

Signalling in Single Cell Wound Healing

The Role of Protein Kinase C

by

Laura Liao

B.Sc., Ryerson University, 2011

A THESIS SUBMITTED IN PARTIAL FULFILLMENT OF
THE REQUIREMENTS FOR THE DEGREE OF

MASTER OF SCIENCE

in

The Faculty of Graduate and Postdoctoral Studies

(Mathematics)

THE UNIVERSITY OF BRITISH COLUMBIA

(Vancouver)

August 2013

© Laura Liao 2013

Abstract

A single cell, such as a frog egg, is able to repair injuries by orchestrating a localized signalling response on the plasma membrane. Proteins called Rho GTPases are recruited to, and form patterns around, the wound site. Patterning allows testable hypotheses to be made about the structure of the signalling network. Here, we extend a Rho GTPase signalling model from Simon et al. (2013) to test how a family of enzymes, protein kinase C (PKC), plays a role in cell repair signalling. Our models let PKCs affect basal Rho GTPase activation and/or inactivation rates, with increasing spatial detail. Ultimately, the model variants do not account for Rho GTPase patterning in all experiments. We suggest a new round of modelling and experiments to correct these issues.

Preface

Chapter 2 is work conducted in University of Wisconsin-Madison's Laboratory of Cell and Molecular Biology by Prof. W. Bement. The unpublished data motivated the modelling work herein.

Table of Contents

Abstract	ii
Preface	iii
Table of Contents	iv
List of Tables	viii
List of Figures	ix
Acknowledgements	xviii
Dedication	xix
1 Introduction	1
1.1 Wound healing in single cell systems	1
1.2 GTPases: RhoA and Cdc42	1
1.3 GTPases signal to actin and myosin	2
1.4 Protein kinase Cs (PKC) influence Rho GTPases	2
1.5 Cell signalling in <i>Xenopus</i> oocyte wound healing	3
1.5.1 Signalling components can be probed and quantified	3
1.5.2 Patterning hints at network's structure	5
1.5.3 Thesis focus	7
2 Protein kinase Cs (PKCs), lipids and their roles	10
2.1 Overview	10
2.2 Diacylglycerol (DAG) overlaps the RhoA zone	13
2.3 PKCs bind DAG, localizing to regions comprising Rho GT- Pase zones	13
2.4 PKC beta and PKC eta play opposing roles in RhoA and Cdc42 activation	15
2.4.1 PKC beta positively influences Rho GTPase activa- tion	16

Table of Contents

2.4.2	PKC eta negatively influences RhoA and Cdc42 activation	18
2.5	Main questions to be addressed	19
3	Models: definitions, background, and logical framework	21
3.1	Overview	21
3.2	Defining the Simon et al. (2013) Rho GTPase model	21
3.2.1	Model features	26
3.2.2	Successes and limitations of the model	26
3.3	The PKCs – revising the basic model	28
3.3.1	Criteria for model validation	29
4	PKCs as spatially constant parameters	30
4.1	Overview	30
4.2	PKCs act on GEFs or GAPs	30
4.2.1	Bifurcations on the basal rates of RhoA (in)activation, k_0^r (k_2)	34
4.2.2	Bifurcations on the basal rates of Cdc42 (in)activation, k_0^c (k_7)	35
4.3	Simulations of PKC manipulations	37
4.3.1	Overexpression of PKC beta	38
4.3.2	Expression of dominant-negative PKC beta	39
4.3.3	Overexpression of PKC eta	41
4.3.4	Expression of dominant-negative PKC eta	42
4.4	Possible ways to achieve inverted Rho GTPase zones	43
4.5	Conclusions	45
5	PKCs as spatially dependent parameters: step function representation	47
5.1	Overview	47
5.2	Defining PKC activity profiles	47
5.2.1	PKC spatial profiles as step functions	48
5.2.2	PKC zone localization	48
5.3	Spatially dependent basal Rho GTPase activation rates	50
5.3.1	Parameter estimation	51
5.3.2	Constraints set by control data	53
5.4	Simulations of PKC manipulations	54
5.4.1	Overexpression of PKC beta	55
5.4.2	Expression of dominant-negative PKC beta	56
5.4.3	Overexpression of PKC eta	58

Table of Contents

5.4.4	Expression of dominant-negative PKC eta	59
5.5	Addressing Cdc42 insensitivity to PKC beta	60
5.5.1	Spatially dependent basal Cdc42 inactivation rate . .	60
5.5.2	Parameter estimation and constraints	61
5.5.3	Simulations	61
5.6	Conclusions	64
6	PKCs as spatially dependent parameters: explicit activity profiles	67
6.1	Overview	67
6.2	Defining PKC activity profiles	67
6.2.1	Explicit PKC activity profiles from data	68
6.2.2	PKC localization to regions overlapping Rho GTPase zones	69
6.3	Spatially dependent basal Rho GTPase activation rates . . .	71
6.3.1	Parameter estimation and constraints	71
6.4	Simulation of the control experiment	73
6.4.1	Revising the $k_0^r(x, t)$, $k_0^c(x, t)$ relationship with PKC beta	74
6.5	Conclusions	77
7	Full nonlinear parameter fitting of model to data	79
7.1	Overview	79
7.2	Fitting spatial background activation rates to control Rho GTPase activities	80
7.2.1	Matching the simulated wound edge to data	80
7.2.2	Fits to control RhoA data	81
7.2.3	Fits to control Cdc42 data	82
7.3	Simulations of PKC manipulations	84
7.3.1	Overexpression of PKC beta	84
7.3.2	Expression of dominant-negative PKC beta	88
7.3.3	Overexpression of PKC eta with inverted Rho GTPase zones	89
7.4	Revisiting fits of background activation rates to Rho GTPase activity	91
7.4.1	Constrained fitting of $k_0^r(x, t)$ to control RhoA activity	92
7.4.2	Constrained fitting of $k_0^c(x, t)$ or $k_7(x, t)$ to control Cdc42 activity	96
7.5	Conclusions	97

Table of Contents

8 Conclusions	98
Bibliography	102
 Appendices	
A Zone amplification factors from box-and-whisker plots . .	104
B Amalgamating PKC and Rho GTPase datasets	106
B.1 Overexpression of PKC beta	107
B.2 Expression of dominant-negative PKC beta	108
B.3 Overexpression of PKC eta with inverted Rho GTPase zones	109

List of Tables

3.1	Parameters in Model 1 from Simon et al. (2013).	25
6.1	Parameterization of $k_0^r(x, t)$ (Equations 6.1-6.3) by method of least-squares. The sum of squared residuals (SSR) is given. .	73
6.2	Parameterization of $k_0^c(x, t)$ by method of least-squares. The sum of squared residuals (SSR) is given.	73
A.1	Fold change in RhoA and Cdc42 zone activities, relative to control, when PKC beta is overexpressed. Based on mean intensity data (in arbitrary units) taken from Figure 2.2 D. Fold changes that are not statistically significant are indicated by —.	104
A.2	Fold change in RhoA and Cdc42 zone activities, relative to control, when dominant-negative PKC beta is expressed. Based on mean intensity data (in arbitrary units) taken from Figure 2.2 E. Fold changes in background activity that are not statistically significant are indicated by —.	104
A.3	Fold change in RhoA and Cdc42 zone activities, relative to control, when PKC eta is overexpressed. Based on mean intensity data (in arbitrary units) taken from Figure 2.2 F. . .	105
A.4	Fold change in RhoA and Cdc42 background activities, relative to control, when dominant-negative PKC eta is expressed. Based on mean intensity data (in arbitrary units) taken from Figure 2.2 G. Fold changes in zones that are not statistically significant are indicated by —.	105

List of Figures

1.1	Rings of active RhoA (inner ring) and active Cdc42 (outer ring) around the wound site (Figure from (Bement et al., 2012)). The wound contracts and closes over the course of a few minutes. Scale bar is 20 μm	2
1.2	Events in single cell wound healing. Upon wounding, an influx of Ca^{2+} into the cell triggers cell repair. Diacylglycerol (DAG), a lipid, accumulates around the wound. Protein kinase Cs (PKC) are lipid targets that are activated by DAG, and influence RhoA and Cdc42 activation. RhoA and Cdc42 play instrumental roles in actin assembly and contraction of the wound. This thesis is focused on later events involving PKCs and Rho GTPases.	3
1.3	Spatial patterns of active RhoA (green) and active Cdc42 (red) in a wounded frog egg (left). Probe intensities are measured in a line scan drawn outwards from the wound center (right). The wound edge is marked with a vertical black line.	4
1.4	Time sequence showing a single cell wound experiment. RhoA and Cdc42 zones rise, narrow, and translocate towards the wound center during wound healing. Late stages of the healing response (zone segregation and zone maintenance; 54 – 84 s) are depicted in these radial concentration profiles. The wound edge is denoted W. Rho GTPase intensities were scaled to concentrations using estimates of basal and elevated Rho GTPase concentrations found in literature (Simon et al., 2013).	5
1.5	The signalling network of RhoA and Cdc42 with interactions mediated through Abr. Reprinted from “Pattern formation of Rho GTPases in single cell wound healing,” by C. M. Simon, 2013, <i>Molecular Biology of the Cell</i> , 24(3), p. 424. Copyright 2013 by the American Society for Cell Biology. Reprinted with permission.	6

List of Figures

1.6	This thesis starts from the Rho GTPase signalling network of Simon et al. (2013) (left), and extends it by investigating the effects of PKCs on background (in)activation rates of RhoA and Cdc42 (center). PKC activation or inhibition of background rates is investigated (right). Potential PKC beta effects are shown in the blue arrows/bar-headed lines. PKC eta (not shown) has the opposite effect. Adapted from “Pattern formation of Rho GTPases in single cell wound healing,” by C. M. Simon, 2013, <i>Molecular Biology of the Cell</i> , 24(3), p. 424. Copyright 2013 by the American Society for Cell Biology. Adapted with permission.	8
1.7	A flow chart summarizing model variants and the chapters in which they are discussed. PKC effects are introduced into the Rho GTPase background (in)activation rates in the Simon et al. (2013) model. Model variations incorporate increasing spatial detail and additional assumptions.	9
2.1	Five lipids characterized by time to appearance, relative to Cdc42 zone formation (15 – 20 s) (Figure from Bement et al. (2012)). Lipid domains of phosphoinositide triphosphate (PIP3), phosphoinositide bisphosphate (PIP2) and phosphatidylserine (PS) organize around the wound edge at late times (A-C). Lipid domains of phosphatidic acid (PA) and diacylglycerol (DAG) organize around the wound edge at early times (D, E). Lipid distributions at 90 s, relative to the Cdc42 zone (A'-E'). Relative positions of lipid compartments by pairwise comparison (F-I). Lipid compartment positions in relation to the wound edge (J). Scale bar = 20 μm . W = Wound edge. Panels are individually reproduced and discussed in the text.	11

List of Figures

2.2	Localization of PKC beta and PKC eta (A) and their distributions at 90 s (Figure from Bement et al. (2012)). Overexpression (OE), or expression of dominant-negative (DN) variants, of PKC beta or PKC eta showing influence on RhoA and Cdc42 zone activation (C). Quantification of average RhoA (green) and Cdc42 (red) zone intensities at 30 s and 60 s for each manipulation (D, F, H). Quantification of average RhoA and Cdc42 zone and background intensities at 60 s for manipulations which show late zone formation (E, H). Top and bottom whiskers indicate maximum and minimum intensities, respectively. Scale bar = 20 μm . W = Wound edge. Panels are individually reproduced and discussed in the text.	12
2.3	Diacylglycerol appears to accumulate around the wound at early times, relative to the formation of the Cdc42 zone (E). DAG localizes to regions close to the wound edge, where the RhoA zone is present (E'). The Cdc42 zone is used to mark a 5 μm distance from the wound edge. W denotes the wound edge. Note that the orientation of the axis is reversed from later simulations, where the wound is on the left.	13
2.4	Localization of PKC beta and PKC eta relative to the Cdc42 zone (A, B). PKC beta overlaps regions of both RhoA and Cdc42 zones (A'). PKC eta overlaps the region containing only the RhoA zone (B').	14
2.5	Time sequence of PKC beta and PKC eta localization show broad zones which narrow as healing progresses (A). Line scans compare the broad PKC beta localization to the narrow PKC eta localization (B).	15
2.6	Time sequence images of a control wound experiment where RhoA (green) and Cdc42 (red) are probed.	16
2.7	Elevated zone activities of RhoA (green) and Cdc42 (red) when PKC beta is overexpressed. Quantification of zone activities at 30 s and 60 s (D).	16
2.8	Diminished zone activities of RhoA (green) and Cdc42 (red) when dominant-negative PKC beta is expressed. Quantification of zone activities and background activities at 60 s (E). .	17
2.9	Diminished zone activities of RhoA (green) and Cdc42 (red) when PKC eta is overexpressed. Quantification of zone activities at 30 s and 60 s (F).	18

List of Figures

2.10	Elevated background activities of RhoA (green) and Cdc42 (red) when dominant-negative PKC eta is expressed. Quantification of zone activities and background activities at 60 s (G).	18
2.11	One-fifth of PKC overexpression experiments result in inverted zones where Cdc42 encircles the wound, with RhoA outside the Cdc42 zone.	19
3.1	RhoA (green) and Cdc42 (red) zones accumulate around the wound on the plasma membrane (left). RhoA and Cdc42 concentrations are tracked in the model through time and space. The two-dimensional spatial domain is represented in radial coordinates where $r = 0$ (in μm) corresponds to the wound center (right).	22
3.2	The signalling network of RhoA and Cdc42 with interactions mediated through Abr. Reprinted from “Pattern formation of Rho GTPases in single cell wound healing,” by C. M. Simon, 2013, <i>Molecular Biology of the Cell</i> , 24(3), p. 424. Copyright 2013 by the American Society for Cell Biology. Reprinted with permission.	23
3.3	The Simon et al. (2013) model captures basic features in Rho GTPase zones such as the speed of amplification and the steady states. RhoGTPases 54 – 84 s post-wounding are simulated (lines), with data shown in circles for comparison. The simulated wound edge is given by the vertical dashed black line, to be compared with the vertical solid black line. Notice that the orientation of the axis is reversed (wound edge towards the left) in comparison to previous line scan data. . .	24
3.4	The effects of PKCs on background Rho GTPase activation rates k_0^r , k_0^c , and background inactivation rates k_2 , k_7 . Potential PKC beta effects are shown in the blue arrows/bar-headed lines. PKC eta (not shown) has the opposite effect. Adapted from “Pattern formation of Rho GTPases in single cell wound healing,” by C. M. Simon, 2013, <i>Molecular Biology of the Cell</i> , 24(3), p. 424. Copyright 2013 by the American Society for Cell Biology. Adapted with permission.	28

List of Figures

4.1	The simulated control (Model 1) possesses two stable steady states in RhoA and three stable steady states in Cdc42. RhoA (green) and Cdc42 (red) have high steady states within the zone, and low steady states at background. Cdc42 has an additional steady state in the Cdc42 bump.	31
4.2	A bifurcation diagram of k_0^r showing RhoA steady states. At the control value (vertical violet line), RhoA possesses stable low and high steady states which correspond to the background and zone activities, respectively (violet arrows). The unstable steady state corresponds to the bistable threshold. The interval 0.87-1.37 marks the bistable region (vertical dashed lines).	32
4.3	A bifurcation diagram of k_0^r showing Cdc42 steady states. As in Figure 4.2, but a third intermediate stable steady state is shown (violet arrows). Cdc42 is bistable over the interval 0-1.37, but only the interval where <i>both</i> GTPases retain bistability is called the bistable region (vertical dashed lines).	33
4.4	Bifurcation diagrams (space-free Equations 3.2-3.4) with respect to RhoA basal activation (top) and inactivation (bottom). Stable branches towards the top (bottom) of each diagram indicate high (low) steady states. Cdc42 possesses an additional intermediate steady state. Bistable region (both GTPases) marked by vertical dashed lines.	34
4.5	As in Figure 4.4 but the intermediate Cdc42 steady state is not shown. RhoA is unaffected by either Cdc42 basal (in)activation rate, and therefore RhoA retains bistability throughout each diagram.	36
4.6	Results for Model 2 where PKC beta is overexpressed. The simulated control is shown for comparison (circles/thick curves).	38
4.7	Results for Model 2 where dominant-negative PKC beta is expressed. The simulated control is shown for comparison (circles/thick curves).	40
4.8	Results for Model 2 where PKC eta is overexpressed. The simulated control is shown for comparison (circles/thick curves).	41
4.9	Results for Model 2 where dominant-negative PKC eta is expressed. The simulated control is shown for comparison (circles/thick curves).	42
4.10	Results for Model 2 where inverted Rho GTPase zones occur because Cdc42 sweeps out in front of the RhoA zone. The simulated control is shown for comparison (circles/thick curves).	44

List of Figures

4.11	Results for Model 2 where inverted Rho GTPase zones occur because the RhoA zone protrudes into a uniform field of Cdc42. The simulated control is shown for comparison (circles/thick curves).	45
5.1	Activity profiles of PKC beta, $\beta(x, t)$, and PKC eta, $\eta(x, t)$, are modelled as normalized step functions with PKC beta covering a greater breadth than PKC eta. The simulated wound edge is marked by the vertical black line, and is towards the left.	48
5.2	Definition of RhoA zone location at early times (left) and late times (right). Top of the thick black line indicates maximum activity above background; base of the black line indicates background activity. Top violet line indicates 40% of height spanned by black line; bottom violet line indicates the defined zone location. A similar determination of the Cdc42 zone location is used with a threshold of 40 %.	49
5.3	Determination of 40 % activity threshold from control data. Time series of Rho GTPases highlighting the RhoA zone location (green interval) and Cdc42 zone location (red interval). Chosen activity threshold corresponds to visual estimation of zone location accuracy.	49
5.4	Distinct regions in the simulated control where both PKCs are present (Region 1), only PKC beta is present (Region 2), and neither PKCs are present (Region 3).	51
5.5	Control simulation for Model 3. Note the appearance of the RhoA shoulder. The control data are shown for comparison (circles/thick curves).	54
5.6	Results for Model 3 where PKC beta is overexpressed by 5 %. The simulated control is shown for comparison (circles/thick curves).	56
5.7	Results for Model 3 where dominant-negative PKC beta is expressed. PKC beta activity is expressed at 80 % of control levels. Initial conditions have been adjusted to guarantee zone maintenance. The simulated control is shown for comparison (circles/thick curves).	57
5.8	Results for Model 3 where PKC eta is overexpressed by 5 %. The simulated control is shown for comparison (circles/thick curves).	58

List of Figures

5.9	Results for Model 3 where dominant-negative PKC eta is expressed. PKC eta activity is expressed at 40 % of control levels. Initial conditions have been adjusted to guarantee zone maintenance. The simulated control is shown for comparison (circles/thick curves).	59
5.10	Control simulation for Model 4. Note the appearance of the RhoA shoulder. The control data are shown for comparison (circles/thick curves).	62
5.11	Results for Model 4 where PKC beta is overexpressed by 210 %. The simulated control is shown for comparison (circles/thick curves).	63
6.1	Normalized intensity profiles of PKC eta and PKC beta activities. Relevant times 54 – 84 s post-wounding are shown. .	68
6.2	PKC activity profiles and Rho GTPase activities from different control datasets are compared. PKC zones do not overlap the RhoA zone. W denotes the wound edge from the Rho GTPase dataset.	69
6.3	Aligning the PKC profiles with the Cdc42 peak at 90 s post-wounding. A 7 μm shift towards the wound center is illustrated.	70
6.4	To correct the PKC localization between datasets, the PKC profiles are merged with Rho GTPase profiles under a 7 μm shift towards the wound center.	71
6.5	PKC zones via the zone localization definition. Mean PKC activity within the zone, and mean PKC activity outside the zone are shown.	72
6.6	Control simulation for Model 5. The control data are shown for comparison (circles/thick curves).	74
6.7	Control simulation for Model 6. The control data are shown for comparison (circles/thick curves).	76
6.8	Control simulation for Model 7. The control data are shown for comparison (circles/thick curves).	77

List of Figures

7.1	Simulated wound edge position (left) and velocity v_c (right) showing the previous choices by Simon et al. (2013) in red, and our improvement in blue. The simulated wound edge position matches data at 54 s and 84 s post-wounding (left, red) when a constant $v_c(t) = 1.12 \mu\text{m}^2/\text{s}$ is used (right, red). The simulated wound edge position matches data at six times points (left, blue) when a time-dependent $v_c(t)$ is used (right, blue).	80
7.2	Model 8 fits to RhoA activity with matched wound edge. Fitted parameters that resulted in a sum of squared residuals of $0.053 \mu\text{M}^2$ were: $k_{\text{basal}}^r = 0.0058 /\text{s}$, $k_{\text{PKC}}^r = 0.38 /\mu\text{M}/\text{s}$, $\alpha_1 = 86 /\mu\text{M}$, $\beta_0^r = 0.60 \mu\text{M}$. Control data are shown as circles/thick curves.	82
7.3	Model 9 fits to Cdc42 activity, as in Figure 7.2. However, the parameters in the basal RhoA activation rate are fixed by the previous RhoA fit. Fitted parameters that resulted in a sum of squared residuals of $0.094 \mu\text{M}^2$ were: $k_{\text{basal}}^c = 0.00025 /\text{s}$, $k_{\text{PKC}}^c = 0.38 /\mu\text{M}/\text{s}$, $\alpha_2 = 85 /\mu\text{M}$, $\beta_0^c = 0.043 \mu\text{M}$. An additional parameter, $C_{\text{shift}} = -2.47 \mu\text{m}$, was introduced so that the offset Cdc42 zone may be fitted.	83
7.4	Results for Model 9 where PKC beta Rho GTPase initial conditions are used and PKCs are at control levels. Rho GTPase data from the corresponding PKC manipulation are shown for comparison (circles/thick curves). However, RhoA data are not shown after 72 s since RhoA activity begins to dive below the focal plane.	85
7.5	As in Figure 7.4, showing results for Model 9 where PKC beta is overexpressed by two-fold.	86
7.6	As in Figure 7.4, showing results for Model 9 where PKC beta is overexpressed by 1.5-fold.	87
7.7	Results for Model 9 where dominant-negative PKC beta Rho GTPase initial conditions are used and PKCs are at control levels. Rho GTPase data from the corresponding PKC manipulation are shown for comparison (circles/thick curves).	88
7.8	Results for Model 9 where dominant-negative PKC beta is expressed at half the control activity. Rho GTPase data from the corresponding PKC manipulation are shown for comparison (circles/thick curves).	89

List of Figures

7.9	Results for Model 9 where overexpressed PKC eta Rho GTPase initial conditions are used and PKCs are at control levels. Rho GTPase data from the corresponding PKC manipulation are shown for comparison (circles/thick curves).	90
7.10	Results for Model 9 where PKC eta is expressed at twice the control activity. Rho GTPase data from the corresponding PKC manipulation are shown for comparison (circles/thick curves).	91
7.11	Model 10 fits to control RhoA activity. Fitted parameters that resulted in a sum of squared residuals of $0.059 \mu\text{M}^2$ were: $k_{\text{basal}}^r = 0.0027 / \text{s}$, $k_{\text{PKC}}^r = 0.29 / \mu\text{M}/\text{s}$, $\alpha_1 = 24.83 / \mu\text{M}$, $\beta_0^r = 0.46 \mu\text{M}$. Control data are shown for comparison (circles/thick curves).	93
7.12	Model 11 fits to control RhoA activity. Fitted parameters that resulted in a sum of squared residuals of $0.071 \mu\text{M}^2$ were: $k_{\text{basal}}^r = 0.0057 / \text{s}$, $k_{\text{PKC}}^r = 0.096 / \mu\text{M}/\text{s}$, $\alpha_1 = 17.25 / \mu\text{M}$, and $\beta_0^r = 42.06 \mu\text{M}$	95
7.13	Results for Model 10 (olive) and Model 11 (blue) where PKC beta is overexpressed by two-fold. The unconstrained fit from Model 8 is shown for comparison (green). RhoA data from the corresponding PKC manipulation are also shown for comparison (circles/thick curves). However, RhoA data are removed after 72 s because RhoA dives below the focal plane.	96
B.1	Alignment of control PKC profiles with Rho GTPase profiles in PKC beta overexpression. PKC profiles are aligned with Rho GTPase data as is (unshifted). The wound edge is not shown but is towards the left. At 72 s, the RhoA zone dives away from the focal plane.	107
B.2	Alignment of control PKC profiles with Rho GTPase profiles in dominant-negative PKC beta expression. PKC profiles are aligned with Rho GTPase data when shifted $5 \mu\text{m}$ away from the wound center. The wound edge is not shown but is towards the left.	108
B.3	Alignment of control PKC profiles with Rho GTPase profiles in PKC eta overexpression. PKC profiles are aligned with Rho GTPase data as is (unshifted). The wound edge is not shown but is towards the left.	109

Acknowledgements

I offer my gratitude to my supervisor Prof. Leah Edelstein-Keshet, who was a fantastic and generous mentor. I thank my readers Profs. William Bement and Dan Coombs for their involvement and encouragement. Special thanks to Raibatak (Dodo) Das who provided invaluable advice on data fitting in this work, and Cory Simon for the inception of this modelling work. I acknowledge funding from NSERC in the form of the Alexander Graham Bell Canada Graduate Scholarship, as well as the NSERC Discovery Grant to Leah Edelstein-Keshet.

I owe thanks to the Keshet research group and all its members. In particular, thanks to my funny conspirators Meghan Dutot and Mayang Mata who worked alongside me throughout my graduate studies at UBC.

Lastly, the students who make up the Institute of Applied Mathematics deserve acknowledgement for the enduring sense of community and support they provided.

To Justin Martel

Chapter 1

Introduction

1.1 Wound healing in single cell systems

A single cell is able to repair injuries and reseal part of its torn membrane. In experiments by our collaborator, W. Bement, egg cells of the frog (*Xenopus*) were injured by laser, and the process of repair was studied (Bement et al., 2012). Wounds seal shut by first orchestrating a localized signalling response, assembling a local cytoskeleton (actin for structure and myosin for force production) and finally contracting shut in a purse-string manner (Bement et al., 1999; Mandato and Bement, 2001).

How is wound healing in single cells orchestrated? In *Xenopus* oocytes, the healing response is triggered by an influx of Ca^{2+} upon wounding. A contractile ring consisting of actin and myosin-II assembles around the wound. As the wound closes, myosin-II segregates into a narrow ring in the interior of the contractile ring, independently of actin, in response to upstream regulators (Bement et al., 1999; Mandato and Bement, 2001). Among possible upstream regulators are a family of small proteins called Rho GTPases, on which *Xenopus* oocyte healing is dependent (Bement et al., 1999). These proteins form radial patterns that motivate the research in this thesis.

1.2 GTPases: RhoA and Cdc42

Rho GTPases are G proteins (GTP-binding regulatory protein) which are typically engaged in signal transduction of an extracellular message to intracellular message. A prototypical example of G protein function begins with an extracellular ligand binding to a plasma membrane-bound cell receptor, inducing a conformational change in the cell receptor. The cell receptor couples to a G protein and promotes exchange of the G protein's GDP to GTP. The now active, membrane-bound G protein binds to and activates other targets until the G protein hydrolyzes its GTP to GDP, thereby terminating signalling.

Since Rho GTPases have an active state (GTP-bound) and an inac-

tive state (GDP-bound), they are considered molecular switches. The Rho GTPases cycle between an inactive, cytosolic state to an active, membrane-bound state. The toggling between these states is regulated by guanine nucleotide exchange factors (GEFs) and GTPase-activating proteins/guanosine nucleotide dissociation inhibitors (GAPs/GDIs) (Jaffe and Hall, 2005). GEFs promote the exchange of GDP to GTP, and thus promote Rho GTPase signalling. GAPs promote hydrolysis of GTP to GDP, and thus inhibit Rho GTPase signalling. GDIs sequester inactive Rho GTPases in the cytosol (DerMardirossian and Bokoch, 2005).

1.3 GTPases signal to actin and myosin

Two Rho GTPases, RhoA and Cdc42, are implicated in driving the assembly of the actomyosin contractile ring during *Xenopus* oocyte wound closure (Benink and Bement, 2005). RhoA promotes phosphorylation of the myosin light chain, inducing contractile forces along actin stress fibers (via an enzyme Rho kinase) (Amano et al., 1996). Cdc42 enhances the growth of actin by branching its filaments (mediated by complexes Arp2/3 and WASP) (Miki and Takenawa, 2003). Thus RhoA regulates contractile forces in the interior domain of the ring, while Cdc42 regulates cytoskeleton remodeling in the exterior domain of the ring (Figure 1.1). The regulation of the contractile array by Rho GTPases falls in line with RhoA and Cdc42's known roles.

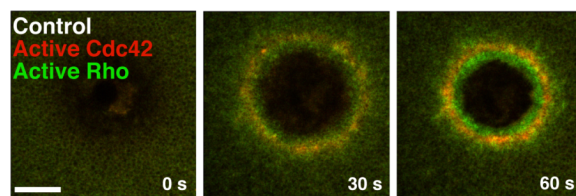


Figure 1.1: Rings of active RhoA (inner ring) and active Cdc42 (outer ring) around the wound site (Figure from (Bement et al., 2012)). The wound contracts and closes over the course of a few minutes. Scale bar is 20 μm .

1.4 Protein kinase Cs (PKC) influence Rho GTPases

The contractile array occupies discrete regions on the plasma membrane. Subcellular domains of Rho GTPase localization are observed (Figure 1.1),

with dynamic Rho GTPases that are in constant flux on and off the membrane (Bement et al., 2006; Benink and Bement, 2005). However, the Rho GTPase-powered contractile array appears late in single cell wound healing. Lipids are involved in the very early response preceding the appearance of Rho GTPases. Rho GTPases, in turn, are influenced by lipids and lipid targets (Figure 1.2) (Bement et al., 2012).

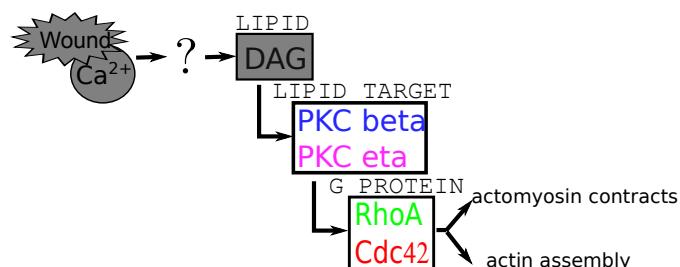


Figure 1.2: Events in single cell wound healing. Upon wounding, an influx of Ca^{2+} into the cell triggers cell repair. Diacylglycerol (DAG), a lipid, accumulates around the wound. Protein kinase Cs (PKC) are lipid targets that are activated by DAG, and influence RhoA and Cdc42 activation. RhoA and Cdc42 play instrumental roles in actin assembly and contraction of the wound. This thesis is focused on later events involving PKCs and Rho GTPases.

As discussed in Chapter 2, the lipid diacylglycerol (DAG) and its target protein kinase C (PKC) are important as upstream signalling components in wound healing. PKCs are shown to influence Rho GTPase activity, and the way in which they do so within the context of *Xenopus* oocyte wound healing becomes our primary focus.

1.5 Cell signalling in *Xenopus* oocyte wound healing

1.5.1 Signalling components can be probed and quantified

Lipids, lipid targets (protein kinase C), and Rho GTPases orchestrate single cell wound healing through a signalling network. *Xenopus* oocytes are a useful experimental system in which to study such cell signalling networks. A key tool are fluorescent probes which visualize processes occurring on the plasma membrane – e.g., membrane resealing and cytoskeleton remodelling. Fluorescent patterns of small molecules on the plasma membrane, such as

active Rho GTPases, can be quantified in a line scan (Figure 1.3). The line scan measures probe intensities which correspond to concentrations of RhoA (green) and Cdc42 (red).

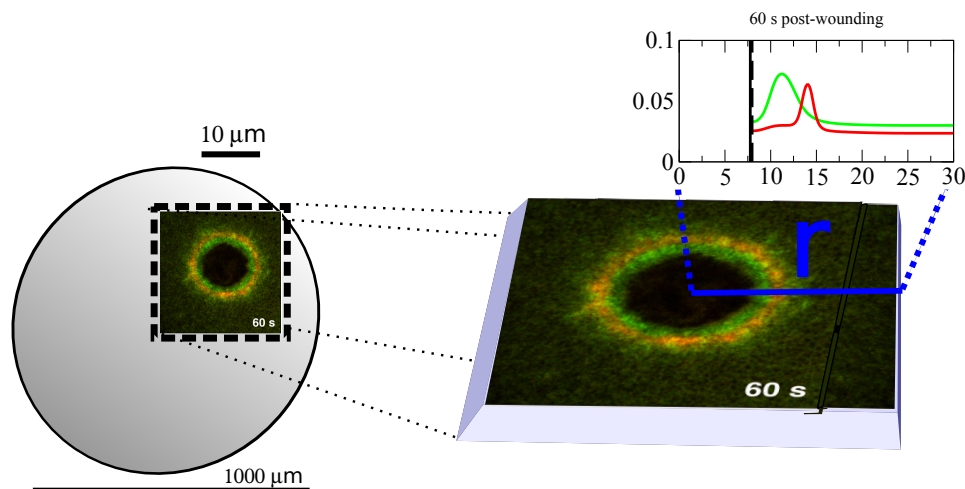


Figure 1.3: Spatial patterns of active RhoA (green) and active Cdc42 (red) in a wounded frog egg (left). Probe intensities are measured in a line scan drawn outwards from the wound center (right). The wound edge is marked with a vertical black line.

Probes reveal zones of Rho GTPases around the wound

Probes reveal spatiotemporal patterning of Rho GTPase activity in images and line scans of the wound. The images show the accumulation of RhoA and Cdc42 around the wound at activities two to five times higher than basal levels in a resting cell. We refer to these regions of elevated activities as discrete *zones*. The zones circumscribe the wound in concentric circles, with RhoA closest to the wound edge, and Cdc42 outside of the RhoA zone (Figure 1.1).

The line scans show the evolution of RhoA and Cdc42 zones (Figure 1.4). Early in wound healing, zones are amplified from an initially shallow Rho GTPase gradient into broad and overlapping zones (**zone formation**). As healing progresses, broad zones narrow into mutually exclusive zones (**zone segregation**). Zone segregation suggests that RhoA inhibits Cdc42, excluding Cdc42 from any region that RhoA occupies. As the zones narrow, they reach a characteristic high concentration as they are pulled forward towards the wound center during closure (**zone maintenance**).

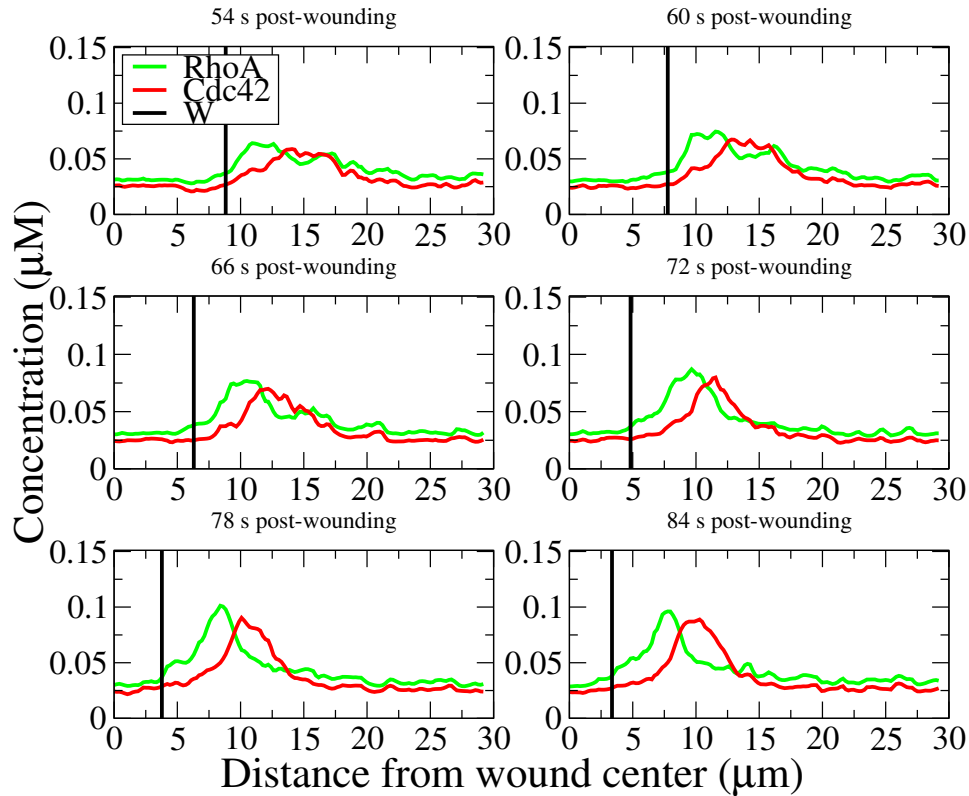


Figure 1.4: Time sequence showing a single cell wound experiment. RhoA and Cdc42 zones rise, narrow, and translocate towards the wound center during wound healing. Late stages of the healing response (zone segregation and zone maintenance; 54 – 84 s) are depicted in these radial concentration profiles. The wound edge is denoted W. Rho GTPase intensities were scaled to concentrations using estimates of basal and elevated Rho GTPase concentrations found in literature (Simon et al., 2013).

1.5.2 Patterning hints at network’s structure

By tracking the patterns in time and space, inferences about the signalling network can be made. For instance, the temporal arrangement of each component in the pathway might be ascertained from observing which probes appear early (upstream) or late (downstream) in the response. The spatial patterns, too, are telling of component interactions with each other. Absences of one component where another component is concentrated might indicate inhibition, whereas amplification in the presence of another compo-

1.5. Cell signalling in *Xenopus* oocyte wound healing

ment might indicate activation. Moreso, manipulations of the experimental system reinforce our ideas about component interactions. Components can be overexpressed (OE), or expressed as functionally impaired versions (DN, dominant-negative), with the resultant changes to patterning also suggestive of regulatory roles. Indeed, the input-output nature of the system allows for perturbation of the signalling network so that we might understand the network's structure.

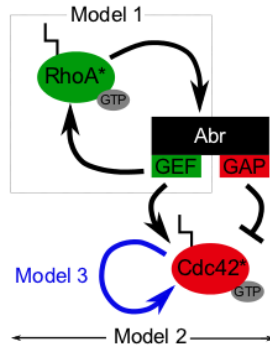


Figure 1.5: The signalling network of RhoA and Cdc42 with interactions mediated through Abr. Reprinted from “Pattern formation of Rho GTPases in single cell wound healing,” by C. M. Simon, 2013, *Molecular Biology of the Cell*, 24(3), p. 424. Copyright 2013 by the American Society for Cell Biology. Reprinted with permission.

Previous work (Simon et al., 2013) viewed *Xenopus* oocyte wound healing as a pattern formation system. They focused on Rho GTPases late in the wound healing response, and asked whether the current hypotheses of Rho, Cdc42 and Abr (a dual GEF/GAP of Rho GTPase (Chuang et al., 1995)) interaction could explain the patterning (Vaughan et al., 2011). Modelling of a network involving RhoA, Cdc42 and Abr, captured key features in Rho GTPase patterns under control conditions, and several experimental manipulations (inhibition of RhoA by C3 exotransferase, overexpression of GEF-dead or GAP-dead Abr, microinjection of Abr) (Figure 1.5). Model validation occurred through predictive experiments involving two wounds at various distances apart. The model made subtle predictions on Rho GTPase patterning in the space between the wounds. The *in silico* predictions were confirmed when two-wound experiments were performed *in vivo*. The authors concluded that Abr, as the chief mediator of Rho GTPase behaviour, was sufficient to account for key aspects of Rho GTPase patterning. Ana-

lyzing cell signalling through the lense of pattern formation was shown to be a valuable perspective.

1.5.3 Thesis focus

In this chapter, we have introduced the actomyosin contractile ring in single cell wound healing and its regulation by RhoA and Cdc42. Both occur late in wound healing, and we have alluded to earlier roles for lipids and lipid targets. We have mentioned that these signalling components can be conveniently probed and quantified in line scans. More importantly, line scans reveal spatiotemporal patterns (zones) that hint at the signalling network's structure. Recent work has tested a Rho GTPase signalling network and successfully recapitulated Rho GTPase patterning (Simon et al., 2013). This thesis extends the previous model, by Simon et al. (2013), of the signalling network in Figure 1.5.

The signalling network describes the following interactions: active RhoA binds to Abr, Abr-bound active RhoA acts as a GEF for RhoA and as a GAP for Cdc42, active Cdc42 regulates itself (Figure 1.6, left). In addition, the network included background activation and background inactivation rates of both RhoA and Cdc42. This thesis is focused entirely on these background (in)activation rates of Rho GTPases, which are clearly marked in Figure 1.6 (center). This thesis investigates PKC activation or inhibition of the background (in)activation rates (Figure 1.6, right).

1.5. Cell signalling in *Xenopus* oocyte wound healing

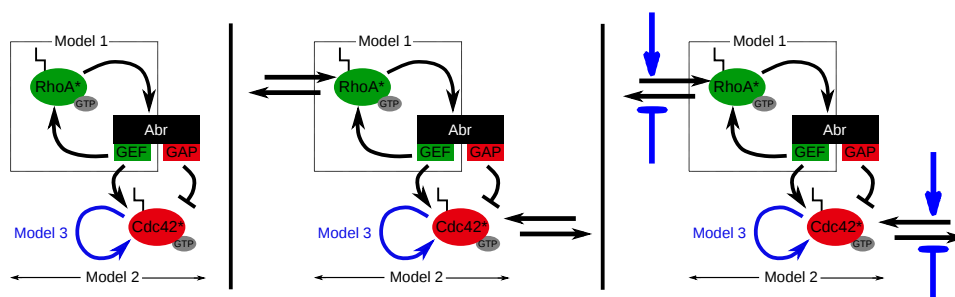


Figure 1.6: This thesis starts from the Rho GTPase signalling network of Simon et al. (2013) (left), and extends it by investigating the effects of PKCs on background (in)activation rates of RhoA and Cdc42 (center). PKC activation or inhibition of background rates is investigated (right). Potential PKC beta effects are shown in the blue arrows/bar-headed lines. PKC eta (not shown) has the opposite effect. Adapted from “Pattern formation of Rho GTPases in single cell wound healing,” by C. M. Simon, 2013, *Molecular Biology of the Cell*, 24(3), p. 424. Copyright 2013 by the American Society for Cell Biology. Adapted with permission.

We use the Rho GTPase network to investigate the roles and effects of PKCs. In Chapter 2, we present *in vivo* experiments which motivate the research in this thesis. The *in vivo* experiments demonstrate PKC interactions with Rho GTPases in the single cell system. In Chapter 3, we define the Simon et al. (2013) Rho GTPase model which is the starting point of this work. We introduce PKC effects with increasing spatial detail into the background (in)activation rates of the model. A flow chart summarizes the model variants detailed in the indicated chapters (Figure 1.7). We begin with the Simon et al. (2013) model and look at the effect of spatially constant PKCs on the background (in)activation rates. We graduate to examining spatially distributed PKCs and their effects on the background (in)activation rates. The spatially distributed PKCs are represented as simple step functions, or as explicit distributions given by data. We work with the explicit distributions, revise some assumptions, and perform rigorous fits. As we shall see, we can improve on the control model, but, given current hypotheses, it is not yet possible to account for all experimental manipulations. In the final chapter, we suggest how future rounds of modelling can correct this.

1.5. Cell signalling in *Xenopus oocyte* wound healing

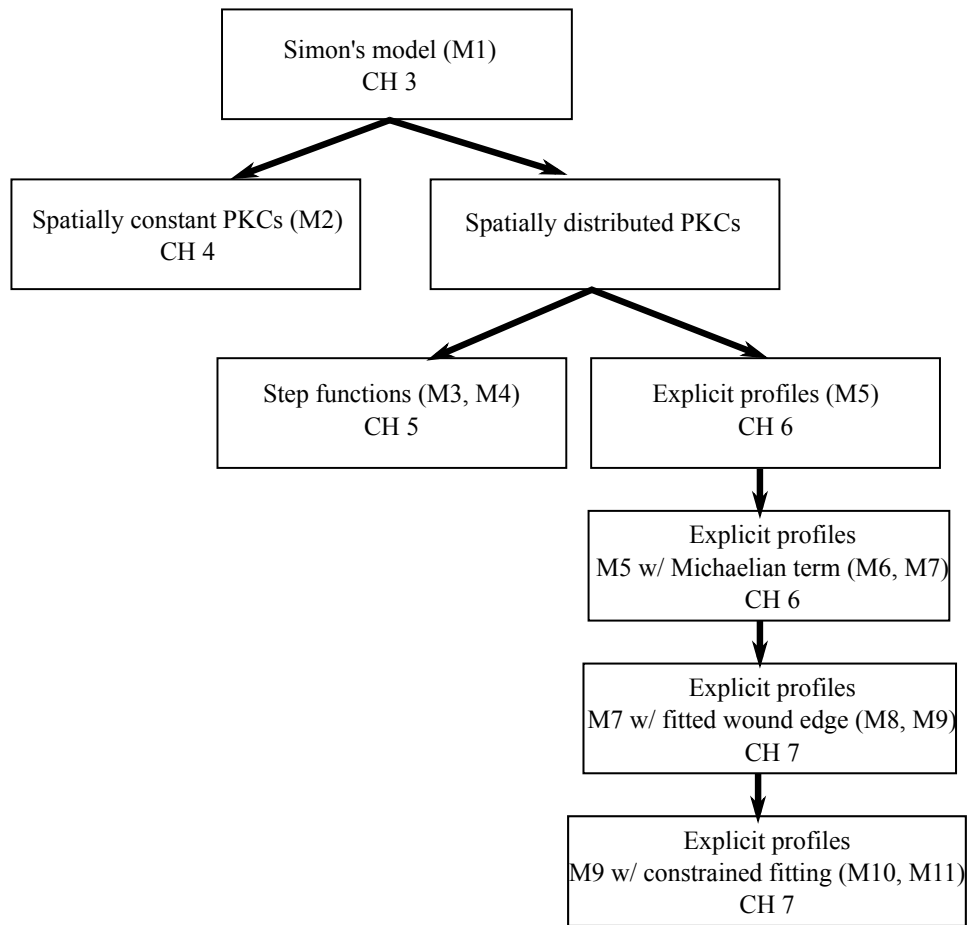


Figure 1.7: A flow chart summarizing model variants and the chapters in which they are discussed. PKC effects are introduced into the Rho GTPase background (in)activation rates in the Simon et al. (2013) model. Model variations incorporate increasing spatial detail and additional assumptions.

Chapter 2

Protein kinase Cs (PKCs), lipids and their roles

2.1 Overview

This chapter presents *in vivo* experiments of Bement et al. (2012) that initiated research described in this thesis. Briefly, the *in vivo* experiments investigated the role of lipids in single cell wound healing. Lipid domains were observed to converge around the wound. Of the five lipids investigated, diacylglycerol (DAG) was shown to be essential to Rho GTPase activation. Further investigation into DAG targets, protein kinase Cs, also showed patterning around the wound edge. PKCs were demonstrated to play opposing roles in wound healing. PKC beta enhanced RhoA and Cdc42 activity, while PKC eta inhibited RhoA and Cdc42 activity.

In these experiments, spherical *Xenopus* oocytes, approximately 1000 μm in diameter, were wounded by a laser. The circular wounds were consistent in size, at diameters of 10 μm . Wounds closed under circumferential tension over the course of a few minutes. Lipids, PKCs and Rho GTPases were probed. Three types of data were shown: images of the wound, line scans through the wound, and box-and-whisker plots quantifying zone intensities. Figures 2.1 and 2.2 were given to us summarizing the experimental results. For reference, we leave the figures intact but repeat panels throughout as we highlight important results.

2.1. Overview

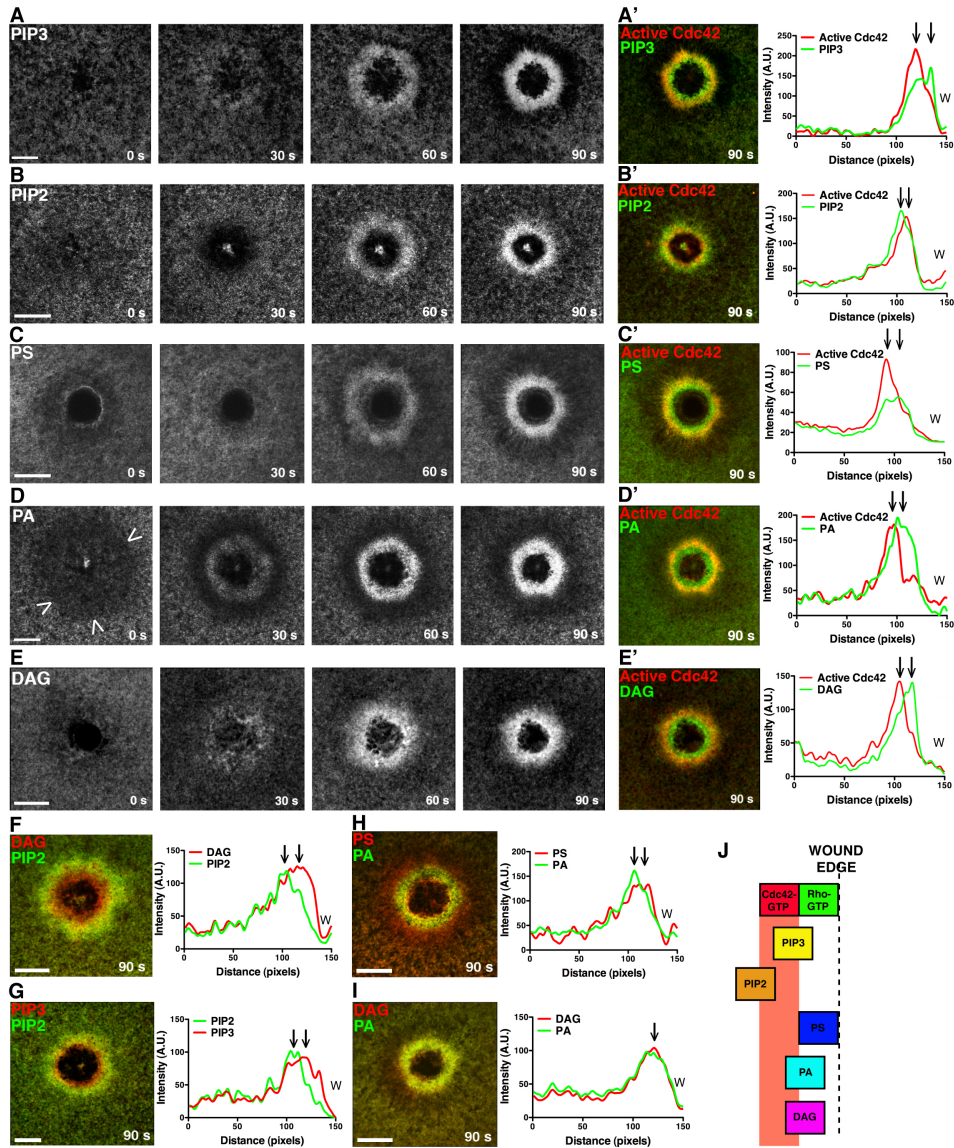


Figure 2.1: Five lipids characterized by time to appearance, relative to Cdc42 zone formation (15 – 20 s) (Figure from Bement et al. (2012)). Lipid domains of phosphoinositide triphosphate (PIP3), phosphoinositide bisphosphate (PIP2) and phosphatidylserine (PS) organize around the wound edge at late times (A-C). Lipid domains of phosphatidic acid (PA) and diacylglycerol (DAG) organize around the wound edge at early times (D, E). Lipid distributions at 90 s, relative to the Cdc42 zone (A'-E'). Relative positions of lipid compartments by pairwise comparison (F-I). Lipid compartment positions in relation to the wound edge (J). Scale bar = 20 μ m. W = Wound edge. Panels are individually reproduced and discussed in the text. 11

2.1. Overview

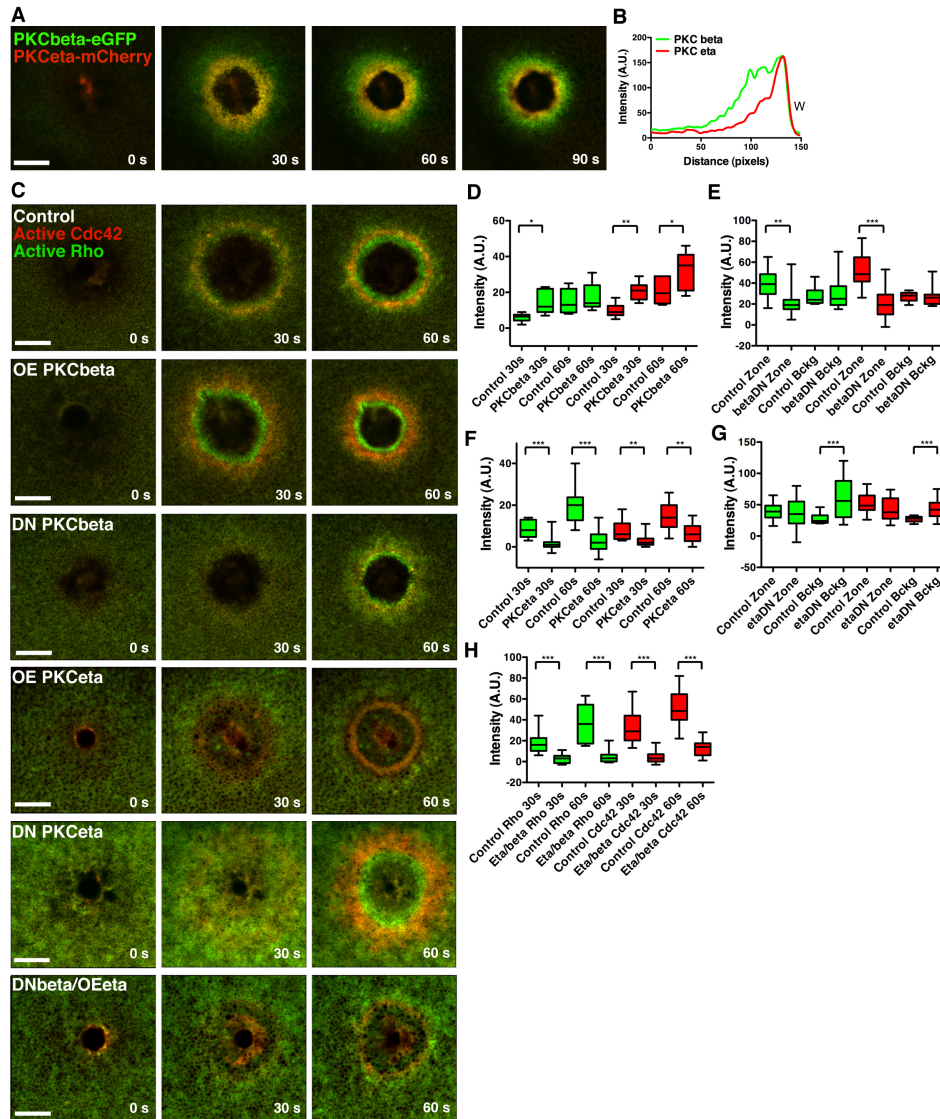


Figure 2.2: Localization of PKC beta and PKC eta (A) and their distributions at 90 s (Figure from Bement et al. (2012)). Overexpression (OE), or expression of dominant-negative (DN) variants, of PKC beta or PKC eta showing influence on RhoA and Cdc42 zone activation (C). Quantification of average RhoA (green) and Cdc42 (red) zone intensities at 30 s and 60 s for each manipulation (D, F, H). Quantification of average RhoA and Cdc42 zone and background intensities at 60 s for manipulations which show late zone formation (E, H). Top and bottom whiskers indicate maximum and minimum intensities, respectively. Scale bar = 20 μ m. W = Wound edge. Panels are individually reproduced and discussed in the text. 12

2.2 Diacylglycerol (DAG) overlaps the RhoA zone

Out of five lipids probed in the study, diacylglycerol was established to be essential to Rho GTPase activation. The black and white time sequence of wound images in Figure 2.3 E depict probes for DAG (white). DAG appeared early, relative to the time of Cdc42 zone formation (at 15 – 20 s), suggesting a role for DAG upstream of Rho GTPase activation. Perturbation to the DAG generation pathway supported that DAG is indeed essential to Rho GTPase activation (not shown). Since DAG was necessary for wound healing, the next component investigated was a DAG target.

Before considering DAG targets, however, we should also note DAG localization from Figure 2.3 E'. At 90 s, wound images show DAG probes (green) in relation to Cdc42 (red). The Cdc42 zone consistently forms 5 μm from the wound edge, and is used to gauge relative positions. The corresponding line scan displays the spatial profile of DAG and Cdc42, with the wound edge towards the right. Here, it is important to notice that DAG localizes to the same region where the RhoA zone would appear.

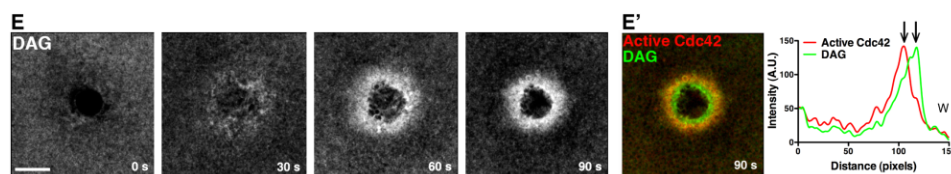


Figure 2.3: Diacylglycerol appears to accumulate around the wound at early times, relative to the formation of the Cdc42 zone (E). DAG localizes to regions close to the wound edge, where the RhoA zone is present (E'). The Cdc42 zone is used to mark a 5 μm distance from the wound edge. W denotes the wound edge. Note that the orientation of the axis is reversed from later simulations, where the wound is on the left.

2.3 PKCs bind DAG, localizing to regions comprising Rho GTPase zones

Diacylglycerol is a well-known activator of a family of enzymes called protein kinase C (PKC). As a result, the DAG targets, PKCs, were subsequently investigated. Members of the PKC family are grouped into three classes – conventional, novel, and atypical – based on their activation requirements.

2.3. PKCs bind DAG, localizing to regions comprising Rho GTPase zones

Conventional PKCs must bind to both Ca^{2+} and DAG in order for catalytic activation to occur. Novel PKCs must bind only to DAG. Atypical PKCs require neither Ca^{2+} nor DAG for their activation. The PKCs considered here are PKC beta (conventional) and PKC eta (novel). They both require DAG as an activator, and must compete for DAG in cell wounding.

Figure 2.4 shows images and line scans of the PKCs (green) in relation to the Cdc42 zone (red). In Figures 2.4 A and A', PKC beta localizes to regions which overlap both the RhoA and Cdc42 zones. In Figures 2.4 B and B', PKC eta localizes to a region which overlaps only the RhoA zone. Since DAG overlaps the RhoA zone, and both PKCs must bind DAG in order to be activated, it is no surprise that both PKC beta and PKC eta also overlap the RhoA zone.

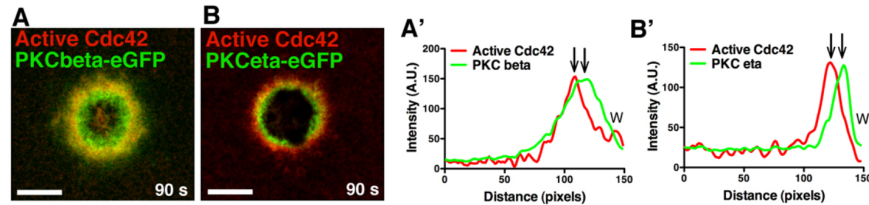


Figure 2.4: Localization of PKC beta and PKC eta relative to the Cdc42 zone (A, B). PKC beta overlaps regions of both RhoA and Cdc42 zones (A'). PKC eta overlaps the region containing only the RhoA zone (B').

Simultaneous probing of PKC beta (green) and PKC eta (red) reveal broad overlapping zones that narrow into well-defined, discrete zones as healing progresses (Figure 2.5 A). A line scan at 90 s shows that PKC beta localizes to a broader region than PKC eta (Figure 2.5 B). The takeaway message on PKC localization is that PKC beta is targeted to a broad region comprising both Rho GTPase zones, while PKC eta is targeted to a narrow region comprising only the RhoA zone.

2.4. PKC beta and PKC eta play opposing roles in RhoA and Cdc42 activation

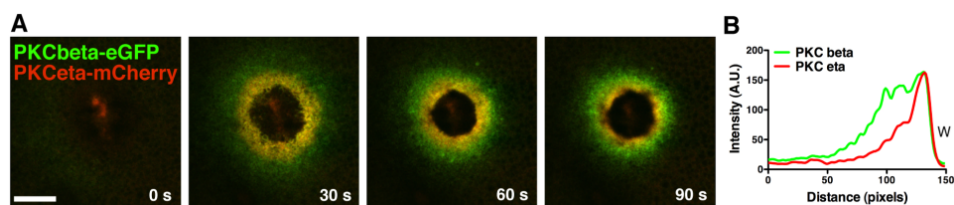


Figure 2.5: Time sequence of PKC beta and PKC eta localization show broad zones which narrow as healing progresses (A). Line scans compare the broad PKC beta localization to the narrow PKC eta localization (B).

2.4 PKC beta and PKC eta play opposing roles in RhoA and Cdc42 activation

In the previous sections, we discussed the spatial profiles of DAG and PKCs with respect to RhoA and Cdc42 localization. Since they were probed in a control wounding experiment, we observed the localization of *endogenous* components. The next panels will show manipulations to the system, and the effect of *exogenous* PKCs on Rho GTPase activation.

The subsequent experiments probed Rho GTPases and monitored for changes in zone activity in response to a PKC manipulation. PKCs can be manipulated through overexpression (OE), or through expression of a dominant-negative (DN) version. Overexpression of PKC means more PKC within the cell, resulting in increased PKC effect. Conversely, a DN PKC is functionally impaired and, when expressed, results in decreased PKC effect. In either manipulation, PKCs retain their capacity to localize. We later assume that exogenous PKCs (OE or DN manipulation) localize in the same way as endogenous PKCs (control).

The following sections show images of wounds with RhoA in green and Cdc42 in red. Each manipulation is labelled as “OE PKC beta”, for example. The images show qualitative changes to Rho GTPase zone activities that are meant to be compared against the control (Figure 2.6). An accompanying box-and-whisker plot quantifies the changes in zone activities in comparison to the control.

2.4. PKC beta and PKC eta play opposing roles in RhoA and Cdc42 activation

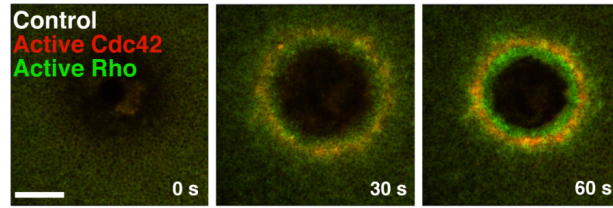


Figure 2.6: Time sequence images of a control wound experiment where RhoA (green) and Cdc42 (red) are probed.

2.4.1 PKC beta positively influences Rho GTPase activation

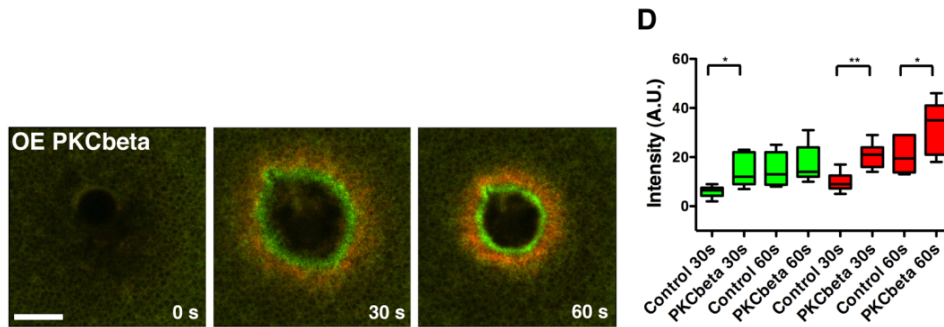


Figure 2.7: Elevated zone activities of RhoA (green) and Cdc42 (red) when PKC beta is overexpressed. Quantification of zone activities at 30 s and 60 s (D).

When PKC beta is overexpressed, both Rho GTPase zones appear brighter (Figure 2.7). The zone quantification shows higher RhoA zone activity at 30 s, compared to control, and higher Cdc42 zone activity at 30 s and 60 s (Figure 2.7 E). We express the difference in zone activities, between the manipulation and control, as fold changes in Table A.1. These are later used in simulations as zone amplification factors.

2.4. PKC beta and PKC eta play opposing roles in RhoA and Cdc42 activation

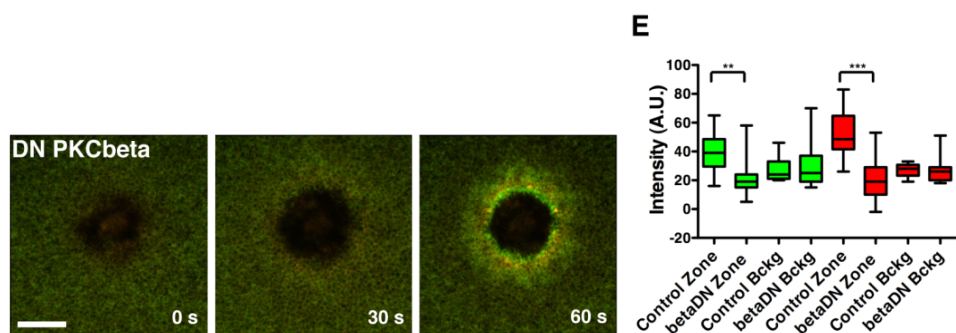


Figure 2.8: Diminished zone activities of RhoA (green) and Cdc42 (red) when dominant-negative PKC beta is expressed. Quantification of zone activities and background activities at 60 s (E).

When dominant-negative PKC beta is expressed, both Rho GTPase zones appear diminished (Figure 2.8). Since zones are not visible at 30 s, zone quantification at only 60 s can be done. The box-and-whisker plot compares zone activities, as well as background activities, to the control. Both RhoA and Cdc42 zone activities are lower than control. No significant changes to background activities are observed. Table A.2 expresses the difference in zone activities as fold changes.

In summary, the overexpression of PKC beta results in upregulation of both RhoA and Cdc42 zone activities, while the expression of dominant-negative PKC beta results in downregulation of both RhoA and Cdc42 zone activities. PKC beta positively influences both RhoA and Cdc42 zone activation.

2.4. PKC beta and PKC eta play opposing roles in RhoA and Cdc42 activation

2.4.2 PKC eta negatively influences RhoA and Cdc42 activation

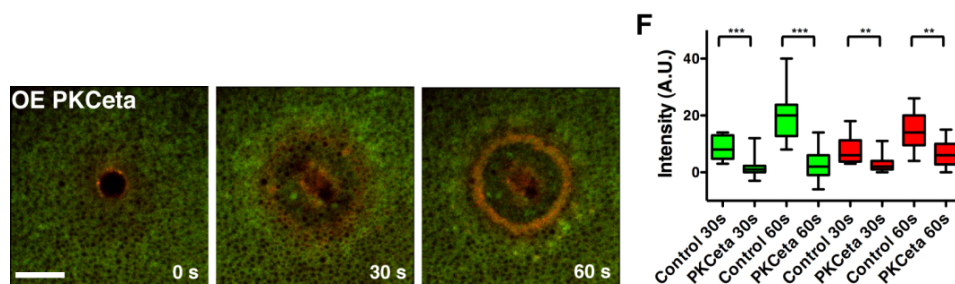


Figure 2.9: Diminished zone activities of RhoA (green) and Cdc42 (red) when PKC eta is overexpressed. Quantification of zone activities at 30 s and 60 s (F).

In comparison to manipulations of PKC beta, manipulations involving PKC eta produce opposite effects on the Rho GTPase zones. In short, overexpression of PKC eta results in qualitatively and quantitatively diminished zones (Figure 2.9). Expression of dominant-negative PKC eta results in qualitatively and quantitatively elevated background activities (Figure 2.10). Thus, PKC eta negatively influences both RhoA and Cdc42 zone activation.

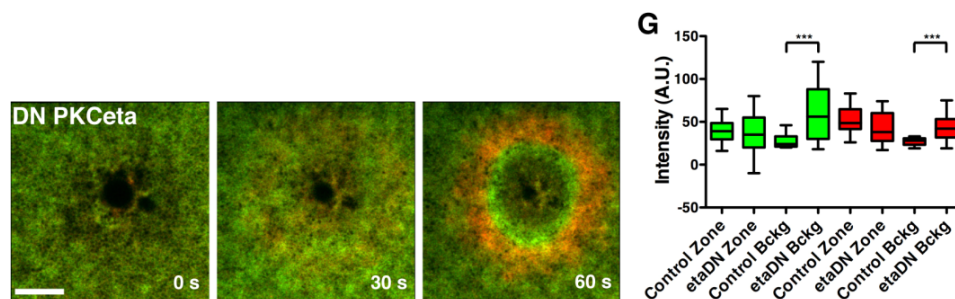


Figure 2.10: Elevated background activities of RhoA (green) and Cdc42 (red) when dominant-negative PKC eta is expressed. Quantification of zone activities and background activities at 60 s (G).

Overall, these results indicate that PKC beta promotes the activation of RhoA and Cdc42. Conversely, PKC eta inhibits the activation of RhoA and Cdc42.

A subset of OE PKC eta manipulations result in inverted RhoA and Cdc42 zones

In the control and the majority of experiments where PKC eta is overexpressed, RhoA encircles the wound, and Cdc42 encircles the RhoA zone (Figure 2.6). However, approximately one-fifth of PKC eta overexpression experiments result in a surprising swap of RhoA and Cdc42 zones (Figure 2.11). The inverted zones are compelling since they are an unusual result that might serve as a way to evaluate hypotheses we make about the signalling network. A successful hypothesis should explain these inverted zones.

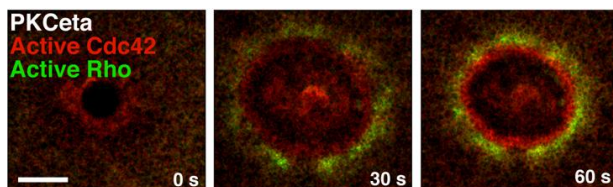


Figure 2.11: One-fifth of PKC overexpression experiments result in inverted zones where Cdc42 encircles the wound, with RhoA outside the Cdc42 zone.

2.5 Main questions to be addressed

What picture of single cell wound healing do these data paint for us? In a control wounding experiment, DAG localizes around the wound, overlapping the RhoA zone. Both PKC eta and PKC beta bind to DAG in the RhoA zone, though PKC beta broadly extends over the Cdc42 zone as well. PKC beta and PKC eta exert opposing effects on both zones of RhoA and Cdc42 activation. In an experiment where PKCs are manipulated, we assume the exogenous PKCs localize in the same way as endogenous PKCs. Overexpression of PKC means there are more PKCs within the cell competing for DAG, and exerting more effect on the GTPases. Expression of dominant-negative PKC means that PKC function is impaired, and their effect on Rho GTPases is diminished.

We plan to use the Simon et al. (2013) model and test hypotheses about how PKCs exert their influence. We formulate questions that will be addressed throughout this thesis.

1. Does PKC beta upregulate Rho GTPase activity by enhancing activation (through a GEF), or by depressing inactivation (through a GAP)? A similar question can be asked about PKC eta.

2.5. *Main questions to be addressed*

2. Is the spatial distribution of PKC beta and PKC eta important in accounting for the observed RhoA and Cdc42 zones?
3. Why does PKC eta only appear in the RhoA zone? Is it possible that PKC eta influences RhoA, but that RhoA also influences PKC eta in order to maintain the discrete eta zone?
4. If PKC eta is present only in the RhoA zone, how does it exert influence over the Cdc42 zone?
5. In what ways does DAG modulate PKC effects on Rho GTPases?

The following chapters address these questions in the above order. Chapter 4 addresses how PKCs affect Rho GTPases, and shows degeneracies between GEF and GAP regulation. Chapter 5 implements spatial distributions of PKCs which further matches the simulated RhoA zone to the observed RhoA zone. Chapter 5 also implements a feedback from RhoA to PKC eta which we ultimately reject. Chapter 6 increases the spatial detail in PKC distributions and also attempts to answer how PKC eta exerts influence over the Cdc42 zone. Chapter 6 places limits on PKC overexpression due to a finite amount of DAG. See Figure 1.7 for a schematic flow chart of the modelling and organization of the thesis. So far, as described in this thesis, the increasingly detailed model variants are not able to account for the RhoA and Cdc42 zone inversion.

Chapter 3

Models: definitions, background, and logical framework

3.1 Overview

In this chapter, the mathematical model is defined and its parameters are explained. We give background on how it was built, and outline model features (i.e., crosstalk and spatial bistability). We discuss the model’s successes and limitations. We then discuss our use of the model and the revisions that we make to it. Finally, we give criteria for model validation.

3.2 Defining the Simon et al. (2013) Rho GTPase model

Our tool for probing the PKC connection to Rho GTPase activation is a set of reaction-diffusion-advection equations (Simon et al., 2013). These equations track the concentrations of three main species – the Rho GTPases RhoA and Cdc42, and the dual GEF/GAP Abr – through time and space. The active forms of Rho GTPases are modelled over a two-dimensional cell surface that is represented in radial coordinates r , centred on the wound (Figure 3.1). Each species in the model reacts, diffuses and advects according to

$$\frac{\partial[G^*]}{\partial t} = \frac{1}{r} \frac{\partial}{\partial r} \left(\underbrace{rD \frac{\partial[G^*]}{\partial r}}_{\text{Diffusion}} + \underbrace{rv[G^*]}_{\text{Advection}} \right) + \underbrace{f([G^*], [G])}_{\text{Reaction}} \quad (3.1)$$

where G denotes the species and an asterisk denotes the active form. The reaction term $f([G^*], [G])$ describes activation and inactivation of G .

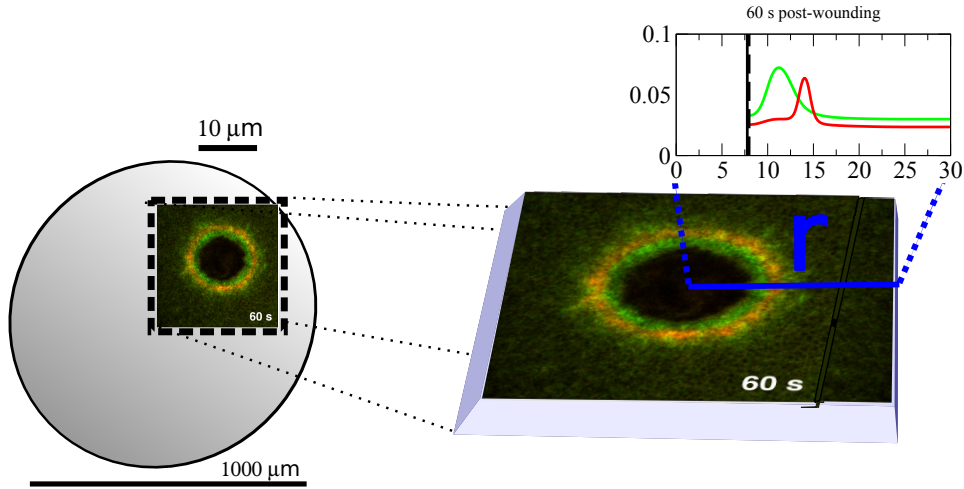


Figure 3.1: RhoA (green) and Cdc42 (red) zones accumulate around the wound on the plasma membrane (left). RhoA and Cdc42 concentrations are tracked in the model through time and space. The two-dimensional spatial domain is represented in radial coordinates where $r = 0$ (in μm) corresponds to the wound center (right).

Active Rho GTPases diffuse in the plane of the plasma membrane (with diffusion coefficient D). They also exchange with inactive GTPases. Since the wounding GTPase pattern is very small relative to the cell size, we assume that inactive GTPases are found in excess and at constant level in the cell. As the wound closes, the membrane advects radially inwards by purse-string closure, leading to GTPase advection. Advection occurs with velocity $v = \frac{v_c(t)}{r}$ which satisfies the continuity equation, and agrees with wound edge data.

The Rho GTPase reaction kinetics are summarized in Figure 3.2. Active RhoA binds to Abr, which acts as a GEF for RhoA, creating a positive feedback loop between RhoA and Abr (Figure 3.2 Model 1). Abr simultaneously acts as both GEF and GAP for Cdc42, but with much stronger GAP activity on Cdc42 (Figure 3.2 Model 2). Cdc42 positively feeds back on itself (Figure 3.2 Model 3).

3.2. Defining the Simon et al. (2013) Rho GTPase model

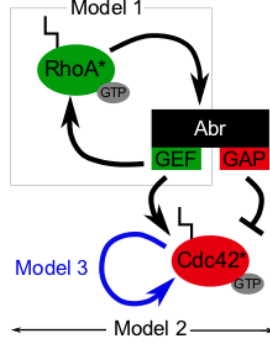


Figure 3.2: The signalling network of RhoA and Cdc42 with interactions mediated through Abr. Reprinted from “Pattern formation of Rho GTPases in single cell wound healing,” by C. M. Simon, 2013, *Molecular Biology of the Cell*, 24(3), p. 424. Copyright 2013 by the American Society for Cell Biology. Reprinted with permission.

The full model from Simon et al. (2013) describing Abr-bound RhoA $[A-R^*]$, RhoA $[R^*]$, and Cdc42 $[C^*]$ is given below.

$$\frac{\partial[A-R^*]}{\partial t} = \mathcal{L}[A-R^*] + k_3[R^*] - k_4[A-R^*] \quad (3.2)$$

$$\frac{\partial[R^*]}{\partial t} = \mathcal{L}[R^*] + \left(\mathbf{k}_0^r + \frac{k_1[A-R^*]^n}{K_A^n + [A-R^*]^n} \right) [R] - (\mathbf{k}_2 + k_3)[R^*] \quad (3.3)$$

$$\frac{\partial[C^*]}{\partial t} = \mathcal{L}[C^*] + \left(\mathbf{k}_0^c + k_5[A-R^*] + \frac{k_6[C^*]^n}{K_C^n + [C^*]^n} \right) [C] - (\mathbf{k}_7 + k_8[A-R^*])[C^*] \quad (3.4)$$

where $\mathcal{L}[G^*] = \frac{1}{r} \frac{\partial}{\partial r} \left(rD \frac{\partial[G^*]}{\partial r} + rv[G^*] \right)$ produces the diffusion-advection terms. We hypothesize that PKCs affect the terms shown in magenta, i.e., the basal rates of activation or inactivation of the GTPases.

Simon et al. (2013) specifically focused on the effect of the GEF/GAP Abr, neglecting other GEF and GAP activity. In Equations 3.3 and 3.4, Abr appears as a GEF for RhoA and Cdc42. Abr activates RhoA at a rate k_1 in a Michaelian way, and linearly activates Cdc42 at a rate k_5 . In Equation 3.4, Abr acts as a GAP for Cdc42 and linearly inactivates Cdc42 at a rate k_8 . Equation 3.2 describes Abr itself, which binds to RhoA at rate k_3 and unbinds at rate k_4 . The remaining Michaelian term describes Cdc42 activation of itself at a rate k_6 . The remaining linear terms describe the basal activation (k_0^r, k_0^c) or basal inactivation (k_2, k_7) of RhoA and Cdc42.

3.2. Defining the Simon et al. (2013) Rho GTPase model

Here we explore the hypothesis that PKCs affect the basal rates of activation or basal rates of inactivation of Rho GTPases.

A control wound healing experiment is simulated using the model and estimated parameters from Table 3.1 (Figure 3.3). Simulated curves are shown against Rho GTPase data plotted as circles (thick curves). The simulated total amount of RhoA (i.e., the sum of active RhoA and Abr-bound RhoA) is plotted in green. Simulated Cdc42 and Abr correspond to red and black, respectively. The simulated wound edge is shown as a vertical dashed line, against wound edge data (vertical solid line).

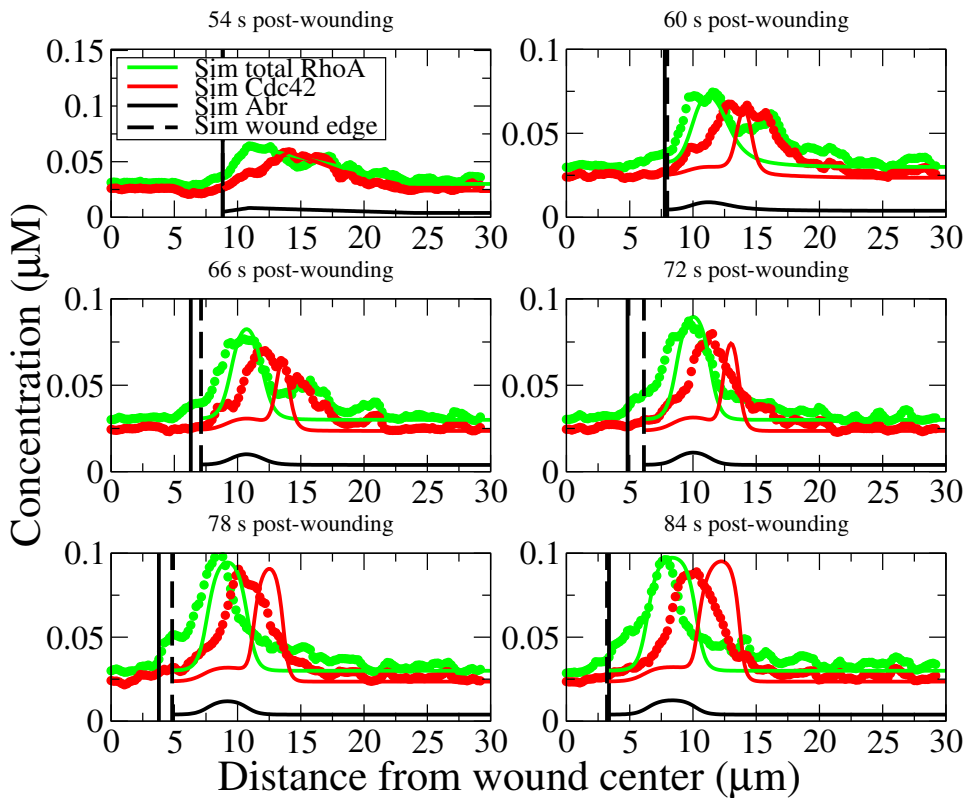


Figure 3.3: The Simon et al. (2013) model captures basic features in Rho GTPase zones such as the speed of amplification and the steady states. RhoGTPases 54 – 84 s post-wounding are simulated (lines), with data shown in circles for comparison. The simulated wound edge is given by the vertical dashed black line, to be compared with the vertical solid black line. Notice that the orientation of the axis is reversed (wound edge towards the left) in comparison to previous line scan data.

3.2. Defining the Simon et al. (2013) Rho GTPase model

Simulations begin with initial conditions specifying each species' concentration profile. The initial conditions are piecewise linear (triangular) profiles fitted to Rho GTPase data. Simulations are computed over a 50 μm domain that begins at the wound edge. Since disrupted plasma membrane cannot support Rho GTPases, a no flux boundary condition is imposed at the wound edge. Far from the wound, Rho GTPases are fixed to basal activities. The wound edge position is given by w , and the wound edge moves with a prescribed velocity, $\frac{dw}{dt} = -\frac{v_c}{w}$. Data on wound edge position through time was used to set the constant v_c .

Parameter	Interpretation	Value	Unit
k_0^r	Basal RhoA activation	0.0091	/s
k_0^c	Basal Cdc42 activation	0.0018	/s
k_1	Maximum GEF activity of Abr on RhoA	0.0241	/s
K_A	Measure of switch location in Hill eqn.	0.0090	μM
K_C	Measure of switch location in Hill eqn.	0.0635	μM
k_2	GAP/GDI inactivation rate of RhoA	1	/s
k_3	Abr binding rate to RhoA	0.1	/s
k_4	GAP/GDI inactivation rate of Abr-RhoA	6/9	/s
k_5	Abr GEF activity on Cdc42	2.0802	/s
k_6	Maximum autocatalysis rate of Cdc42	0.0326	/s
k_7	Background GAP/GDI inactivation rate of Cdc42	0.6889	/s
k_8	Abr GAP activity on Cdc42	79.5006	/s
v_c	Advection velocity parameter	2.1231	$\mu\text{m}^2/\text{s}$
n	Hill coefficient	6	

Table 3.1: Parameters in Model 1 from Simon et al. (2013).

In order to conveniently keep track of changes between model variants, we provide model definitions. All model variants start from Model 1 (M 1) base assumptions. Subsequent model definitions note modifications to the basic assumptions.

Model 1. The Simon et al. (2013) model.

Equations 3.2-3.4

Parameters Table 3.1

Initial conditions Piecewise linear (triangular) profiles fitted to control data.

Boundary conditions No flux condition at wound edge, basal activity far from the wound.

Advection velocity Constant v_c such that initial and final wound edge locations agree with data.

3.2.1 Model features

The equations in Model 1 were developed by Simon et al. (2013) in a systematic way. Simon began with simple, linear reaction terms which were successively replaced by complex, nonlinear terms until key Rho GTPase features were captured. The two key features were crosstalk and spatial bistability.

Crosstalk is the inhibition of one species by another. In the context of single cell wound healing, crosstalk is evident in zone segregation where initially overlapping RhoA and Cdc42 zones narrow into mutually exclusive zones. Through inhibition, RhoA excludes Cdc42 from regions that it occupies. This crosstalk feature is present in the model as Abr-mediated RhoA inhibition of Cdc42.

Spatial bistability refers to Rho GTPase activities occupying either a stable high steady state or a stable low steady state across the spatial domain. High and low steady states are separated by a threshold. Activities below the threshold rapidly fall down to the low steady state, while activities above the threshold rapidly rise up to the high steady state. Switching between the two requires significant perturbation. Spatial bistability is present in the model as the Rho GTPase zones: a peak at high steady state within the zone, and background activity (low steady state) elsewhere.

3.2.2 Successes and limitations of the model

Model 1 successfully simulates Rho GTPase zones in a control experiment (Figure 3.3). It captures zone segregation and zone maintenance from 54 – 84 s post-wounding. In the simulation, the initial profiles narrow into zones that are rapidly amplified. The speed of rise in both zones, as well as peak and background activities, compare well with data.

While the approximate patterns are accounted for, the model is unable to capture several features. For one, the simulated zones are too narrow at the base, and the Cdc42 zone is offset from the RhoA zone (Figure 3.3, 84 s). Then, if we look at the amount of Cdc42 within the RhoA zone, the simulated Cdc42 activity shows a “bump” above background. We know this bump should not be present since the data shows Cdc42 at background

levels within the RhoA zone. On the other hand, if we look at the amount of RhoA within the Cdc42 zone, the simulated RhoA activity is as low as background. The data instead show a “shoulder” of RhoA within the Cdc42 zone, above background. We find that the inclusion of PKCs refines Rho GTPase patterning. In particular, we improve the shape of each zone and capture the RhoA shoulder. Correcting the Cdc42 zone offset and bump require Abr-related changes which we do not consider.

It is worth mentioning that the RhoA shoulder is a subtle, yet relevant, detail in patterning. In wounded cells where contraction has been inhibited, a faint rim of RhoA is visible outside the ring of Cdc42. At its most extreme, the rim can be very broad, manifesting as zones on either side of the Cdc42 zone. The rim of RhoA is very likely the RhoA shoulder which peeks out from underneath the Cdc42 zone.

Model 1 is also limited to portraying wound healing during 54 – 84 s. It does not recapitulate wound healing from the very beginning, because it was not intended to model calcium or early events in signalling. It does not recapitulate zone formation at times slightly before 54 s because the Rho GTPase gradient is too shallow for amplification, and because components other than Abr likely play a role. Lastly, the model does not account for times after 84 s, due to broadening of the simulated zones. When the simulated zones rise up and plateau, the trailing edge bleeds outwards due to a constant supply of inactive, cytosolic GTPase fuelling activation. As such, discrete zones are no longer retained after 84 s. Biologically, a non-Abr GAP is hypothesized to act on the trailing edge of the RhoA zone (Vaughan et al., 2011). Thus, the model which accounts for Rho GTPase patterning through Abr, is limited to simulating this window of time. Incorporating PKCs does not expand this window, but we suspect that they assist in maintaining discrete zones by curbing the outwards spread of the trailing edge.

3.3 The PKCs – revising the basic model

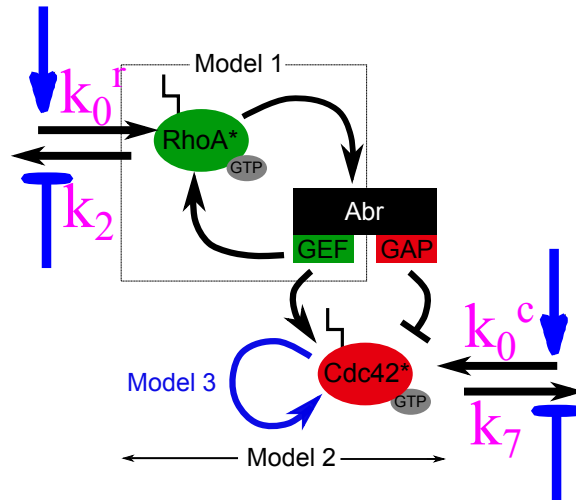


Figure 3.4: The effects of PKCs on background Rho GTPase activation rates k_0^r , k_0^c , and background inactivation rates k_2 , k_7 . Potential PKC beta effects are shown in the blue arrows/bar-headed lines. PKC eta (not shown) has the opposite effect. Adapted from “Pattern formation of Rho GTPases in single cell wound healing,” by C. M. Simon, 2013, *Molecular Biology of the Cell*, 24(3), p. 424. Copyright 2013 by the American Society for Cell Biology. Adapted with permission.

How do we investigate the effects of PKCs on Rho GTPases? We begin with Model 1 and assume that PKCs affect Rho GTPases through background GEFs and GAPs. That is, PKCs affect the background (in)activation rates of Rho GTPases: k_0^r , k_0^c , k_2 , k_7 (Figure 3.4). We progress from model to model by increasing the spatial detail of the PKCs, and hence, the spatial dependence of the background (in)activation rates (See flowchart in Figure 1.7). In Chapter 4, we assume that PKCs are spatially uniform across the domain. In Chapter 5, we assume that PKCs localize to the RhoA zone, and represent their spatial profiles as simple step functions. In Chapters 6 and 7, we assume that PKCs overlap regions where the RhoA zone is present, and that their spatial profiles are given explicitly by data.

With each model variant, we simulate the control and fit the model parameters. In order to validate the model variant, we reproduce a battery of PKC manipulations by making fold changes in parameters k_0^r , k_0^c , k_2 and

k_7 . The simulated Rho GTPase zones are model outputs evaluated against quantitative and qualitative criteria listed in the next section. Ideally, inverted zones in the overexpression of PKC η would also be reproduced.

Under the current assumptions, we do not successfully reproduce the PKC manipulations. In the final chapter, we make suggestions for future modelling of PKCs through the basal rates of Rho GTPase activation. In principle, however, the PKCs can eventually be modelled as dynamic variables.

3.3.1 Criteria for model validation

With each model variant, we evaluate how well it reproduces Rho GTPase zones in the set of PKC manipulations. A manipulation is recapitulated if the following criteria are met.

- C1** Given appropriate initial Rho GTPase spatial profiles, zones are maintained.
- C2** The quantitative fold changes to zone activities, relative to the control, match the extent seen in data (Tables A.1-A.4).
- C3** Qualitative features such as zone breadth, gaps, inversion and otherwise, match experimental images (Figure 2.2 C).

Chapter 4

PKCs as spatially constant parameters

4.1 Overview

In this chapter, we consider a simplified view in which the effect of the PKCs is uniform in space, ignoring their known spatial distribution. Using Model 1, we first investigate two hypotheses for the effect of PKCs:

- (i) PKCs modulate the basal Rho GTPase activation rate.
- (ii) PKCs modulate the basal Rho GTPase inactivation rate.

The first possibility implies that PKCs act on GEFs, while the second implies GAPs. Next, we simulate PKC manipulations (OE, DN) and find that the current assumptions do not explain their effect on the Rho GTPase zones. We conclude that PKC localization is necessary.

4.2 PKCs act on GEFs or GAPs

We are interested in whether Rho GTPases are affected by PKCs through GAPs or GEFs. For instance, PKC beta could upregulate Rho GTPase activity either by activating GEFs, or by depressing GAPs. GEF (GAP) regulation is synonymous with the GTPase basal (in)activation rates k_0^r , k_0^c (k_2 , k_7). To look at differences between GEF and GAP regulation by PKCs, we examine bifurcation diagrams with respect to each parameter (k_0^r , k_0^c , k_2 , k_7) in turn¹.

If we consider a space-free version of Equations 3.2-3.4, we are left with ordinary differential equations (ODE) which describe Rho GTPase reaction kinetics. By carrying out a bifurcation analysis of the ODEs, we find two

¹Aside from the bifurcation parameter, all other parameters retain values from Table 3.1.

4.2. PKCs act on GEFs or GAPs

stable RhoA steady states and three stable Cdc42 steady states (s.s.). Figure 4.1 illustrates that simulated RhoA has a high s.s. within the zone, and low s.s. at background. Simulated Cdc42 has similar high and low steady states, but also possesses a third stable s.s. which manifests as the Cdc42 bump in Figure 4.1.

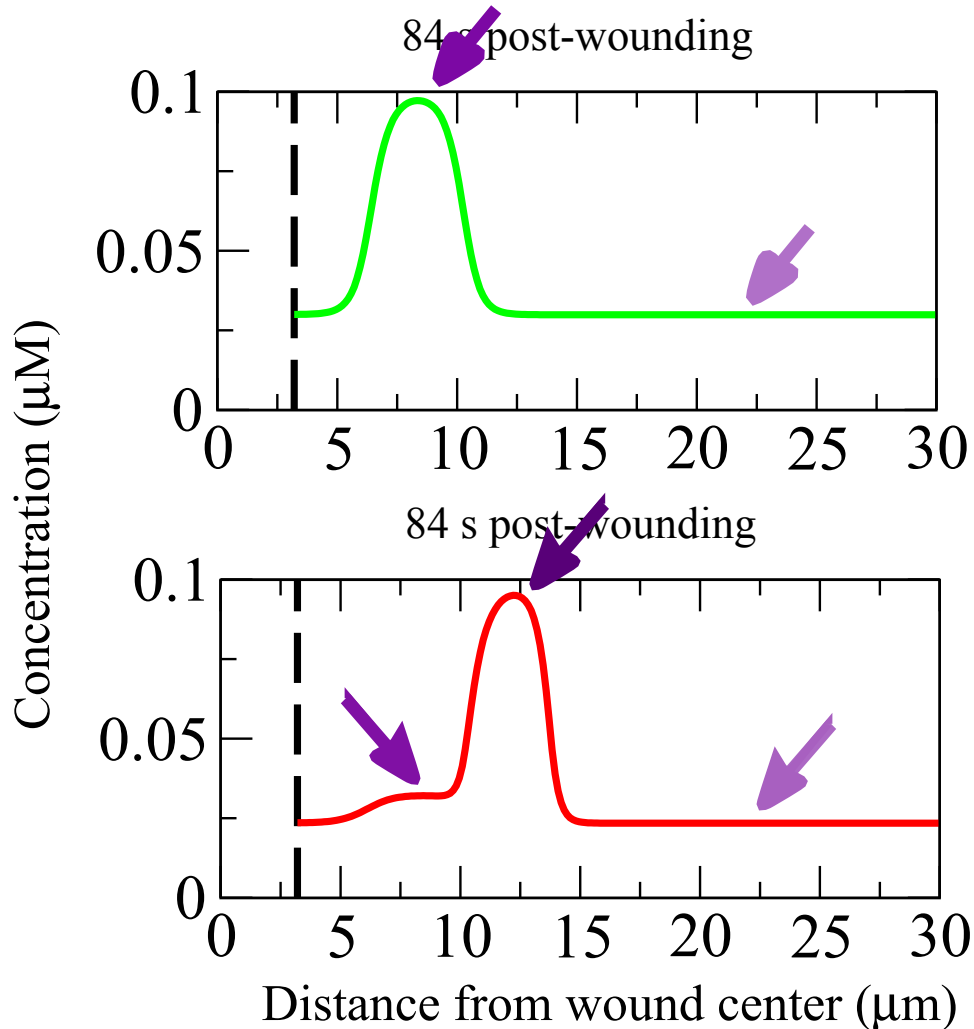


Figure 4.1: The simulated control (Model 1) possesses two stable steady states in RhoA and three stable steady states in Cdc42. RhoA (green) and Cdc42 (red) have high steady states within the zone, and low steady states at background. Cdc42 has an additional steady state in the Cdc42 bump.

4.2. PKCs act on GEFs or GAPs

To ease comprehension of a bifurcation diagram, we show the bifurcation diagram of RhoA steady states on k_0^r (Figure 4.2). The normalized control parameter value ($k_0^r = 1$) is marked with a vertical violet line which crosses through two stable branches (solid green) and an unstable branch (dashed green). Arrows mark features in patterning which correspond to the stable steady states. The RhoA threshold corresponds to an unstable steady state. As the parameter k_0^r is increased (right of violet line), the unstable steady state and low steady state converge and disappear. A fold change in k_0^r greater than 1.37 (dashed-solid black vertical line) results in a single high steady state, and thus RhoA monostability. Conversely, a fold change in k_0^r less than 0.87 (dashed black vertical line) results in a single low steady state, and also RhoA monostability. Consequently, the region within a fold change of 0.87-1.37 in k_0^r is a regime where bistability is possible. Bistability is necessary for zone maintenance and thus we only consider this range of possible variation of k_0^r in the next simulations.

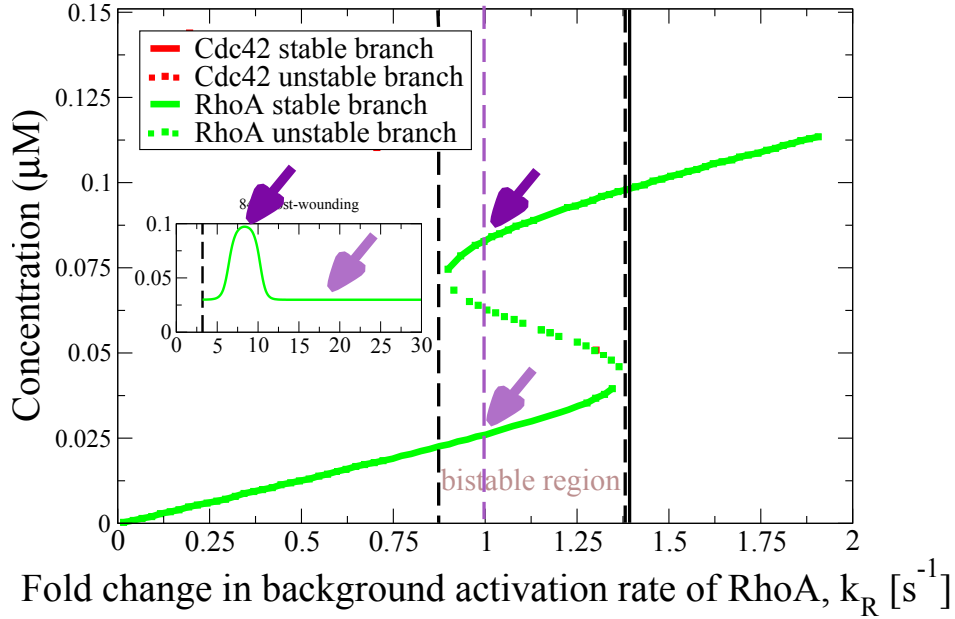


Figure 4.2: A bifurcation diagram of k_0^r showing RhoA steady states. At the control value (vertical violet line), RhoA possesses stable low and high steady states which correspond to the background and zone activities, respectively (violet arrows). The unstable steady state corresponds to the bistable threshold. The interval 0.87-1.37 marks the bistable region (vertical dashed lines).

4.2. PKCs act on GEFs or GAPs

The bifurcation diagram of Cdc42 steady states on k_0^r can be read in a similar manner (Figure 4.3). Notice the presence of the third stable steady state that corresponds to the Cdc42 bump. Additionally, the region of Cdc42 bistability extends from 0-1.37 fold change in k_0^r . However, the bistable region that we indicate in the diagram is narrower, because we indicate the regime where *both* RhoA and Cdc42 exhibit bistability. The vertical dashed-solid black line marks the loss of both RhoA and Cdc42 bistability, while the vertical dashed black line marks the loss of only one GTPase's bistability. Subsequent bifurcation diagrams show RhoA and Cdc42 steady states in the same plot.

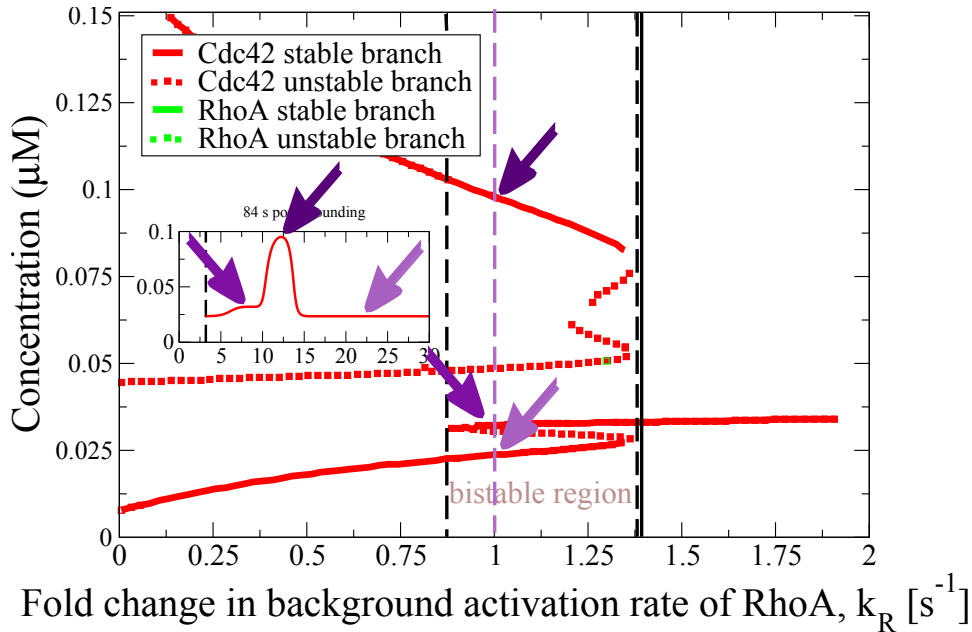


Figure 4.3: A bifurcation diagram of k_0^r showing Cdc42 steady states. As in Figure 4.2, but a third intermediate stable steady state is shown (violet arrows). Cdc42 is bistable over the interval 0-1.37, but only the interval where *both* GTPases retain bistability is called the bistable region (vertical dashed lines).

4.2.1 Bifurcations on the basal rates of RhoA
(in)activation, k_0^r (k_2)

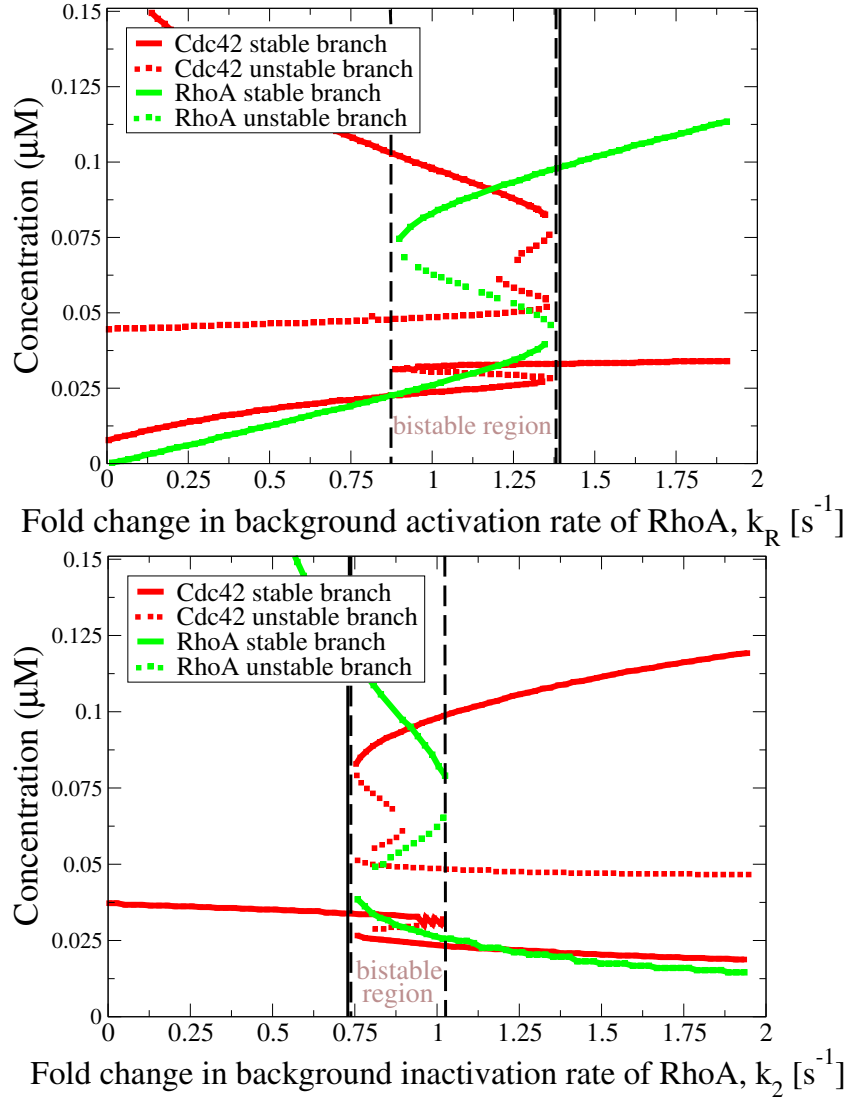


Figure 4.4: Bifurcation diagrams (space-free Equations 3.2-3.4) with respect to RhoA basal activation (top) and inactivation (bottom). Stable branches towards the top (bottom) of each diagram indicate high (low) steady states. Cdc42 possesses an additional intermediate steady state. Bistable region (both GTPases) marked by vertical dashed lines.

We first consider the bifurcation diagram on the background activation rate of RhoA (Figure 4.4, top). Within the bistable region, increasing k_0^r leads to higher RhoA zone activity, and higher RhoA and Cdc42 background activities. With increasing RhoA zone activity also comes a lowering of the threshold. Lower thresholds tend to result in broad zones, as we shall see in the simulations. Outside of the bistable region, two scenarios occur. Either RhoA (monostable) fills the domain at high background activity with Cdc42 at low background activity, or RhoA fills the domain at low background activity with zones of Cdc42 still possible.

A similar bifurcation diagram on the background inactivation rate of RhoA is shown in Figure 4.4 (bottom). The k_2 bifurcation diagram appears as a mirror image of the k_0^r diagram, though not all features are exactly reflected. The k_2 diagram possesses a narrower bistable region and a very steep stable RhoA branch. It appears that RhoA activity can be tuned with similar effects through either RhoA basal rate. However, k_2 is restricted to a narrower bistable region, which means reduced prospects of zone maintenance under manipulations that change k_2 .

4.2.2 Bifurcations on the basal rates of Cdc42 (in)activation, k_0^c (k_7)

In the bifurcation diagram on the background activation rate of Cdc42 (Figure 4.5, top), we first notice that RhoA steady states are unaffected by Cdc42 parameters. Therefore, RhoA is bistable for all changes in the Cdc42 basal rate. Within the bistable region, increasing k_0^c leads to higher Cdc42 zone and background activities, with an accompanying decline of the threshold value. Outside the bistable region, Cdc42 fills the domain at high background activity, while RhoA zones are possible.

Again, a similar mirrored bifurcation diagram on the background inactivation rate of Cdc42 occurs (Figure 4.5, bottom). It appears that Cdc42 activity can be tuned through either Cdc42 basal rate. However, some values of k_0^c are inaccessible since they fall below zero. As well, k_7 possesses a steep stable upper branch allowing for Cdc42 zones with much higher activity.

4.2. PKCs act on GEFs or GAPs

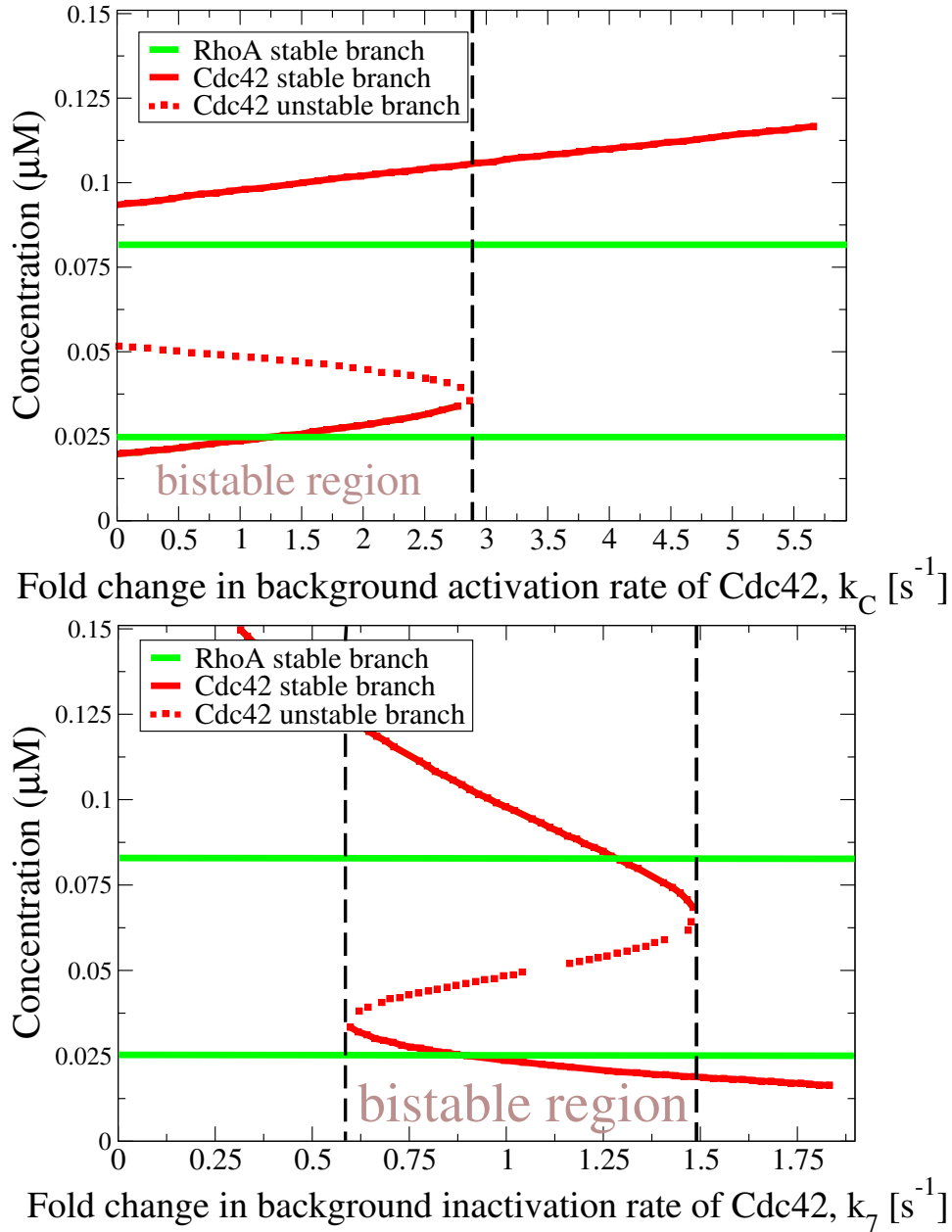


Figure 4.5: As in Figure 4.4 but the intermediate Cdc42 steady state is not shown. RhoA is unaffected by either Cdc42 basal (in)activation rate, and therefore RhoA retains bistability throughout each diagram.

Overall, these bifurcation diagrams show degeneracies between the basal activation and inactivation rates. Discriminating between GEF and GAP regulation might entail further interpretation of the narrowness of each bistable region, or consideration of the steepness of each diagram’s upper stable branch. We cannot immediately rule out that PKCs exclusively act on a GEF or GAP, so we test how changing any of the four parameters k_0^r , k_0^c , k_2 and k_7 affects RhoA and Cdc42 activities.

4.3 Simulations of PKC manipulations

In this section, we simulate the PKC manipulations using information obtained from the bifurcation diagrams (Figures 4.4, 4.5). Simulating spatially uniform PKCs does not require changes to the equations in Model 1, and only requires fold changes to control initial conditions and control parameter values. We can define Model 2 in the following way:

Model 2. The spatially uniform PKC model.

Parameters Fold changes in the bistable region according to bifurcation diagrams (Figures 4.4, 4.5).

Initial conditions Piecewise linear (triangular) profiles fitted to control data, and scaled by amplification factors in Tables A.1-A.4 at 30 s.

The Model 2 control simulation is the same as the control from Model 1 since no fold changes to control parameter values or initial conditions are made. Thus, the Model 2 control simulation is shown in Figure 3.3.

We reproduce PKC manipulations by specifying initial conditions and the parameter fold changes which mimic overexpression or expression of dominant-negative PKC. The initial conditions have the same shape as the control profiles, but are amplified by factors in Tables A.1-A.4 (at 30 s). Recall that the amplification factors were derived from the box-and-whisker plot zone quantifications (Figure 2.2). Parameters are adjusted according to the significant experimental outcome we aim to reproduce, e.g., an upregulated Cdc42 zone is achieved by decreasing Cdc42 background inactivation rate. In order to guarantee zone maintenance, the corresponding parameter fold changes are chosen from the bistable regions given by the bifurcation diagrams (Figures 4.4-4.5).

To evaluate whether the simulated manipulations are successful, we refer to criteria in Section 3.3.1. Zone maintenance (**C1**) and qualitative aspects

4.3. Simulations of PKC manipulations

of the simulated zones (**C2**) can be visually scrutinized. We quantitatively assess the fold change in simulated zone activities at 84 s (**C3**), relative to the control, and compare them to fold changes in Tables A.1-A.4 at 60 s. As such, the simulated GTPases in a PKC manipulation are plotted over the simulated control so that changes in zone activities can be readily compared.

4.3.1 Overexpression of PKC beta

Simulated results are shown in Figure 4.6. In the 54 s panel we show the adjusted initial conditions based on Table A.1. In all panels, the control simulation is shown for comparison (circles/thick curves). Experimentally, the overexpression of PKC beta results in a significantly upregulated Cdc42 zone, so we decrease the background inactivation rate k_7 (fold change of 0.625).

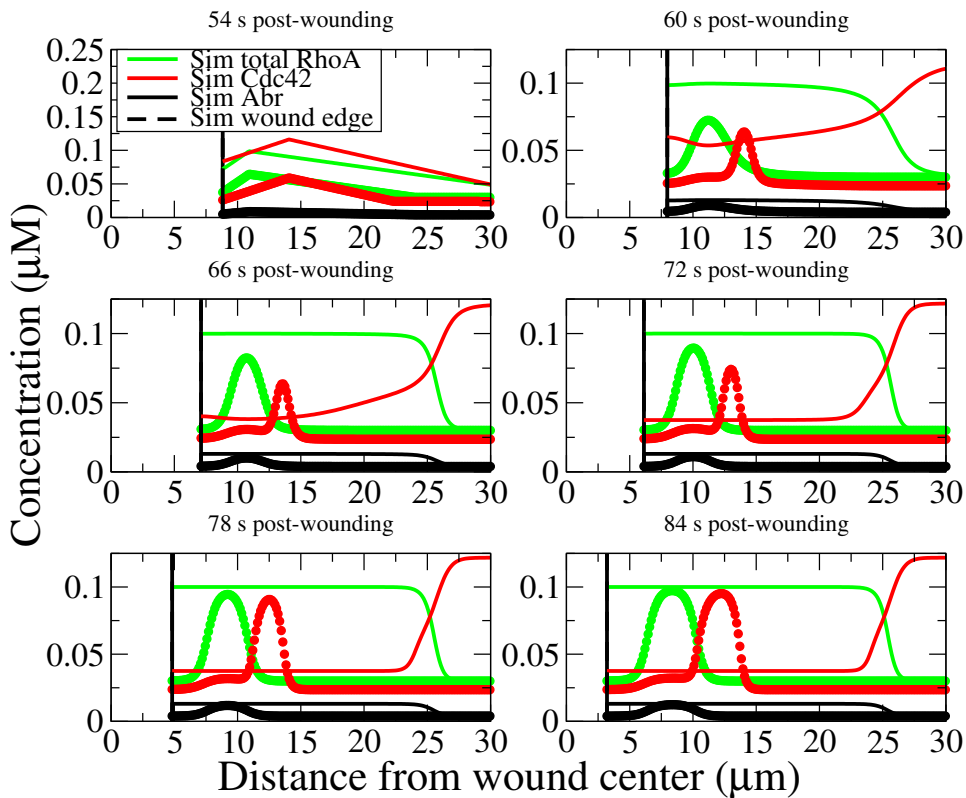


Figure 4.6: Results for Model 2 where PKC beta is overexpressed. The simulated control is shown for comparison (circles/thick curves).

4.3. Simulations of PKC manipulations

In the last panel, we observe the RhoA zone with the same level of activity as the control, but the zone broadens. The breadth of the RhoA zone is a result of initial conditions with greater activity levels than the threshold value, allowing faster plateau to high steady state, and outwards bleeding. We also observe a very broad Cdc42 zone whose activity is elevated above the control. The breadth of the Cdc42 zone is a combination of initial conditions with greater activity levels, and a lowering of the threshold due to the decrease in k_7 .

While zones are maintained (**C1**), Model 2 fails to satisfy criteria **C2** and **C3**. Quantitatively, the Cdc42 zone is elevated by a 1.3 fold change above the control. This falls short of what is observed (Table A.1, 60 s). Qualitatively, both zones are much broader than the control zones. This is simply not observed in wounding images (Figure 2.2 C). Consequently, the simplest model cannot account for experimental observations.

4.3.2 Expression of dominant-negative PKC beta

Simulated results are shown in Figure 4.7. In the 54 s panel, we show slightly elevated initial conditions. Experimentally, zones do not form at early times, cannot be quantified, and therefore this leaves us without a 30 s zone amplification factor in Table A.2. Instead, we adjust the initial conditions by the smallest amount such that zone maintenance is guaranteed. Experimentally, the expression of dominant-negative PKC beta results in downregulated zones. To simulate this, we decrease the basal RhoA activation rate k_0^r (fold change of 0.9) and increase the basal Cdc42 inactivation rate k_7 (fold change of 1.25).

4.3. Simulations of PKC manipulations

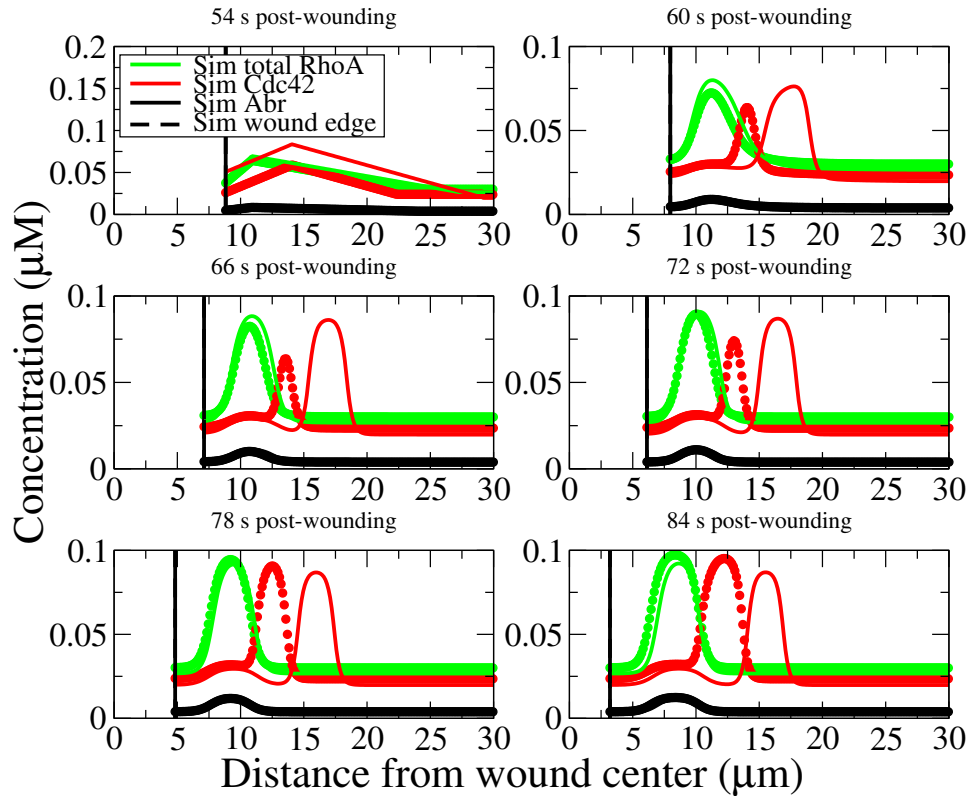


Figure 4.7: Results for Model 2 where dominant-negative PKC beta is expressed. The simulated control is shown for comparison (circles/thick curves).

At 84 s, we observe both RhoA and Cdc42 zones whose activities are depressed. Both zones maintain widths similar to the control. The zone widths are narrow despite elevated initial conditions because the corresponding parameter manipulations effectively raise the thresholds. Lastly, we observe a curious gap between the RhoA and Cdc42 zones.

In the simulation of dominant-negative PKC beta, zone maintenance (**C1**) was enforced. Regardless, Model 2 fails to satisfy criteria **C2** and **C3**. Quantitatively, we expect to see zones depressed by more than half the control activity (Table A.2). Qualitatively, no such gap between zones is observed (Figure 2.2 C). Therefore, Model 2 cannot account for experimental observations.

4.3.3 Overexpression of PKC ϵ

Figure 4.8 shows the simulated results where PKC ϵ is overexpressed. In the first panel, we show the adjusted initial conditions (Table A.3). Experimentally, overexpression of PKC ϵ results in the downregulation of both RhoA and Cdc42 zones. To simulate this, we decrease the basal RhoA activation rate k_0^r (fold change of 0.89), and increase the basal Cdc42 inactivation rate k_7 (fold change of 1.25).

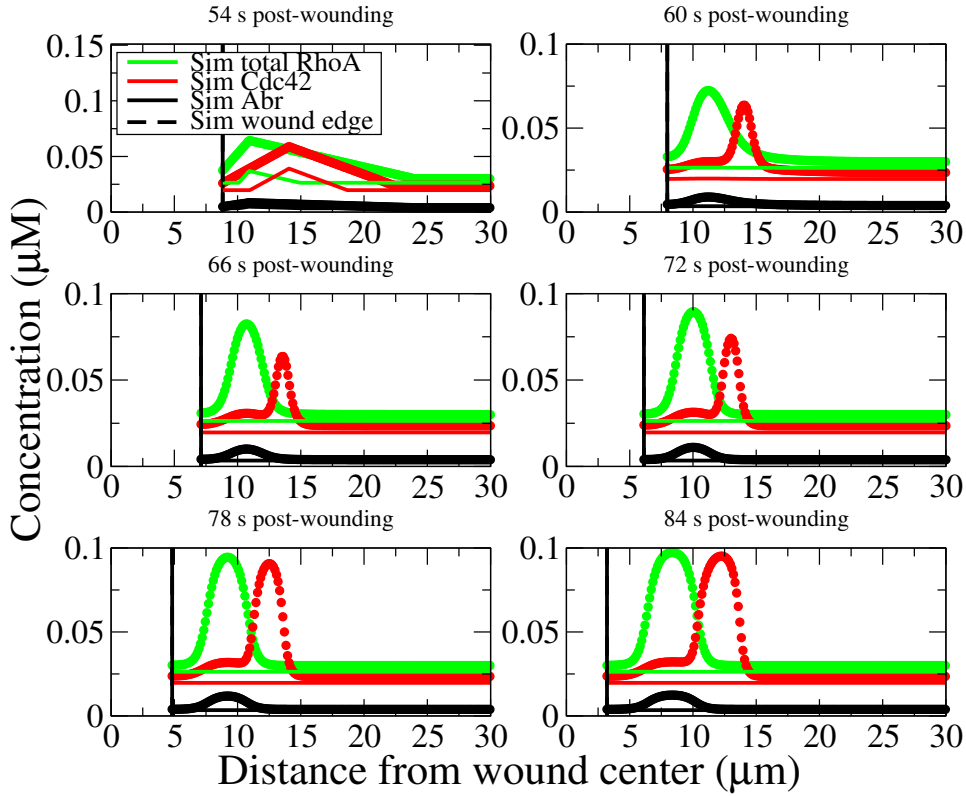


Figure 4.8: Results for Model 2 where PKC ϵ is overexpressed. The simulated control is shown for comparison (circles/thick curves).

We observe the rapid decay of both RhoA and Cdc42 zones. Zones cannot be maintained due to a combination of diminished initial conditions and increased thresholds. In this simulation where PKC ϵ is overexpressed, zone maintenance is not achieved. Therefore, Model 2 fails to satisfy criterion **C1** and cannot be assessed on the remaining criteria. As a result, our

current assumptions do not account for experimental observations.

4.3.4 Expression of dominant-negative PKC ϵ

Simulated results are shown in Figure 4.9. In the first panel, the initial conditions are unchanged from the control. Experimentally, zones do not form at early times, and we do not have 30 s amplification factors in Table A.4. Instead, we use control initial conditions which guarantee zone maintenance. To simulate the experimental result where dominant-negative PKC ϵ up-regulates both background activities, we decrease the basal RhoA inactivation rate k_2 (fold change of 0.9), and decrease the basal Cdc42 inactivation rate k_7 (fold change of 0.8).

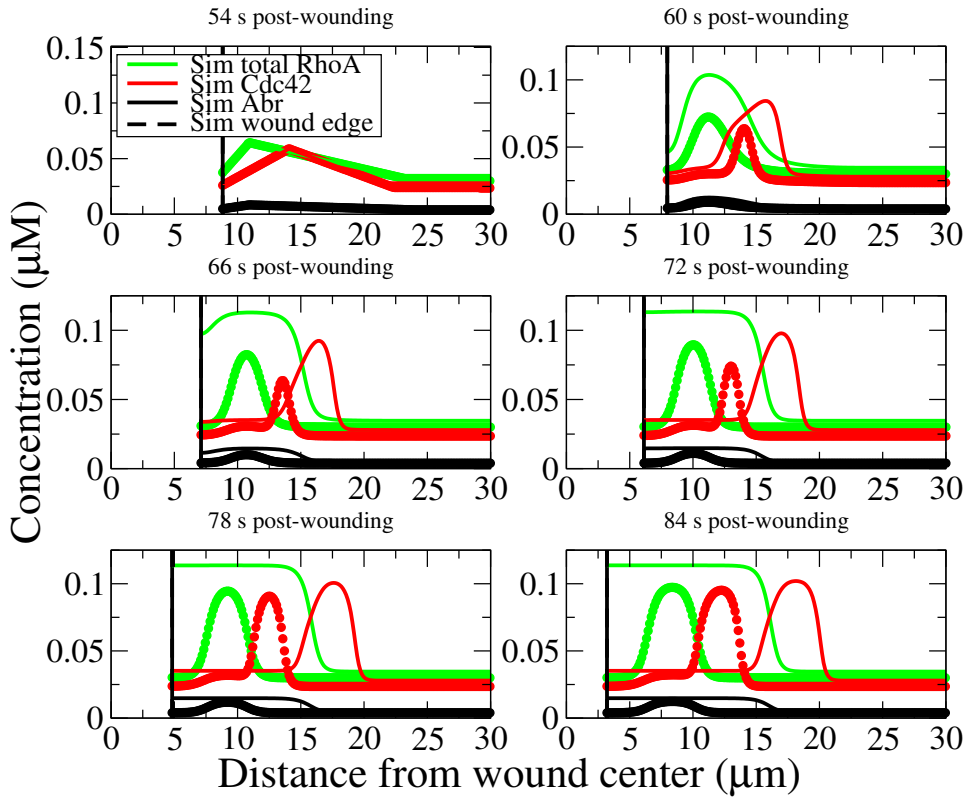


Figure 4.9: Results for Model 2 where dominant-negative PKC ϵ is expressed. The simulated control is shown for comparison (circles/thick curves).

In the last panel, we observe RhoA and Cdc42 zones with elevated activities. The RhoA zone is broad, due to a decreased threshold. More importantly, the background activities are only slightly above control.

While zones are maintained (**C1**), Model 2 fails to satisfy criteria **C2** and **C3**. Quantitatively, we expect to see background activities that are almost twice the control (Table A.4). Qualitatively, the simulated RhoA zone is broader than Cdc42, though experimental wound images show the opposite (Figure 2.2 C). We conclude that this model cannot recapitulate experimental observations.

4.4 Possible ways to achieve inverted Rho GTPase zones

Given that PKC η overexpression could not be qualitatively or quantitatively reproduced by Model 2, we cannot infer how zone inversion occurs in that circumstance. The simulated manipulation failed because RhoA and Cdc42 zones could not be sustained since the initial conditions were below the threshold. Now we wonder: outside of PKC η overexpression, can we ever observe inverted Rho GTPase zones? We relax the constraint used to adjust the initial conditions (Table A.3), and find two ways of achieving inverted zones.

In the first example, we see the simulation begin with reduced initial conditions (Figure 4.10). The basal RhoA inactivation rate k_2 is decreased (0.89 fold change) and the basal Cdc42 inactivation rate k_7 is decreased (0.8 fold change). We observe the simulated Cdc42 zone spreading close to the wound edge *before* the RhoA zone can establish. In this way, Cdc42 is able to sandwich the RhoA zone. Here is one possible way to see the Cdc42 zone in front of the RhoA zone.

4.4. Possible ways to achieve inverted Rho GTPase zones

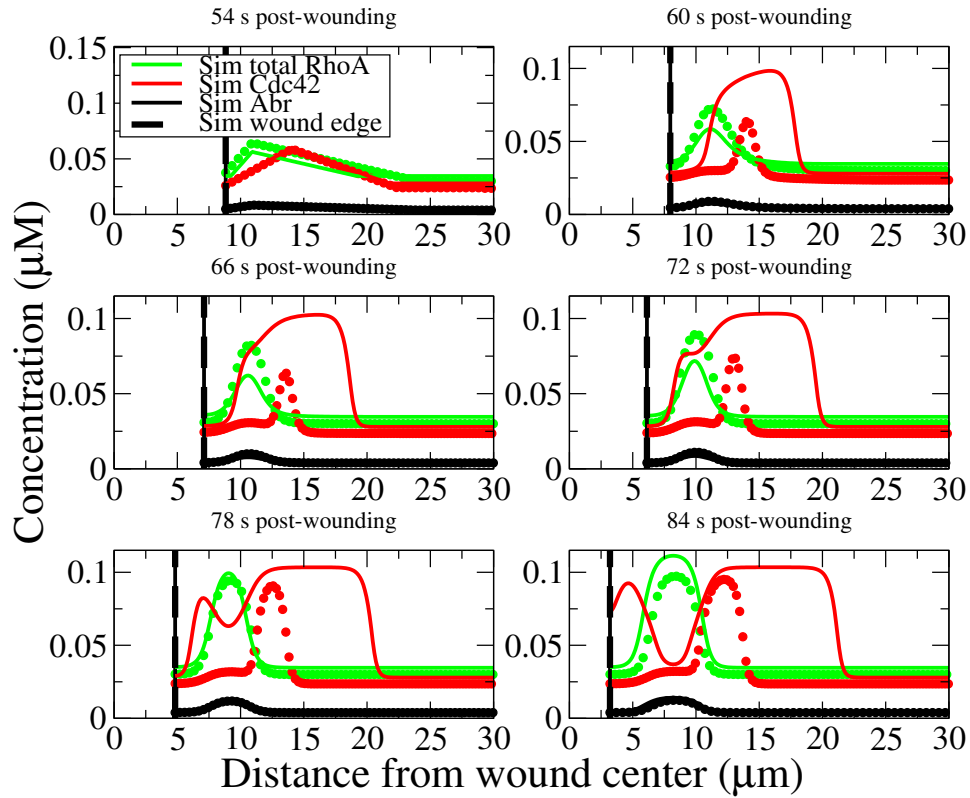


Figure 4.10: Results for Model 2 where inverted Rho GTPase zones occur because Cdc42 sweeps out in front of the RhoA zone. The simulated control is shown for comparison (circles/thick curves).

In the second example, we decrease the basal Cdc42 inactivation rate k_7 (0.5 fold change). We observe the monostable Cdc42 establish a uniform field of Cdc42 over the domain (Figure 4.11). The simulated RhoA zone establishes, suppressing Cdc42, creating a divot in the uniform field. Again, Cdc42 sandwiches the RhoA zone, but also fills the domain far from the wound.

4.5. Conclusions

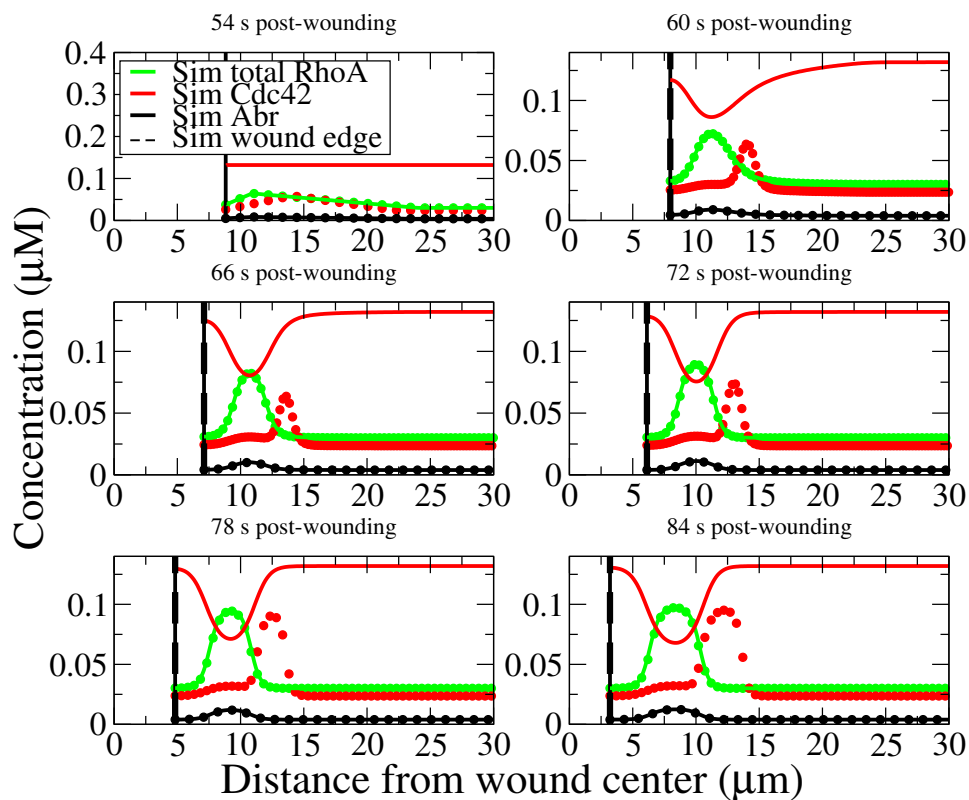


Figure 4.11: Results for Model 2 where inverted Rho GTPase zones occur because the RhoA zone protrudes into a uniform field of Cdc42. The simulated control is shown for comparison (circles/thick curves).

It appears that inverted zones can be achieved through the use of precarious initial conditions, or by enabling Cdc42 monostability. In both examples, the parameter fold changes resemble a manipulation where PKC beta is overexpressed. Thus, we are unable to investigate how zone inversion occurs within the context of PKC eta overexpression. We are, however, convinced that inverted zones are not impossible using Model 2.

4.5 Conclusions

In this chapter, we showed that using a model with spatially constant PKCs fails to account for quantitative and qualitative observations in experiments where PKCs are manipulated. At best, simulations of the overexpression of

PKC beta and the expression of dominant-negative PKC eta result in the correct trend of upregulated zones. However, features such as zone breadth and peak zone activity do not match what is observed. Even when zone breadth is not an issue, like in the simulation of dominant-negative PKC beta, qualitative features such as a gap between zones works against model validation. At worst, this model can never account for the overexpression of PKC eta. Zones are simply never sustained due to initial conditions below threshold.

With respect to zone inversion, we sought any manipulation that would produce the Cdc42 zone in front of the RhoA zone, even if it meant choices dissimilar to PKC eta overexpression. Manipulations resembling PKC beta overexpression were found to produce Cdc42 zones which sandwiched the RhoA zone. Though these results are unconvincing in explaining inversion in PKC eta overexpression, they illustrate that Model 2 is capable of such phenomena.

In this chapter, we also showed that PKC impact on Rho GTPases can be through either GEFs or GAPs. We examined bifurcation diagrams on four key parameters (k_0^r, k_0^c, k_2, k_7) and showed that basal activation rates shared similarities with basal inactivation rates. The bifurcation diagrams identified parameter regimes where bistability, and therefore zone maintenance, was possible.

Based on these results, we asked whether taking into account the nonuniform spatial distribution of PKCs could correct the flawed model predictions. In the next chapter, we explore localized PKC effects modulating the basal Rho GTPase activation rates (i.e., through GEFs).

Chapter 5

PKCs as spatially dependent parameters: step function representation

5.1 Overview

Based on the failure of the simplest model variant, we revise the approach to represent spatially distributed PKC activity. To do so, we use experimental data to define PKC activity profiles $\beta(x, t)$ and $\eta(x, t)$. Here we consider simple representations of that spatial dependence, namely piecewise constant functions of space. As a result the quantities k_0^r and k_0^c are in turn functions.

In this chapter, we implement PKC activity profiles without using explicit data on their temporal evolution². Instead, we use observations from Chapter 2 to inform their shape and localization relative to the Rho GTPase zones. For simplicity, we let PKCs modulate the basal Rho GTPase activation rates. With this model variant, we calibrate the control simulation. PKC manipulations are then simulated, but we find that the current assumptions do not explain the experimental observations. We conclude that more detailed PKC activity profiles are necessary.

5.2 Defining PKC activity profiles

In order to make a simplified approximation of the PKC activity profiles, several features demand attention:

- (i) PKC beta and PKC eta accumulate around wounds as zones of elevated activity (Figure 2.5). Both PKC beta and PKC eta overlap the RhoA zone, though PKC beta also encompasses the Cdc42 zone (Figures 2.4).

²We do eventually receive explicit data on PKC activity profiles, and use them in the next chapter.

- (ii) The PKC zones appear to exhibit zone segregation and zone maintenance in concert with the Rho GTPase zones (Figure 2.5 A).

5.2.1 PKC spatial profiles as step functions

The spatial profile of PKC activity (Feature (i)) can be approximated as a step function (Figure 5.1). Both PKC step functions are normalized to 1, representing the elevated activity within zones. Outside of each step function, the corresponding PKC activity is assumed to be essentially zero. The PKC beta step function $\beta(x, t)$ is broader than the PKC eta step function $\eta(x, t)$.

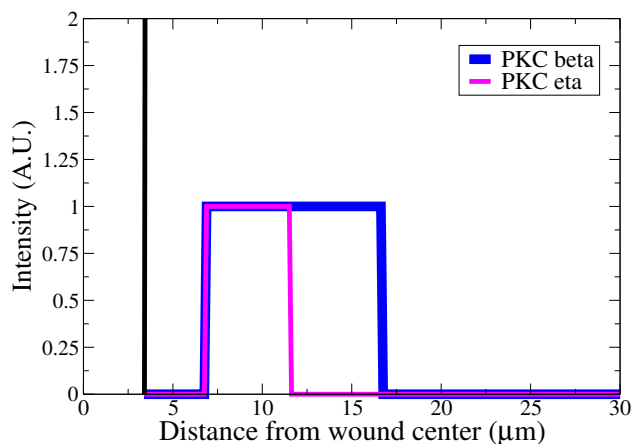


Figure 5.1: Activity profiles of PKC beta, $\beta(x, t)$, and PKC eta, $\eta(x, t)$, are modelled as normalized step functions with PKC beta covering a greater breadth than PKC eta. The simulated wound edge is marked by the vertical black line, and is towards the left.

5.2.2 PKC zone localization

We have picked our simplified representation of the PKC activity profiles, but how do we determine where these PKC zones should localize? Based on Feature (ii), they should track the Rho GTPase zones. For us to recognize where a Rho GTPase zone is located, we adopt the following quantitative definition.

Zone Localization The RhoA (Cdc42) zone localization is defined as the region of the domain with RhoA (Cdc42) activity exceeding 40 % the maximum RhoA (Cdc42) activity above background.

5.2. Defining PKC activity profiles

The zone localization definition is illustrated in Figure 5.2. The 40 % activity threshold was chosen by applying various thresholds to Rho GTPase control data and visually estimating the accuracy of zone locations (Figure 5.3). We let PKC beta follow the union of RhoA and Cdc42 zone locations, and PKC eta follow the RhoA zone location.

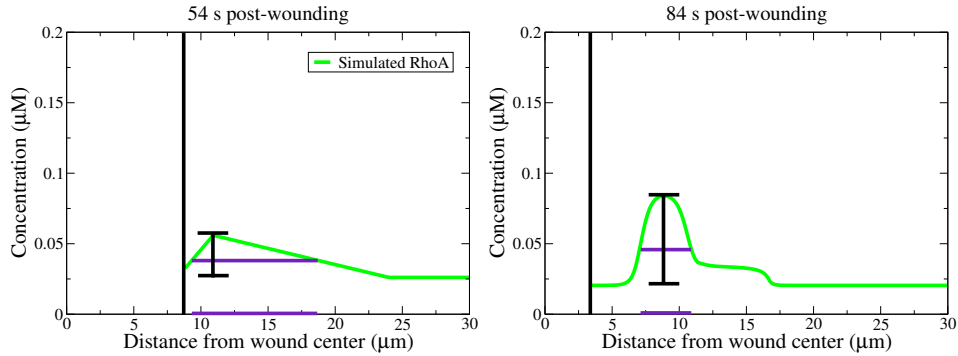


Figure 5.2: Definition of RhoA zone location at early times (left) and late times (right). Top of the thick black line indicates maximum activity above background; base of the black line indicates background activity. Top violet line indicates 40% of height spanned by black line; bottom violet line indicates the defined zone location. A similar determination of the Cdc42 zone location is used with a threshold of 40 %.

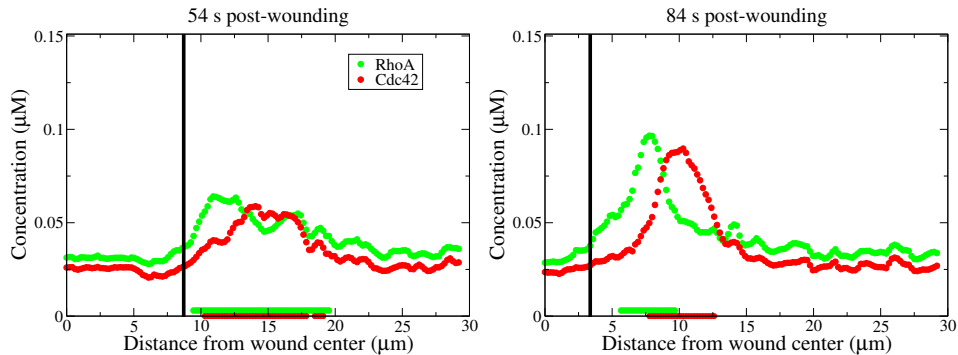


Figure 5.3: Determination of 40 % activity threshold from control data. Time series of Rho GTPases highlighting the RhoA zone location (green interval) and Cdc42 zone location (red interval). Chosen activity threshold corresponds to visual estimation of zone location accuracy.

By defining Rho GTPase zone locations which dictate the localization of PKCs, we have imposed implicit feedbacks between the two. That is, PKCs localize to the GTPase zones, while simultaneously regulating GTPase activity. In turn, PKCs impact Rho GTPase zone widths and locations, which feeds back into dictating PKC recruitment. Without yet considering the role of the lipid DAG, this is one way to implement the coordinated movement of PKC zones with Rho GTPase zones.

5.3 Spatially dependent basal Rho GTPase activation rates

The above arguments defined the functions $\beta(x, t)$ and $\eta(x, t)$. With this, we revise the background activation rates k_0^r and k_0^c . The simplest assumption is that these functions take a form:

$$k_0^r(x, t) = k_{\text{basal}}^r + k_{\text{PKC}}^r \frac{\beta(x, t)}{1 + \alpha_1 \eta(x, t)} \quad (5.1)$$

$$k_0^c(x, t) = k_{\text{basal}}^c + k_{\text{PKC}}^c \frac{\beta(x, t)}{1 + \alpha_2 \eta(x, t)} \quad (5.2)$$

where k_{basal} is the basal rate of Rho GTPase activation, k_{PKC} is the contribution of Rho GTPase activation from PKCs, and α is the strength of PKC eta relative to PKC beta. $\beta(x, t)$ is 1 on the spatial domain wherever both Rho GTPase zones are located, and 0 elsewhere. $\eta(x, t)$ is 1 on the domain where the RhoA zone is located, and 0 elsewhere.

We chose these forms for the following reasons:

1. In the absence of PKCs ($\beta(x, t) = \eta(x, t) = 0$), we obtain a basal activation rate $k_0^{r,c}(x, t) = k_{\text{basal}}^{r,c}$.
2. PKC beta enhances the basal activation rate.
3. PKC eta counteracts PKC beta and reduces the basal activation rate.

Based on the forms 5.1 and 5.2, we must identify six parameters values, namely $k_{\text{PKC}}^{r,c}$, $k_{\text{basal}}^{r,c}$ and $\alpha_{1,2}$.

We consider three separate regions, each with its own PKC beta and PKC eta level (Figure 5.4).

- Region 1 where both PKCs are present and influence RhoA zone activity.

5.3. Spatially dependent basal Rho GTPase activation rates

- Region 2 where only PKC beta is present and influences Cdc42 zone activity.
- Region 3 where neither PKCs are present.

We apply constraints in each region to estimate the parameter values. We follow a sequence of steps each time, first considering Region 3 (PKCs absent), then Region 1 (PKCs present), and finally Region 2 (PKC beta present).

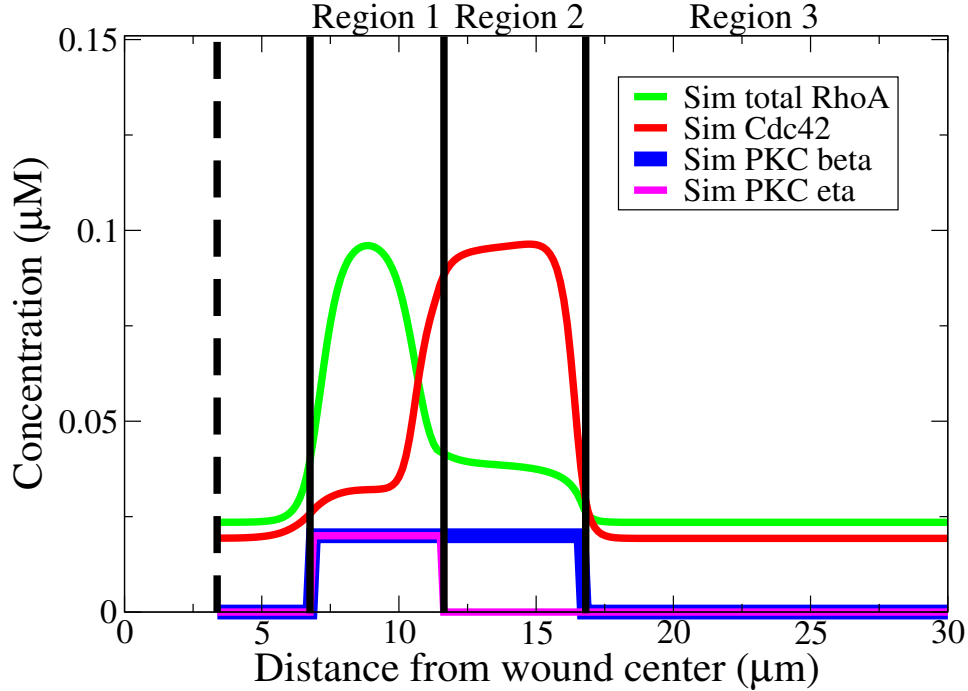


Figure 5.4: Distinct regions in the simulated control where both PKCs are present (Region 1), only PKC beta is present (Region 2), and neither PKCs are present (Region 3).

5.3.1 Parameter estimation

In Region 3, both PKCs are absent ($\beta(x, t) = \eta(x, t) = 0$) and the RHS of Equation 5.1 is now k_{basal}^r . We constrain the basal rate to

$$k_{\text{basal}}^r = \mu_1 k_{\text{ctrl}}^r \quad (5.3)$$

5.3. Spatially dependent basal Rho GTPase activation rates

where μ_1 (Region 3 constraint) is a fold change of the base parameter value, k_0^r (from Table 3.1), which we have called k_{ctrl}^r . The first parameter k_{basal}^r is now determined.

In Region 1, both PKCs are present ($\beta(x, t) = \eta(x, t) = 1$) and we constrain the RHS of Equation 5.1 to the base value of the RhoA basal activation rate k_{ctrl}^r

$$k_{\text{basal}}^r + \frac{k_{\text{PKC}}^r}{1 + \alpha_1} = k_{\text{ctrl}}^r. \quad (5.4)$$

This constraint ensures that the simulated control RhoA zone behaves the same as the control RhoA zone from Model 1. The above allows us to determine the second parameter k_{PKC}^r in terms of the remaining parameter α_1 and the base value k_{ctrl}^r

$$\Rightarrow k_{\text{PKC}}^r = (1 - \mu_1)(1 + \alpha_1)k_{\text{ctrl}}^r. \quad (5.5)$$

In Region 2, only PKC beta is present ($\beta(x, t) = 1, \eta(x, t) = 0$). We constrain the RHS of Equation 5.1 to $\omega_1 k_{\text{ctrl}}^r$, and substitute determined parameters from 5.3 and 5.5. The last parameter α_1 is now determined:

$$k_{\text{basal}}^r + k_{\text{PKC}}^r = \omega_1 k_{\text{ctrl}}^r \quad (5.6)$$

$$\begin{aligned} k_{\text{ctrl}}^r(\mu_1 + (1 - \mu_1)(1 + \alpha_1)) &= \omega_1 k_{\text{ctrl}}^r \\ \Rightarrow \alpha_1 &= \frac{\omega_1 - \mu_1}{1 - \mu_1} - 1. \end{aligned} \quad (5.7)$$

The prefactor ω_1 (Region 2 constraint) describes the fold change necessary for setting the RhoA activation rate in Region 2 to match the activity of the RhoA shoulder.

Altogether, with the three determined parameters, the basal RhoA activation rate (Equation 5.1) can be expressed in terms of constraints μ_1 and ω_1 :

$$k_0^r(x, t) = k_{\text{ctrl}}^r \left(\mu_1 + (1 - \mu_1)(1 + \alpha_1) \frac{\beta(x, t)}{1 + \alpha_1 \eta(x, t)} \right) \quad (5.8)$$

where $\alpha_1 = \frac{\omega_1 - \mu_1}{1 - \mu_1} - 1$.

Repeating the same process for Cdc42, we have

$$k_0^c(x, t) = k_{\text{ctrl}}^c \left(\mu_2 + (1 - \mu_2)(1 + \alpha_2) \frac{\beta(x, t)}{1 + \alpha_2 \eta(x, t)} \right). \quad (5.9)$$

So far, we have defined the PKC activity profiles as step functions which localize to Rho GTPase zones. We have further assumed that the background RhoA and Cdc42 activation rates are spatially dependent on the

PKC activity profiles. The basal activation rates take on a particular form (Equations 5.1, 5.2) which can be parameterized under several constraints. Next, we specify how we choose the exact constraints to simulate the control experiment.

5.3.2 Constraints set by control data

In this section, we detail how we set constraints $\mu_{1,2}$ and $\omega_{1,2}$ to faithfully simulate the control. We consult the bifurcation diagrams (Figures 4.4, 4.5) when matching control data on Rho GTPase activity (Figure 1.4) to approximate k_0^r and k_0^c values. We discuss the constraints for each region in turn.

What do we expect to happen when PKCs are absent? We expect that zone formation and maintenance would not be possible, and that Rho GTPases are essentially monostable. Furthermore, we expect background levels of Rho GTPase activities. For these reasons, we set the constraint on k_{basal}^r to $\mu_1 = 0.75$. This is outside the RhoA bistable region, and also results in background activity comparable to data. Similarly, we set $\mu_2 = 0.01$, which is inside the bistable region³ with a high threshold, and still results in background activity comparable to data.

In Region 2, we match the control RhoA shoulder activity (0.05 μM) to the bifurcation diagram. According to Figure 4.4, $\omega_1 = 1.25$ will produce activities close to what is observed. We also match the control Cdc42 zone activity ($[C^*] = 0.09 \mu\text{M}$). To do this, we consider Cdc42 steady state kinetics (Equation 3.4) which sets $\omega_2 = 2.7$ for us:

$$(k_7 + k_8) \frac{[C^*]}{[C]} - k_5[A-R^*] - \frac{k_6[C^*]^n}{K_C^n + [C^*]^n} = 2.7k_{\text{ctrl}}^c \quad (5.10)$$

where $[A-R^*]$ is the stable low steady state determined from Equations 3.2 and 3.3, with $k_0^r = 1.25k_{\text{ctrl}}^r$.

With these constraints, we initiate a control simulation using background activation rates of RhoA and Cdc42 with the following parameterizations:

$$k_0^r(x, t) = k_{\text{ctrl}}^r \left(0.75 + 0.5 \frac{\beta(x, t)}{1 + \eta(x, t)} \right) \quad (5.11)$$

$$k_0^c(x, t) = k_{\text{ctrl}}^c \left(0.01 + 2.71 \frac{\beta(x, t)}{1 + 1.73\eta(x, t)} \right) \quad (5.12)$$

³Recall that regions of low monostability are inaccessible when modulating the parameter k_0^c .

5.4 Simulations of PKC manipulations

In this section, we simulate the PKC manipulations by modifying PKC beta and PKC eta activities. We can define Model 3 in the following way:

Model 3. The spatially distributed PKC (as step functions) model.

Equations 5.11, 5.12

Initial conditions Piecewise linear (triangular) profiles fitted to control data, and scaled by amplification factors in Tables A.1-A.4 at 30 s.

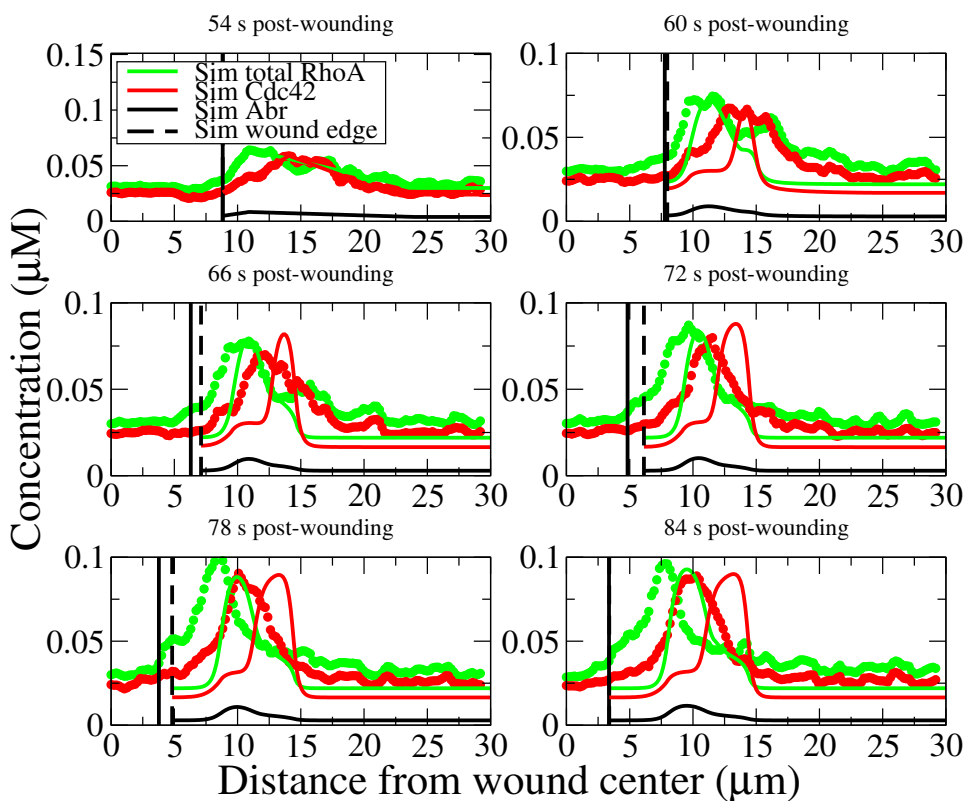


Figure 5.5: Control simulation for Model 3. Note the appearance of the RhoA shoulder. The control data are shown for comparison (circles/thick curves).

The Model 3 control simulation is shown in Figure 5.5. The simulated control captures the speed of rise in the RhoA and Cdc42 zone, as well as

peak GTPase zone activities. A few improvements are visible in the RhoA activity. The first notable feature is the appearance of the RhoA shoulder which was emphasized in Section 3.2.2. The second improvement follows from the RhoA shoulder, and is a widening in the base of the zone, with close coupling between the GTPase zones.

To simulate a PKC manipulation, we specify initial conditions as in Section 4.3, and modify the relevant PKC activity. When a particular PKC is overexpressed, its activity is increased from control levels. When a dominant-negative PKC is expressed, its activity is decreased from control levels. The simulated manipulation is evaluated against criteria in Section 3.3.1, just as in the previous chapter. The following results show simulated GTPases plotted over the Model 3 simulated control for comparison.

5.4.1 Overexpression of PKC beta

Simulations of PKC beta overexpression is shown in Figure 5.6. The first panel shows the adjusted initial conditions (Table A.1). The simulated manipulation overexpresses PKC beta activity by 5 %. Further overexpression results in a very broad RhoA zone annihilating the Cdc42 zone.

Throughout the simulation, we observe an extremely broad RhoA zone, trailed by the Cdc42 zone which has a width comparable to the control. The broad RhoA zone is a result of initial conditions with greater activity than control, in conjunction with lowering of the threshold by the manipulation. The Cdc42 zone does not broaden as extremely because the RhoA zone expands at the Cdc42 zone's expense.

At 84 s, both zones have activities that are comparable to the control. The RhoA zone appears slightly elevated, while the Cdc42 appears unchanged from control. Cdc42 insensitivity to PKC beta overexpression, and thereby k_0^c , can be simply explained by the bifurcation diagram in Figure 4.5. The diagram shows that the Cdc42 upper stable branch has a range between 0.093 – 0.1 μM over a fold change of 0-3 in k_0^c (bistable region). Thus, the very narrow range in Cdc42 stable high steady states over the bistable region is responsible for the Cdc42 zone's insensitivity to PKC modulation. The PKC beta overexpression might have been very slight, but does indeed exert effects on both zones.

In this manipulation, the simulated results exhibit zone maintenance, satisfying the first criterion **C1**. Qualitatively, we expect upregulation of the zones, though the simulations do not strongly reflect this. Furthermore, we expect similar zone widths, but the simulated RhoA zone becomes extremely broad (Figure 2.2 C). Since the zones are not significantly upregulated, this

5.4. Simulations of PKC manipulations

simulation does not satisfy criteria **C2** and **C3** (Table A.1). Model 3 is unable to recapitulate experimental observations.

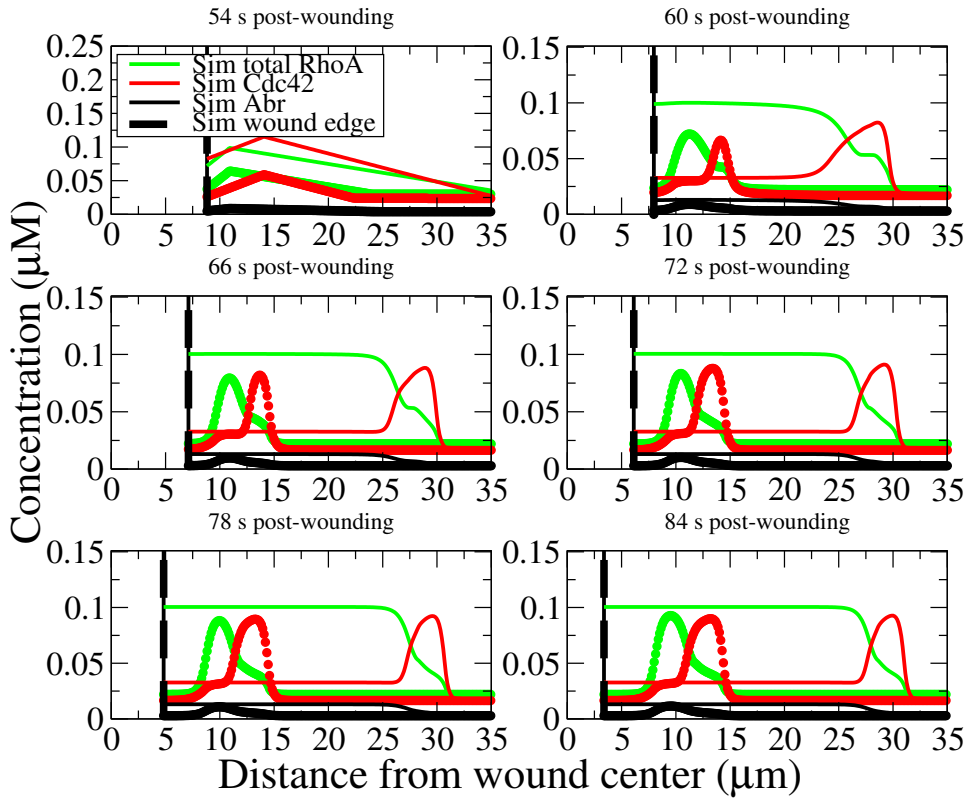


Figure 5.6: Results for Model 3 where PKC beta is overexpressed by 5 %. The simulated control is shown for comparison (circles/thick curves).

5.4.2 Expression of dominant-negative PKC beta

Simulated results are shown in Figure 5.7. The first panel shows slightly elevated initial conditions. Experimentally, zones do not form early, so we do not have zone amplification factors at 30 s (Table A.2). We asked whether adjusting the initial conditions could improve this result. Consequently, we adjusted the initial conditions by the minimum amount needed to guarantee zone formation. To simulate expression of dominant-negative PKC beta, the PKC beta activity is expressed at 80 % of the control activity. Further underexpression does not lead to very different results.

In the simulation, we observe zones with heights and widths very similar

5.4. Simulations of PKC manipulations

to the control. We observe the RhoA zone slightly above control activity, and the (insensitive) Cdc42 very slightly below the control activity. The counterintuitive result where RhoA is slightly elevated can be explained simply. We raised the initial conditions, guaranteeing zone maintenance, because the PKC manipulation raised the bistability threshold. The amplified RhoA initial conditions rose to high steady state faster than the control RhoA zone, thus appearing slightly elevated at 84 s. In fact, seconds after the last panel, the RhoA zone downregulation becomes fully apparent.

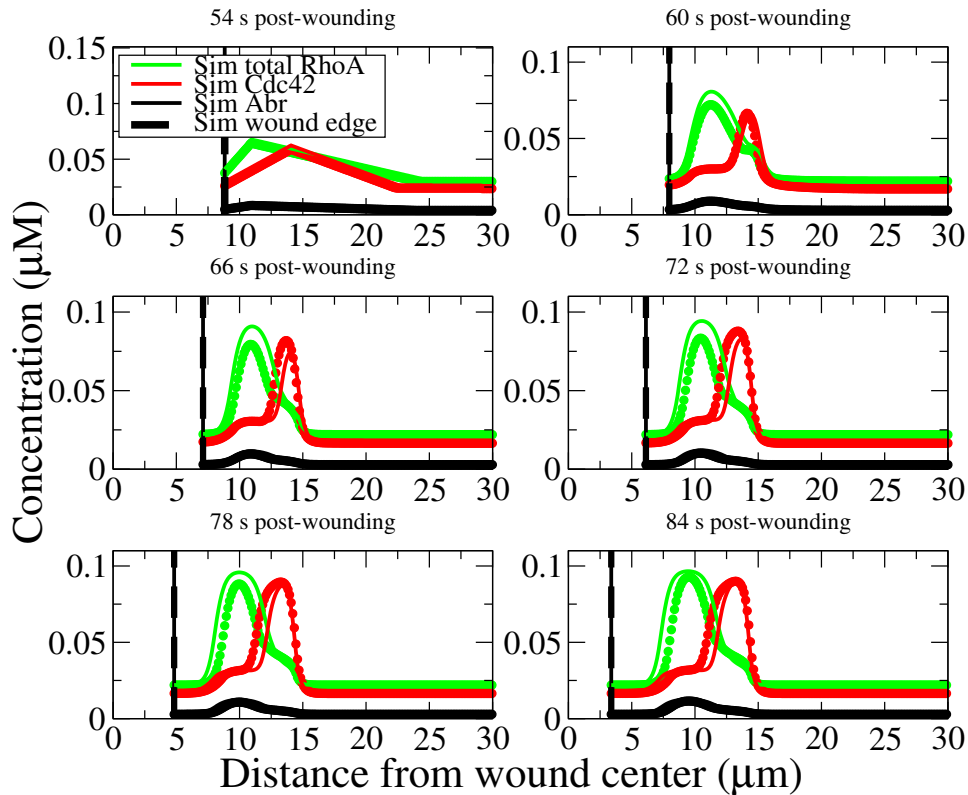


Figure 5.7: Results for Model 3 where dominant-negative PKC beta is expressed. PKC beta activity is expressed at 80 % of control levels. Initial conditions have been adjusted to guarantee zone maintenance. The simulated control is shown for comparison (circles/thick curves).

While the simulation exhibits zone maintenance (**C1**), it fails to satisfy criteria **C2** and **C3**. Under this manipulation, we expect to observe significantly downregulated zone activities (Table A.2). Since the simulated

5.4. Simulations of PKC manipulations

zones are not qualitatively and quantitatively downregulated to the extent we expect, Model 3 cannot reproduce experimental observations.

5.4.3 Overexpression of PKC ϵ

Simulated results are shown in Figure 5.8. The first panel shows the adjusted initial conditions (Table A.3). PKC ϵ is overexpressed by 5 %, and further overexpression does not change the results.

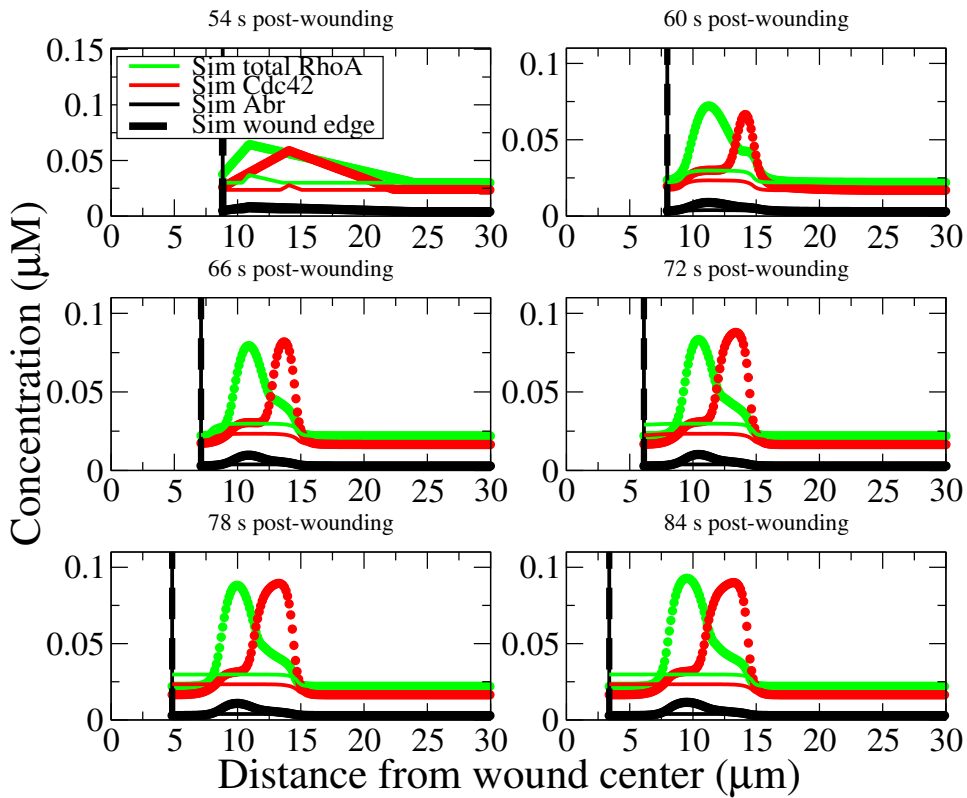


Figure 5.8: Results for Model 3 where PKC ϵ is overexpressed by 5 %. The simulated control is shown for comparison (circles/thick curves).

The simulation shows rapid decay of both RhoA and Cdc42 zones. The zones cannot be sustained because the initial conditions are set below the threshold, and the threshold is increased by the manipulation. This simulation fails to satisfy the criterion on zone maintenance (**C1**), and thus cannot be evaluated on remaining criteria. Under the current assumptions, Model 3

cannot reproduce the experimental observations.

5.4.4 Expression of dominant-negative PKC ϵ a

Simulation results are shown in Figure 5.9. The first panel shows initial conditions exactly as in the control. Experimentally, zones do not form early, so we do not have zone amplification factors at 30 s (Table A.4). Instead, we tested initial conditions which guarantee zone maintenance. The expression of dominant-negative PKC ϵ a was simulated by expressing PKC ϵ a at 40 % of PKC ϵ a control activity. Further underexpression produces similar results.

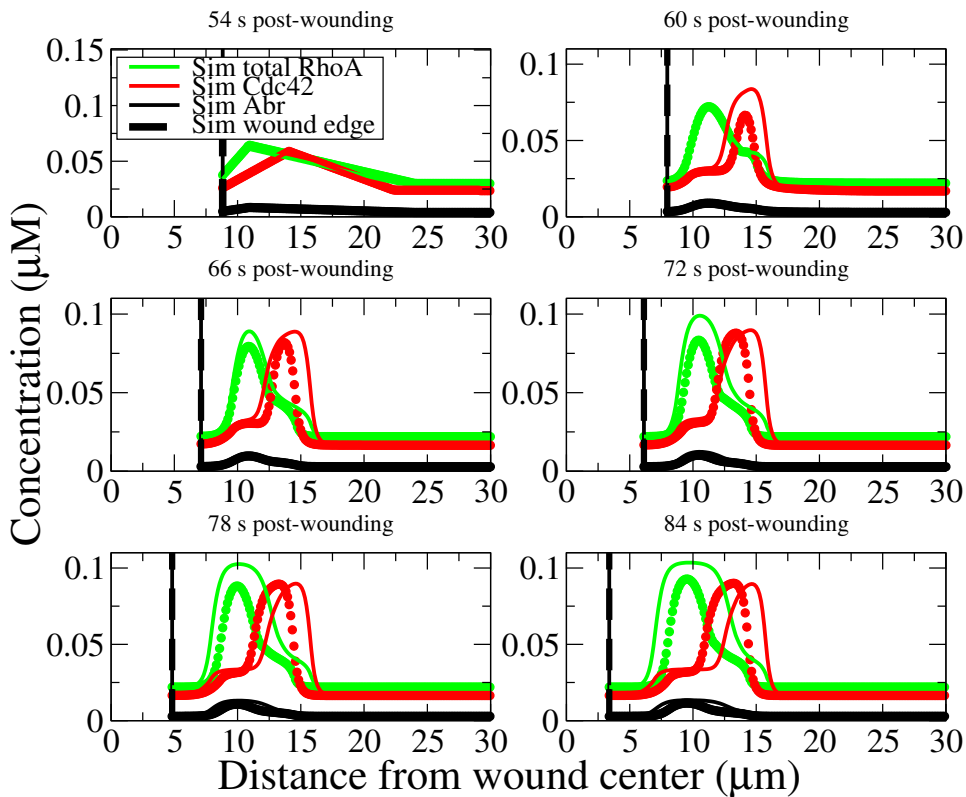


Figure 5.9: Results for Model 3 where dominant-negative PKC ϵ a is expressed. PKC ϵ a activity is expressed at 40 % of control levels. Initial conditions have been adjusted to guarantee zone maintenance. The simulated control is shown for comparison (circles/thick curves).

At 84 s, we observe a RhoA zone with elevated activity. The RhoA zone is slightly broader than control. We also observe the Cdc42 zone whose activity and width remains comparable to control. In fact, the Cdc42 zone is completely unaffected by changes in PKC eta. By definition, PKC eta localizes solely to the RhoA zone, and is absent from the Cdc42 zone. Moreover, because PKCs were assumed to be essentially zero outside the GTPase zones, the background activities are completely unaffected by the PKCs.

In this simulation, the first criterion on zone maintenance is satisfied (**C1**). Qualitatively, we expect upregulation of both RhoA and Cdc42 zone activity, but only observe RhoA upregulation. Experimental images also show that the Cdc42 zone is slightly broader than the RhoA zone, but we observe the opposite (does not satisfy **C2**; Figure 2.2 C). Quantitatively, the data show that background activities should be significantly elevated, but no change is observed in the simulation (does not satisfy **C3**; Table A.4). Therefore, Model 3 and the current assumptions are unable reproduce experimental observations.

5.5 Addressing Cdc42 insensitivity to PKC beta

In Sections 5.4.1 and 5.4.2, we simulated PKC beta manipulations. Simulation results showed that Cdc42 activity was insensitive to PKC beta. Furthermore, we discussed that Cdc42 insensitivity was primarily due to PKC effects via the basal Cdc42 activation rate k_0^c . Instead, we attempt to address this issue by allowing PKC beta effects through the basal Cdc42 inactivation rate k_7 . If we recall the bifurcation diagram in Figure 4.5, we expect dramatic changes in Cdc42 activity from modest fold changes in k_7 (due to the steep Cdc42 upper stable branch).

In this section, we allow the PKCs to affect the Rho GTPases through k_0^r and k_7 . We simulate the control and overexpression of PKC beta. We demonstrate that the Cdc42 zone can be tuned more effectively through the basal Cdc42 inactivation rate k_7 .

5.5.1 Spatially dependent basal Cdc42 inactivation rate

We assume that k_7 takes on the form:

$$k_7(x, t) = k_{7\text{basal}} - k_{7\text{PKC}} \frac{\beta(x, t)}{1 + \alpha_3 \eta(x, t)}. \quad (5.13)$$

Here, we have a negative term for the contribution of PKC effects. The negative sign is necessary because k_7 , a GAP term, has the opposite effect

of k_0^c , a GEF term. The above assumption allows the inactivation rate to decrease with PKC beta, and approach the background level with increases in PKC eta.

5.5.2 Parameter estimation and constraints

To estimate the parameters $k_{7\text{basal}}$, $k_{7\text{PKC}}$ and α_3 , we apply constraints to each region, as previously done. In terms of the constraints, the parameters can be expressed as:

$$k_{7\text{basal}} = \mu_3 k_{7\text{ctrl}} \quad (5.14)$$

$$k_{7\text{PKC}} = (1 + \alpha_2)(\mu_3 - 1)k_{7\text{ctrl}} \quad (5.15)$$

$$\alpha_3 = \frac{\mu_3 - \omega_3}{\mu_3 - 1} - 1 \quad (5.16)$$

where μ_3 is the Region 3 constraint, ω_3 is the Region 2 constraint, and $k_{7\text{ctrl}}$ is the base value of the basal *Cdc42* inactivation rate (Table 3.1). The background *Cdc42* inactivation rate expressed in terms of constraints is then

$$k_7(x, t) = k_{7\text{ctrl}}(\mu_3 - (\mu_3 - 1)(1 + \alpha_3)\frac{\beta(x, t)}{1 + \alpha_3\eta(x, t)}). \quad (5.17)$$

To set the constraints, we match the control data on GTPase activities to fold changes in parameters suggested by the bifurcation diagram (Figure 4.5). Since we expect monostable *Cdc42* in the absence of PKCs, we set $\mu_3 = 1.6$, outside the bistable region. The constraint in Region 2, $\omega_3 = 0.85$, is set in a similar way as in Section 5.3.2.

5.5.3 Simulations

We now define Model 4 in the following way:

Model 4. The spatially distributed PKC (as step functions) model.

Equations 5.11, 5.17

Initial conditions Piecewise linear (triangular) profiles fitted to control data, and scaled by amplification factors in Tables A.1-A.4 at 30 s.

The Model 4 control simulation is shown in Figure 5.10. The Rho GTPase zones look very similar to the Model 3 control simulation (Figure 5.5), and the RhoA shoulder still appears. The only difference between the simulated controls is a narrower *Cdc42* zone when Model 4 is used.

5.5. Addressing *Cdc42* insensitivity to *PKC* beta

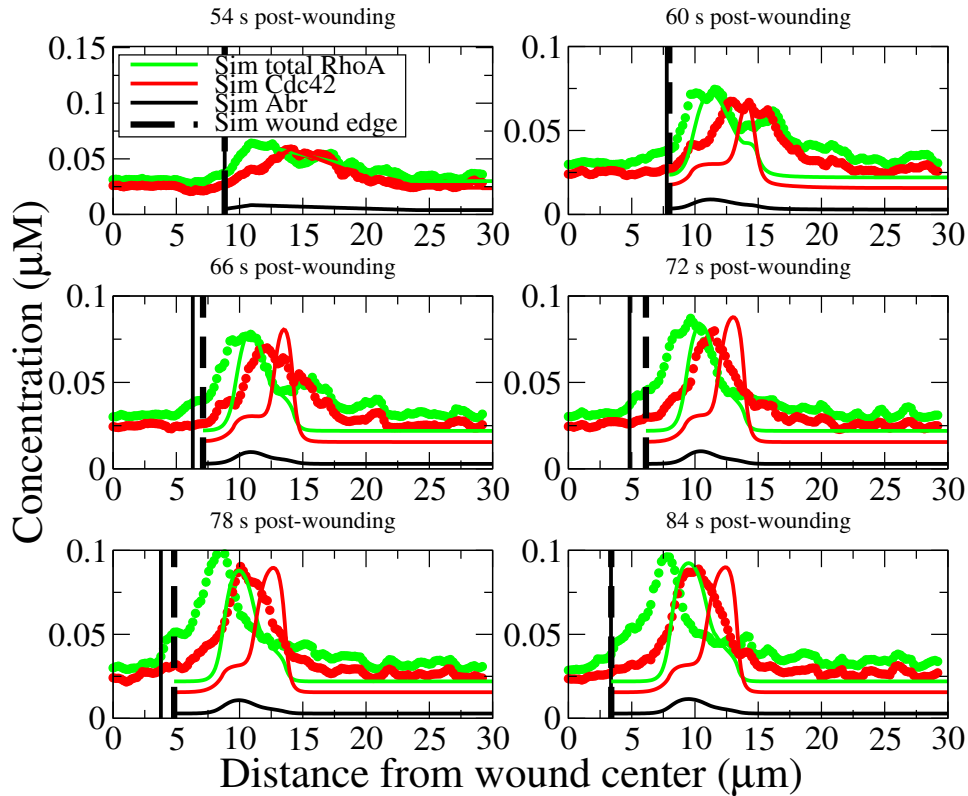


Figure 5.10: Control simulation for Model 4. Note the appearance of the RhoA shoulder. The control data are shown for comparison (circles/thick curves).

Overexpression of *PKC* beta

Figure 5.11 shows the simulation results for the overexpression of *PKC* beta. In the first panel, the adjusted initial conditions are shown. *PKC* beta is overexpressed by 210 %. Further overexpression is not possible since this would result in non-positive values of k_7 which is inconsistent with its definition.

We observe that the initial zones quickly plateau to high steady state and broaden outwards. Both RhoA and Cdc42 zones are upregulated above control activities. At 84 s, the Cdc42 zone is more elevated than in previous simulations where the basal rate of Cdc42 activation (k_0^c) was affected by *PKCs*. Here, we demonstrate that varying k_7 is more effective in upregulating Cdc42 zone activity.

5.5. Addressing *Cdc42* insensitivity to *PKC* beta

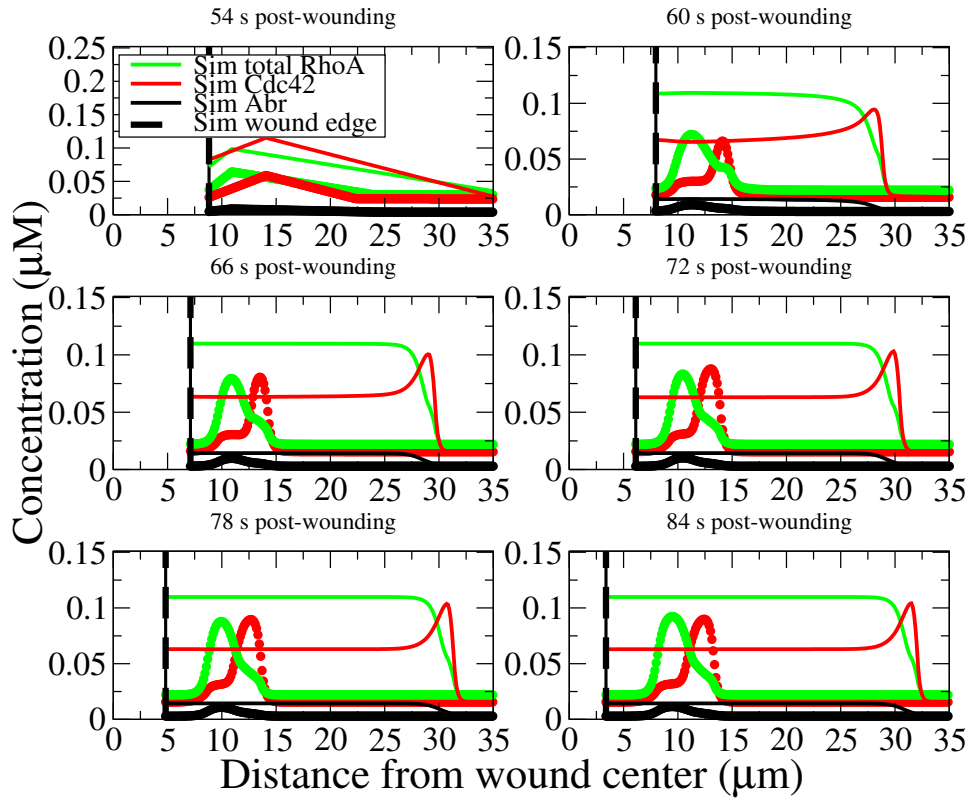


Figure 5.11: Results for Model 4 where *PKC* beta is overexpressed by 210 %. The simulated control is shown for comparison (circles/thick curves).

In this simulation, zone maintenance is achieved (**C1**), as well as a qualitative upregulation of both zones. However, the simulated RhoA zone breadth is still too broad, so this simulation does not satisfy criterion **C2** (Figure 2.2 C). Quantitatively, the upregulation of either zone does not match the extent observed in data (Table A.1, **C3** not satisfied). Therefore, under these assumptions, Model 4 is unable to reproduce experimental observations. From this, we conclude that the basal *Cdc42* inactivation rate k_7 might improve our simulation results, but only with respect to the *Cdc42* zone's peak activity.

5.6 Conclusions

In this chapter, we constructed a model (Model 3) with the simplest representation of PKC activity profiles. We used step functions to represent the PKC activity profiles, and allowed them to localize to the Rho GTPase zones. Simulated PKC beta overlapped both RhoA and Cdc42 zones, while simulated PKC eta overlapped the RhoA zone. The PKCs affected the Rho GTPase basal rates of activation ($k_0^r(x, t), k_0^c(x, t)$). By consulting bifurcation diagrams and experimental GTPase control activities, we parameterized the basal rates' dependence on PKCs.

Model 3 reproduced a notable feature in the Rho GTPase control data. It captured the prominent RhoA shoulder and improved the zone width. While Model 3 was able to simulate the control quite well, it did not account for any of the PKC manipulations. In particular, we could not account for the overexpression of PKC eta, meaning we also could not account for the inverted Rho GTPase zones. Generally, trends in upregulation or downregulation of RhoA activity were qualitatively captured. However, the model had trouble with PKC modulation of Cdc42 activity. The failure of the model in each manipulation highlights its shortcomings.

In simulations where PKC beta is manipulated, we noticed that Cdc42 activity was insensitive to modulations in PKC beta activity. We found that the insensitivity was due to PKC effects through the basal Cdc42 rate of activation (k_0^c). In contrast, PKC effects through the basal Cdc42 rate of inactivation (k_7) produced more noticeable changes to Cdc42 zone activity. It is possible that PKCs regulate GAP activity, though we were unable to successfully reproduce a PKC manipulation even with this modification.

In simulations where PKC eta is manipulated and zones were maintained, we noticed that Cdc42 activity was completely unaffected by modulations in PKC eta activity. By definition, simulated PKC eta is absent from the Cdc42 zone, and thus does not exert its influence there. This is one of several major issues we will address in turn.

Model 3 is fraught with many problems. We need to reconsider the PKC activity profiles, PKC localization, and the Rho GTPase initial conditions. Our first observation is that the simple representation of PKC activity profiles is insufficient in accounting for the manipulations. In simulated manipulations, PKC eta is zero within the Cdc42 zone, rendering the zone unaffected by PKC eta. We can think of two possible ways to correct this. First, we are inclined to increase the realism and spatial detail of the PKC activity profiles. If they were peak-like (Figure 2.5), with a gradual transition from peak to baseline, a non-zero amount of PKC eta would be present

within the Cdc42 zone. A small amount of PKC η in the Cdc42 zone might “cure” the Cdc42 insensitivity. Second, we might need to implement PKC competition for DAG. Our model variants assumed that PKC η and PKC β were independent of each other. However, if they competed for DAG, PKC η would affect PKC β in the RhoA zone. And, since PKC β is broad and extends over the Cdc42 zone, PKC η indirectly affects Cdc42 zone activity. In the next chapter, we implement the first possibility.

Our second observation concerns our implementation of PKC localization. Biologically, we know that PKCs localize to DAG. There is no reason to believe that PKC localization is Rho GTPase-dependent, as we have assumed in our models. Allowing PKCs to localize to the Rho GTPase zones is therefore unjustified. Since we also made this erroneous assumption in the control, as well as the manipulations, we further presumed that exogenous PKCs localize differently than endogenous PKCs. Seeing that we want to test very simple assumptions, our next models assume that PKCs are not Rho GTPase-dependent in the control. And, we use control PKC localization (endogenous) in the simulated PKC manipulations (exogenous).

Our third observation concerns the appropriateness of the Rho GTPase initial conditions. We used initial conditions that were fitted to the Rho GTPase control data, and scaled them appropriately in order to simulate PKC manipulations. This strategy preceded our receipt of explicit data and might have confounded the simulation results. For example, simulations of PKC β overexpression began with very broad initial conditions which resulted in very broad Rho GTPase zones. Thus, our results were in qualitative disagreement with experimental observations. As another example, simulations of PKC η overexpression began with very small zones which negated zone maintenance. Moreover, we had to guess at the initial conditions in both the simulations where dominant-negative PKCs were expressed. To remove further ambiguity, in the next chapter we use explicit data on Rho GTPase activities, under specific PKC manipulations, as our initial conditions.

Lastly, we would like to note one more interesting possibility. When we parameterized the basal activation rates, we constrained k_{basal} to a monostable regime. This means that in regions of zero (or low) PKC activity, simulated Rho GTPase zones simply cannot be sustained. Due to the constraint, extreme broadening of simulated Rho GTPase zones, beyond regions of high PKC activity, should not be observed. In this chapter, however, extremely broad simulated Rho GTPase zones were observed because of another reason: our artificial implementation of PKC localization. In the next chapter, we implement this monostable constraint again, in regions of low PKC ac-

5.6. Conclusions

tivity, and expect focused, discrete Rho GTPase zones. We propose that PKC activity profiles are partly responsible for the discrete Rho GTPase zones. They might also have the effect of curbing the backwards spread of the Rho GTPase zone's trailing edge. Therefore, no additional GAP at the trailing edge needs to be hypothesized.

Based on these results, in the next chapter we replace the step functions with data on the explicit PKC activity profiles, and ask whether model predictions could be corrected.

Chapter 6

PKCs as spatially dependent parameters: explicit activity profiles

6.1 Overview

Based on the failure to explain experimental data using step function representations of the PKC activities, we asked whether more detailed spatiotemporal PKC activity profiles would improve the results. Consequently, we requested detailed profiles of both PKC beta and PKC eta from W. Bement. We received a PKC dataset from a control experiment, as well as Rho GTPase data from each manipulation. In addition, we also had previous control Rho GTPase data at hand (Figure 1.4).

In this chapter, we implement explicit spatiotemporal PKC activity profiles given by control data. For proper PKC localization, we merge the two different control PKC and control Rho GTPase datasets. Given differences between datasets, we must horizontally shift the PKC data so that the RhoA zone and PKC peaks overlap. As in Chapter 5, we let PKCs modulate the basal Rho GTPase activation rates. We calibrate the model variant by first approximating the detailed PKC activity profiles with a step function profile, and then apply constraints to estimate parameters. With this model variant, the simulated control experiment did not account for the control data. As such, we revise a major assumption, namely that PKC beta expression should saturate. We conclude that this revision is appropriate, and that we should continue with a rigorous fit of the control simulation, before simulating PKC manipulations.

6.2 Defining PKC activity profiles

We received data on PKC activity profiles in the control wound experiment. These data remove ambiguity about the shape of the profiles, and

also the temporal evolution of PKC localization. We discuss how our functions $\beta(x, t)$ and $\eta(x, t)$ are defined by the shape and localization of PKC activity profiles.

6.2.1 Explicit PKC activity profiles from data

We use PKC activity profiles from 54 – 84 s, at every 6 s interval. The activity profiles begin at the wound center and end 50 μm away. Here, we show normalized PKC activity profiles of PKC beta and PKC eta (Figure 6.1). PKC beta spans a broader region than PKC eta, though both their peak activities overlap in the same place. The two activity peaks move towards the wound center, while amplifying between 54 – 78 s, until subsiding at 84 s.

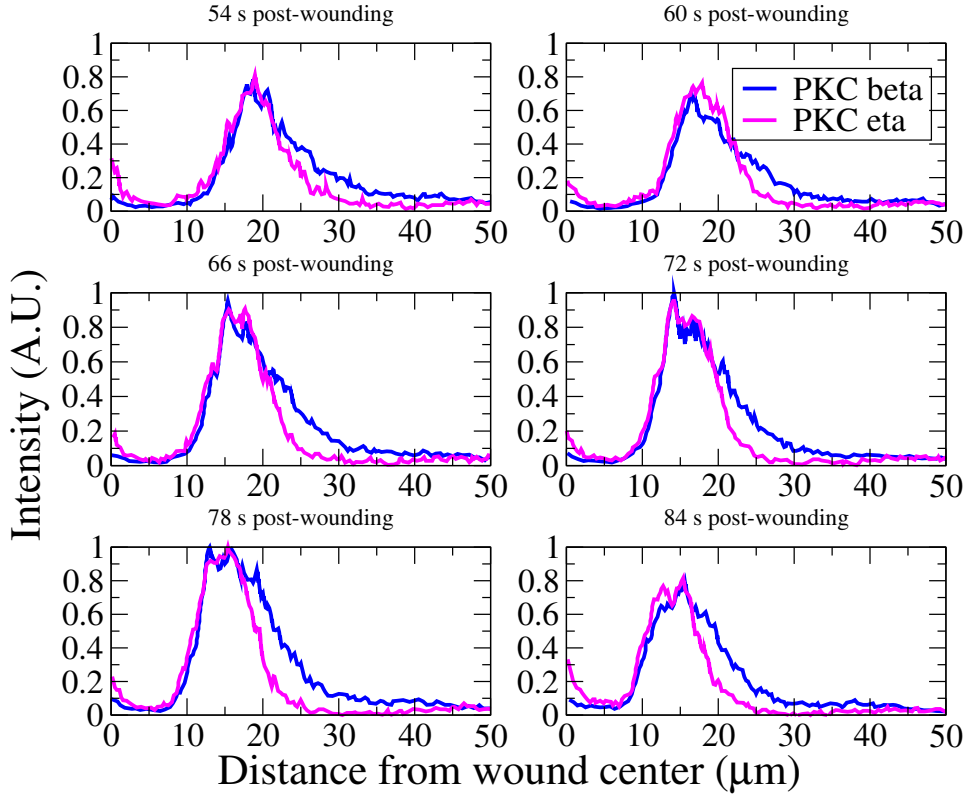


Figure 6.1: Normalized intensity profiles of PKC eta and PKC beta activities. Relevant times 54 – 84 s post-wounding are shown.

According to Figure 2.4, we assume that we can scale the PKC activity

profiles to units of concentration in the same way that Cdc42 activity was scaled at 90 s. The scaled PKC activity profiles are shown in Figure 6.2. Next, we make one more adjustment before defining $\beta(x, t)$ and $\eta(x, t)$.

6.2.2 PKC localization to regions overlapping Rho GTPase zones

The PKC activity profiles were obtained from a different control experiment than the Rho GTPase profiles. Because of this, the two different datasets cannot be directly amalgamated. If we merge the two profiles, we see that the PKCs do not overlap the RhoA zone as we expect (Figure 6.2).

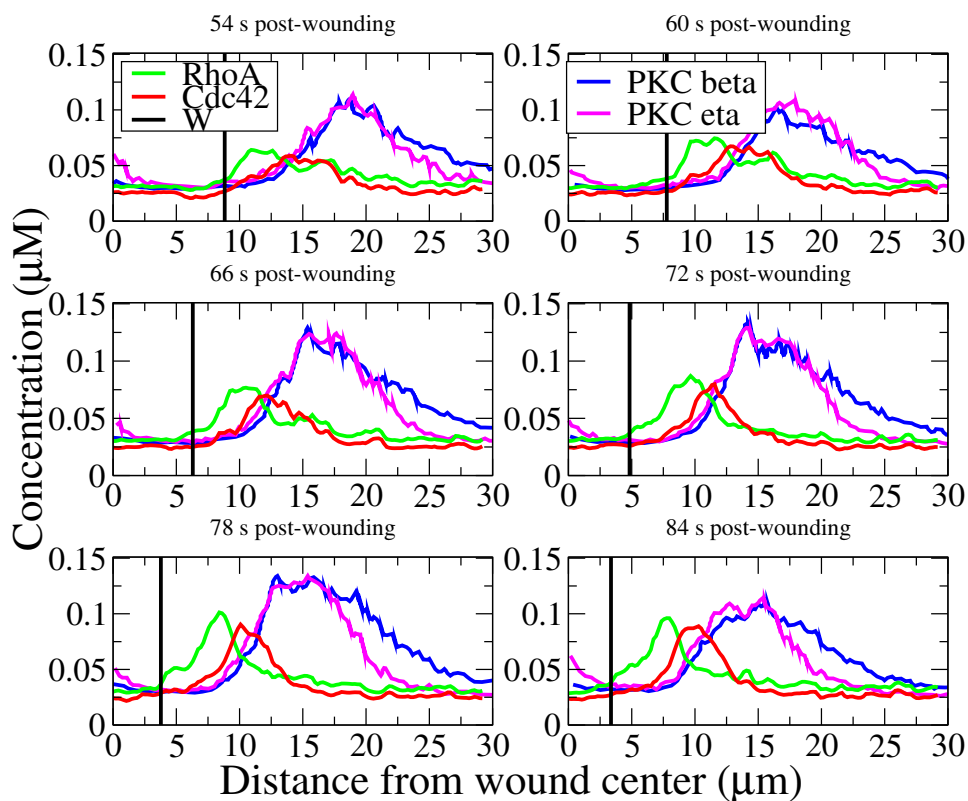


Figure 6.2: PKC activity profiles and Rho GTPase activities from different control datasets are compared. PKC zones do not overlap the RhoA zone. W denotes the wound edge from the Rho GTPase dataset.

In order to resolve this issue, we translate the PKC profiles by a fixed

6.2. Defining PKC activity profiles

amount. A clue is provided in Figure 2.4 B', where we observe a gradient of PKC eta crossing through the Cdc42 zone at 90 s. Accordingly, we make a 7 μm shift to the PKC profile relative to Cdc42 activity, at 90 s (Figure 6.3). The final merged datasets show appropriate PKC localization to the same regions as the RhoA zone (Figure 6.4).

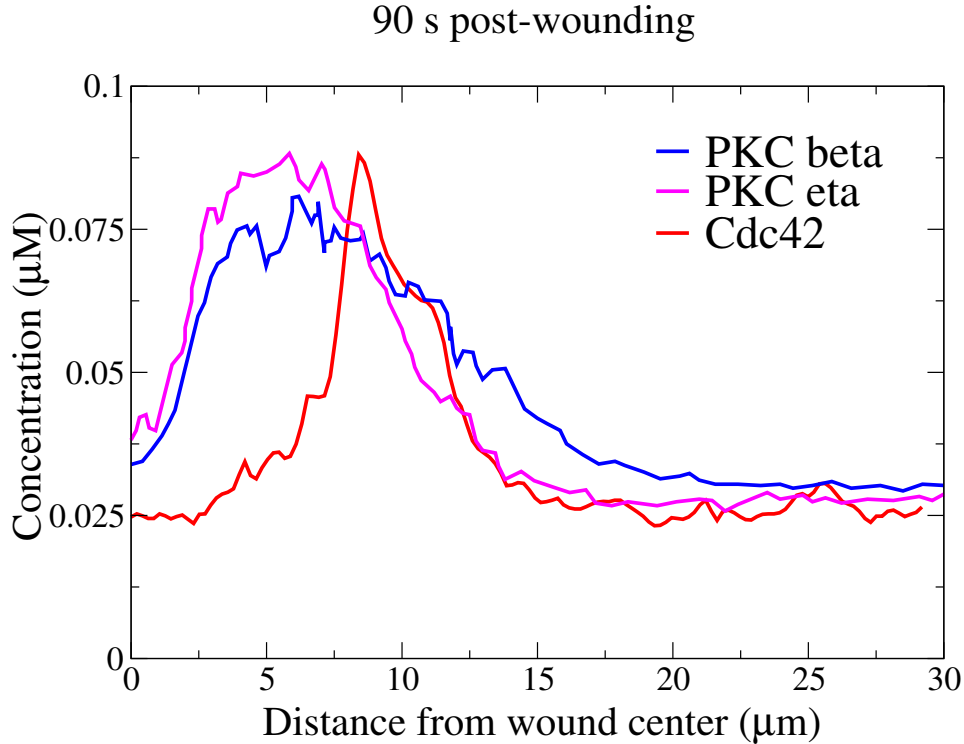


Figure 6.3: Aligning the PKC profiles with the Cdc42 peak at 90 s post-wounding. A 7 μm shift towards the wound center is illustrated.

We emphasize that we are merely correcting for the differences between datasets, so that PKCs localize to regions where the RhoA zone manifests. We do not implement any sort of PKC dependence on GTPases, as in Chapter 5. With this correction, we can now define our PKC profile functions. To define $\beta(x, t)$ and $\eta(x, t)$, we interpolate the explicit PKC activity profiles over the spatial domain, as well as between time points.

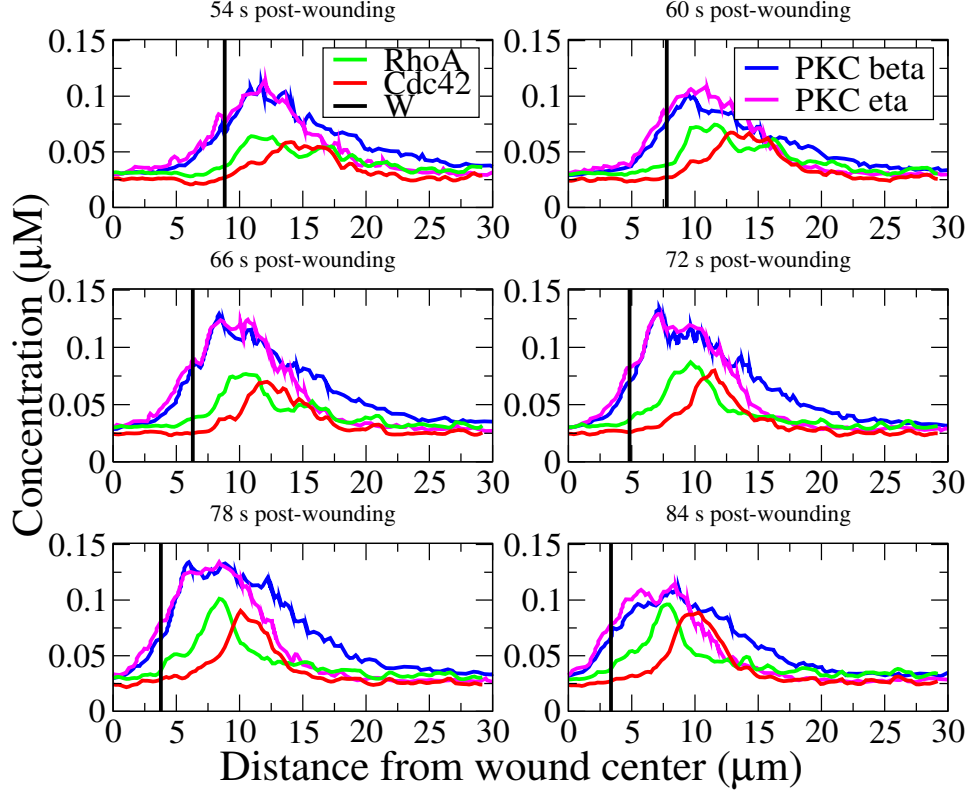


Figure 6.4: To correct the PKC localization between datasets, the PKC profiles are merged with Rho GTPase profiles under a 7 μm shift towards the wound center.

6.3 Spatially dependent basal Rho GTPase activation rates

The PKC activity profiles $\beta(x, t)$ and $\eta(x, t)$, explicitly given by data, influence the Rho GTPase basal activation rates. The rates $k_0^r(x, t)$ and $k_0^c(x, t)$ assume the forms in Equations 5.1 and 5.2. Again, six parameter values must be identified.

6.3.1 Parameter estimation and constraints

We would like to take advantage of constraining $k_0^r(x, t)$ and $k_0^c(x, t)$ in distinct regions of PKC activity, as we have done in the previous chapter.

6.3. Spatially dependent basal Rho GTPase activation rates

To do so, we apply the zone localization definition to the PKCs, to delineate regions of high and low PKC activity. The mean activity within a PKC zone, and the mean activity outside the zone are shown in Figure 6.5.

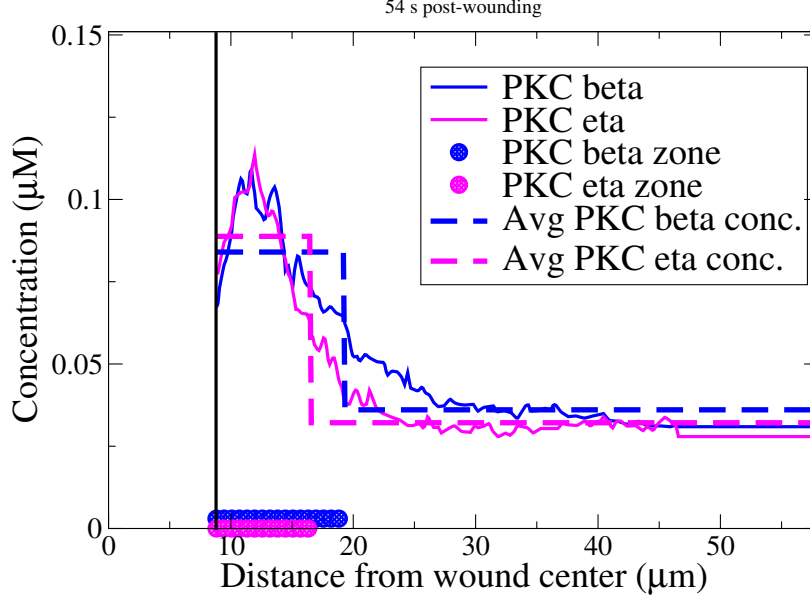


Figure 6.5: PKC zones via the zone localization definition. Mean PKC activity within the zone, and mean PKC activity outside the zone are shown.

As in Section 5.3, we consider three separate regions, each with its own PKC beta and PKC eta level of activity. In Region 1, PKC beta activity is high (β_H) and PKC eta activity is high (η_H). In Region 2, PKC beta activity is high and PKC eta activity is low (η_L). In Region 3, PKC beta activity is low (β_L) and PKC eta activity is low. Parameter estimation is set up in the same way as in Section 5.3.1, however $\beta_{H,L}$ and $\eta_{H,L}$ are used. Equations 6.1-6.3 show the constraints applied in each region (LHS) and the $k_0^r(x, t)$ parameters we must determine.

$$\text{Region 1} \quad k_{\text{ctrl}}^r = k_{\text{basal}}^r + k_{\text{PKC}}^r \frac{\beta_H}{1 + \alpha_1 \eta_H} \quad (6.1)$$

$$\text{Region 2} \quad 1.25k_{\text{ctrl}}^r = k_{\text{basal}}^r + k_{\text{PKC}}^r \frac{\beta_H}{1 + \alpha_1 \eta_L} \quad (6.2)$$

$$\text{Region 3} \quad 0.75k_{\text{ctrl}}^r = k_{\text{basal}}^r + k_{\text{PKC}}^r \frac{\beta_L}{1 + \alpha_1 \eta_L} \quad (6.3)$$

6.4. Simulation of the control experiment

Using MATLAB's `leasqr`, we determine the parameters by minimizing the sum of squared residuals (SSR) of the LHS of Equations 6.1-6.3. The Cdc42 rate parameter $k_0^c(x, t)$ is treated similarly. The resulting parameters are shown in Tables 6.1 and 6.2. In the parameterization of $k_0^c(x, t)$, the basal rate was fixed to zero because fitting leads to a negative value on the order of 10^{-3} .

k_{basal}^r (/s)	0.0034
k_{PKC}^r (/μM/s)	0.12
α_1 (/μM)	9.1
SSR	1.4×10^{-25}

Table 6.1: Parameterization of $k_0^r(x, t)$ (Equations 6.1-6.3) by method of least-squares. The sum of squared residuals (SSR) is given.

k_{basal}^c (/s)	0
k_{PKC}^c (/μM/s)	0.15
α_2 (/μM)	85
SSR	2.53×10^{-6}

Table 6.2: Parameterization of $k_0^c(x, t)$ by method of least-squares. The sum of squared residuals (SSR) is given.

6.4 Simulation of the control experiment

In this section, we simulate the control experiment using detailed PKC activity profiles and the parameterized basal activation rates. We define Model 5 in the following way:

Model 5. The spatially distributed PKC (as detailed profiles) model.

Equations 5.1, 5.2, where $\beta(x, t)$ and $\eta(x, t)$ are detailed PKC activity profiles from control data.

Parameters Tables 6.1 and 6.2

The Model 5 simulation is shown in Figure 6.6. The RhoA zone appears to rise as the data does, while the Cdc42 zone prematurely rises before the data. At 84 s post-wounding, the RhoA zone is significantly wider than the data but still centered correctly. The Cdc42 zone matches the width of the data but is offset from the data. We also observe the loss of a prominent

6.4. Simulation of the control experiment

RhoA shoulder. Due to discrepancies in RhoA activity, Model 5 cannot account for the experimental control.

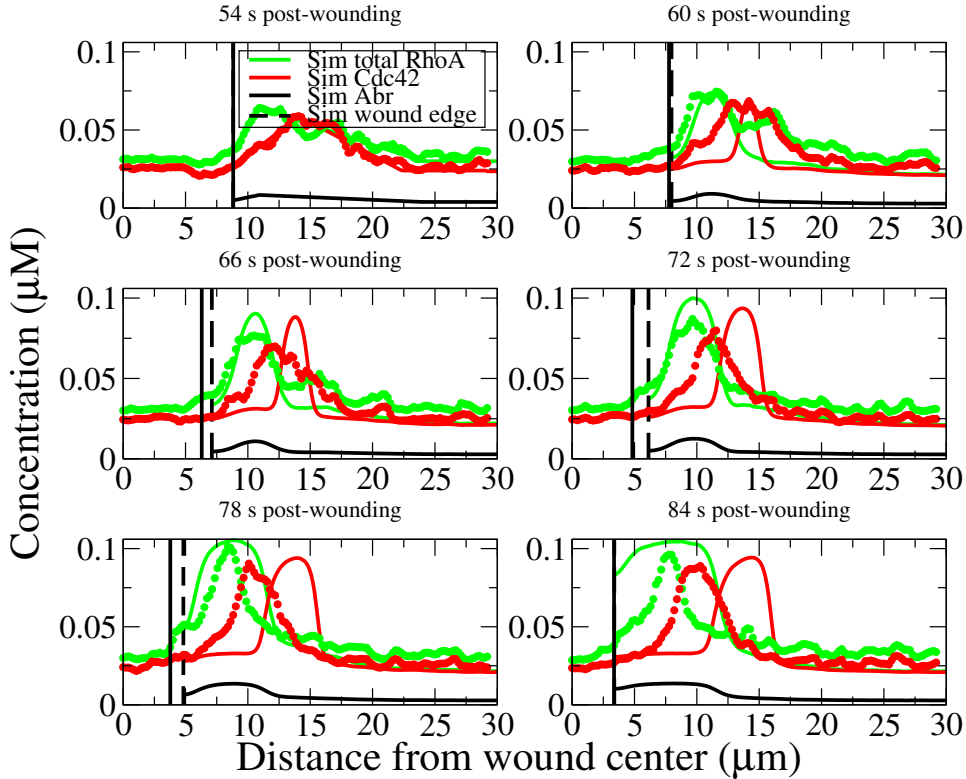


Figure 6.6: Control simulation for Model 5. The control data are shown for comparison (circles/thick curves).

6.4.1 Revising the $k_0^r(x, t)$, $k_0^c(x, t)$ relationship with PKC beta

The Model 5 control simulation does not successfully recapitulate the RhoA zone's width (Figure 6.6). To correct this, we re-examine the relationship between $k_0^r(x, t)$ and PKC beta. The current assumption is that $k_0^r(x, t)$ is proportional to $\beta(x, t)$ (Equation 5.1). Our current parameterization of the background activation rate produces a RhoA zone that is too broad (Figure 6.6). This suggests that PKC beta upregulation of the basal activation rate is too strong. This also suggests revising the PKC contribution term in Equation 5.1 which is currently linear and unbounded.

6.4. Simulation of the control experiment

Instead, we expect that PKC beta's effect should saturate, and we revise the relationship to a Michaelian term in $\beta(x, t)$,

$$k_0^r(x, t) = k_{\text{basal}}^r + k_{\text{PKC}}^r \frac{1}{1 + \alpha_1 \eta(x, t)} \frac{\beta_0^r \beta(x, t)}{\beta_0^r + \beta(x, t)} \quad (6.4)$$

where β_0^r is the concentration of PKC beta at which the added rate is half of its maximal value $k_{\text{PKC}}^r \frac{\beta_0^r}{1 + \alpha_1 \eta(x, t)}$. For low PKC activity (small $\beta(x, t)$), the Michaelian term is well approximated by a linear relationship, reducing to our previous approximation in Equation 5.1.

We want to estimate β_0^r so that this linearity gradually tapers off for higher PKC beta activity and ultimately reduces the broad RhoA zone in the control simulation. Other parameters need no revision and are retained from the fits in the previous section. We sample a variety of β_0^r to find that $\beta_0^r = 2.26 \mu\text{M}$ sufficiently reduces the width of the RhoA zone and improves its height (Figure 6.7, Model 6). We define the model variant in the following way:

Model 6. The model with PKC beta saturation in $k_0^r(x, t)$.

Equations 6.4, 5.2, where $\beta(x, t)$ and $\eta(x, t)$ are detailed PKC activity profiles from control data.

Parameters $\beta_0^r = 2.26 \mu\text{M}$, Tables 6.1 and 6.2

6.4. Simulation of the control experiment

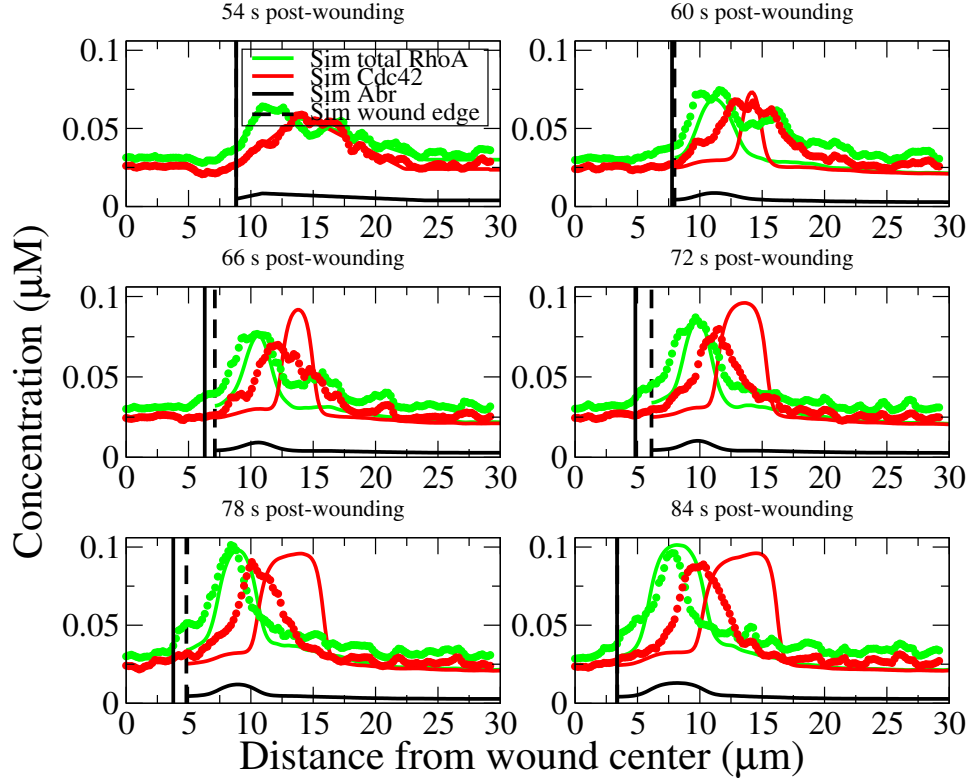


Figure 6.7: Control simulation for Model 6. The control data are shown for comparison (circles/thick curves).

We similarly treat the basal Cdc42 activation rate and find that a Michaelian expression with $\beta_0^c = 1.02 \mu\text{M}$ improves the Cdc42 zone's height, width and speed of rise (Figure 6.8, Model 7). This model variant is defined as:

Model 7. The model with PKC beta saturation in $k_0^r(x, t)$ and $k_0^c(x, t)$.

Equations 6.4 and analogous $k_0^c(x, t)$ equation, where $\beta(x, t)$ and $\eta(x, t)$ are detailed PKC activity profiles from control data.

Parameters $\beta_0^r = 2.26 \mu\text{M}$, $\beta_0^c = 1.02 \mu\text{M}$, Tables 6.1 and 6.2

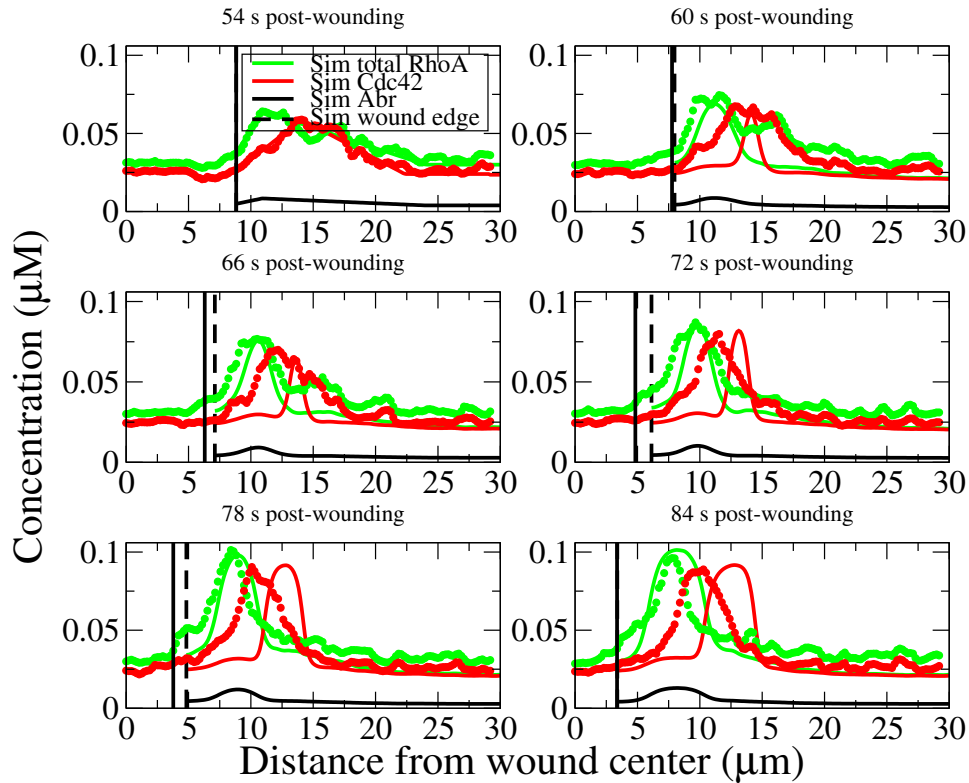


Figure 6.8: Control simulation for Model 7. The control data are shown for comparison (circles/thick curves).

6.5 Conclusions

In this chapter, we used control data of PKC activity profiles to define the functions $\beta(x,t)$ and $\eta(x,t)$. We had to combine two different control datasets, and ensured that PKCs localized to regions overlapping the RhoA zone. The PKCs acted on the basal rates of activation $k_0^r(x,t)$ and $k_0^c(x,t)$. With the current linear dependence of the basal activation rate on PKC beta, we saw the model fail to explain control data. The simulated control lost the RhoA shoulder, and the simulated RhoA zone grew too broad.

We revised a major assumption in the basal activation rate's dependence on PKC beta. We let the basal activation rate saturate with high PKC beta activity. The saturation is a reasonable assumption because PKC beta expression should be limited. In experiments, PKC beta can only be overexpressed by a certain amount before the Rho GTPase zones cease up-

regulation. This makes sense when we consider that the lipid DAG, for which PKCs compete, is finite, and that PKCs depend on DAG for activation. Thus, PKC activity should be bounded, as well as the activation rates.

So far, increasing the spatial detail in the PKC activity profiles has demanded a major revision in our assumptions on $k_0^r(x, t)$ and $k_0^c(x, t)$. We have only simulated the control experiments in this chapter, but see preliminary improvements. Before we simulate PKC manipulations, we further modify the latest model variant so that a rigorous fit of the control simulation can be done.

Chapter 7

Full nonlinear parameter fitting of model to data

7.1 Overview

In the previous chapter, we used explicit PKC activity profiles and found that the basal activation rates had to saturate with PKC beta expression. After this modification, the control was simulated and improvements were made in the simulated RhoA and Cdc42 zones. In this chapter, we use the same modification but rigorously fit the control simulation to determine the parameters in the basal activation rates. With the parameters, we then simulate PKC manipulations.

To perform a fit to control data, we modify the advection velocity so the simulated wound edge is pulled forwards at the same speed as the observed wound edge. Matching the wound edge aligns the simulated RhoA zone with the data, making a fit possible. We proceed by decoupling the RhoA fit from the Cdc42 fit. We can do so since RhoA activity affects Cdc42 activity, but not vice versa. Thus, we can first fit simulated RhoA to data, and determine parameters in $k_0^r(x, t)$. Then with $k_0^r(x, t)$ fixed, we fit simulated Cdc42 to data, determining parameters in $k_0^c(x, t)$.

With the calibrated model, we simulate PKC manipulations. Recall that we requested and received data on the PKC manipulations. In addition to the control PKC profiles previously discussed, we received Rho GTPase activity profiles for each manipulation. This allows us to initiate each simulated manipulation with the corresponding Rho GTPase initial conditions from data. Additionally, we assume that PKCs localize in the same way as PKCs in the control simulation. Under the current assumptions, the model is unable to account for experimental observations.

We therefore revisit the fitted basal rates and notice that GTPase zones are possible even at background PKC activity. At low PKC activity, both fitted basal activation rates lie within the bistable region. For consistency to previous model variants, we give the fitting routine a nonlinear constraint

7.2. Fitting spatial background activation rates to control Rho GTPase activities

which enforces the basal activation rates to lie in a monostable regime wherever PKC activity is low. Under this constraint, we find fits to control RhoA data successful, while fits to Cdc42 are not. Cdc42 fits invariably lead to loss of the Cdc42 zone. We further show that the PKC activity profiles are partly responsible for discrete RhoA zones. However, we conclude that we need to assess the validity of this assumption by way of experiment.

7.2 Fitting spatial background activation rates to control Rho GTPase activities

7.2.1 Matching the simulated wound edge to data

In order to easily fit Rho GTPase data at all six time points, we match the simulated velocity of the wound edge to data. By solving the ODE describing wound edge velocity, $\frac{dw}{dt} = -\frac{v_c(t)}{w}$, the constant v_c can be determined using data on wound edge position.

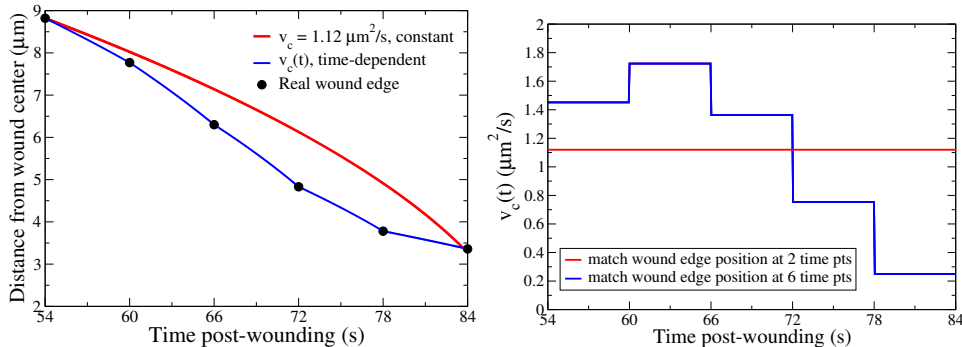


Figure 7.1: Simulated wound edge position (left) and velocity v_c (right) showing the previous choices by Simon et al. (2013) in red, and our improvement in blue. The simulated wound edge position matches data at 54 s and 84 s post-wounding (left, red) when a constant $v_c(t) = 1.12 \mu\text{m}^2/\text{s}$ is used (right, red). The simulated wound edge position matches data at six times points (left, blue) when a time-dependent $v_c(t)$ is used (right, blue).

Previously, v_c was constant in time and was determined using wound edge positions at 54 s and 84 s (Figure 7.1, right). This resulted in the wound edge being pulled at a constant speed early in the simulation, eventually speeding up to meet the exact final location observed in data (Figure 7.1, left). Instead, we choose to allow a time-dependent $v_c(t)$ which is determined

7.2. Fitting spatial background activation rates to control Rho GTPase activities

using wound edge position data at each six second interval (Figure 7.1, right). This results in the wound edge being pulled at a velocity which matches the wound edge position at all six time points (Figure 7.1, left).

7.2.2 Fits to control RhoA data

We strategically decouple our fitting procedure by first fitting $k_0^r(x, t)$ to RhoA activities, since Cdc42 activity has no impact on RhoA (Figure 3.2). The model is still governed by Equations 3.2-3.4, but the basal activation rate has been revised to the function $k_0^r(x, t)$ (Equation 6.4). We solve a nonlinear curve-fitting problem using MATLAB's `lsqcurvefit`. The fit to RhoA activity is shown in Figure 7.2, and we define Model 8 as follows:

Model 8. The RhoA fitted model with PKC beta saturation in $k_0^r(x, t)$.

Equations 6.4, where $\beta(x, t)$ and $\eta(x, t)$ are detailed PKC activity profiles from control data.

Parameters Listed in Figure 7.2.

Advection velocity $v_c(t)$ such that wound edge locations agree with control data throughout (Figure 7.1).

Model 8 simulates the control well, but does not reproduce the RhoA shoulder. It captures the rise in the RhoA zone adequately, as well as the width of the zone base. Compared to Model 7 results, the background activities are also much improved.

7.2. Fitting spatial background activation rates to control Rho GTPase activities

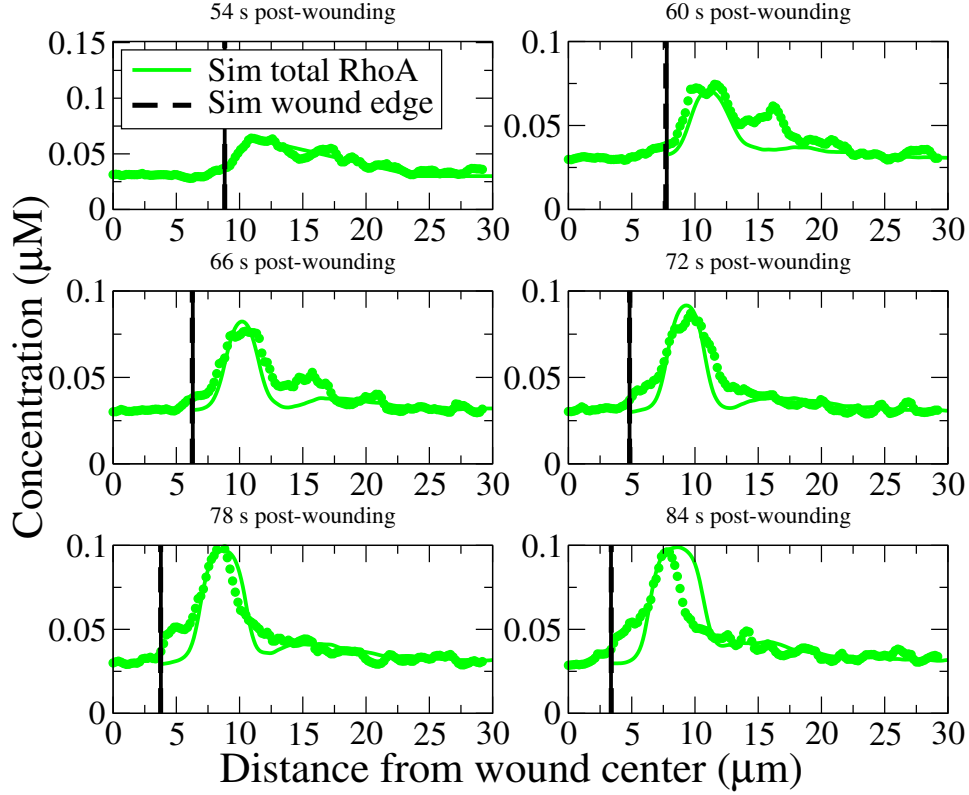


Figure 7.2: Model 8 fits to RhoA activity with matched wound edge. Fitted parameters that resulted in a sum of squared residuals of $0.053 \mu\text{M}^2$ were: $k_{\text{basal}}^r = 0.0058 \text{ /s}$, $k_{\text{PKC}}^r = 0.38 \text{ /}\mu\text{M/s}$, $\alpha_1 = 86 \text{ /}\mu\text{M}$, $\beta_0^r = 0.60 \mu\text{M}$. Control data are shown as circles/thick curves.

7.2.3 Fits to control Cdc42 data

Recall that Model 1 simulated a control Cdc42 zone that was slightly offset from data (Figure 3.3). In Model 1, and all model variants presented, the offset remains uncorrected. In order to fit the Cdc42 activity, we introduce an additional parameter to adjust for the Cdc42 offset. The subsequent fit to Cdc42 activity is shown in Figure 7.3, using Model 9 which is defined as:

Model 9. The fitted model with PKC beta saturation in $k_0^r(x, t)$ and $k_0^c(x, t)$.

Equations 6.4 and analogous $k_0^c(x, t)$ equation, where $\beta(x, t)$ and $\eta(x, t)$ are detailed PKC activity profiles from control

7.2. *Fitting spatial background activation rates to control Rho GTPase activities*

data.

Parameters Listed in Figures 7.2, 7.3.

Initial conditions Rho GTPase activity profiles from data.

Advection velocity $v_c(t)$ such that wound edge locations agree with control data throughout (Figure 7.1).

The fully fitted model (Model 9) is successful in reproducing the control Cdc42 activity. The rise in the simulated Cdc42 zone is slightly faster than data, but the shape and width at the final time point matches well. Simulated Cdc42 background activities match well too.

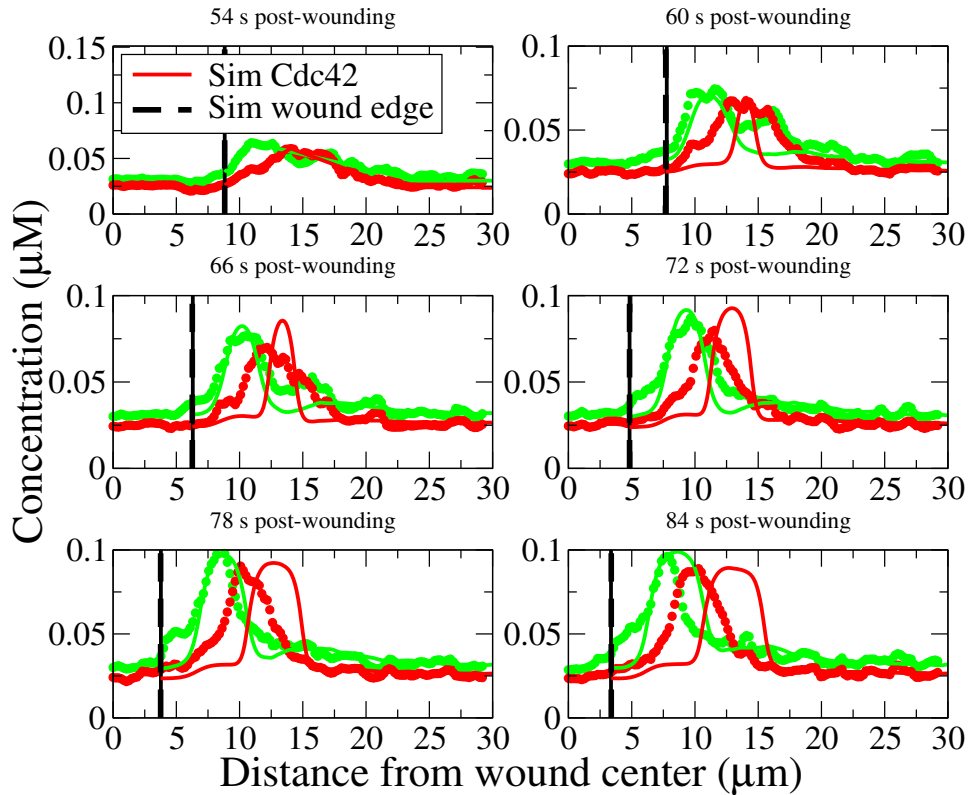


Figure 7.3: Model 9 fits to Cdc42 activity, as in Figure 7.2. However, the parameters in the basal RhoA activation rate are fixed by the previous RhoA fit. Fitted parameters that resulted in a sum of squared residuals of $0.094 \mu\text{M}^2$ were: $k_{\text{basal}}^c = 0.00025 / \text{s}$, $k_{\text{PKC}}^c = 0.38 / \mu\text{M}/\text{s}$, $\alpha_2 = 85 / \mu\text{M}$, $\beta_0^c = 0.043 \mu\text{M}$. An additional parameter, $C_{\text{shift}} = -2.47 \mu\text{m}$, was introduced so that the offset Cdc42 zone may be fitted.

7.3 Simulations of PKC manipulations

After the full nonlinear parameter fits, we simulate the PKC manipulations using Model 9. We reproduce PKC manipulations by specifying Rho GTPase initial conditions and changes in PKC activities. Furthermore, we use the control PKC localization in the PKC manipulations. This assumes that exogenous PKCs localize in the same way as endogenous PKCs.

For each manipulation, the corresponding Rho GTPase initial conditions are specified by data. To gauge the effects of the Rho GTPase initial conditions, we perform a simulation where PKC activities are at their control levels. We then mimic overexpression, or expression of dominant-negative PKC, by modifying the relevant PKC activity by two-fold, or by half. The simulated manipulation is evaluated against criteria in Section 3.3.1, as in previous chapters. In contrast to previous model validation, we have Rho GTPase data from each experimental PKC manipulation. We use these data for direct qualitative and quantitative comparison to simulated Rho GTPase results. The following results show the simulated Rho GTPases plotted over Rho GTPase data.

7.3.1 Overexpression of PKC beta

To gauge the effect of the Rho GTPase initial conditions, Figure 7.4 shows simulation results where PKC beta activity remains at control levels. In the first panel, the Rho GTPase initial conditions are given by data. In all panels, the Rho GTPase data are shown for comparison (circles/thick curves).

Throughout the simulation, we observe the Cdc42 zone broaden and sandwich the RhoA zone. The height of the Cdc42 zone matches data at 54 – 60 s and 84 s. The width of the Cdc42 zone is too broad, and the sandwich effect is largely due to the initial profile. When comparing simulated RhoA to data, we are limited to 54 – 66 s. After this time, the RhoA data are not shown because the RhoA band begins to dive below the focal plane. For early times, simulated RhoA peak zone activity is higher than data, though the background activities match well.

Since this simulation is not a PKC manipulation where we have modified the PKC activities from control levels, we do not evaluate these results against criteria for model validation. These results are to be contrasted with the following simulations where the PKC activities are modified.

7.3. Simulations of PKC manipulations

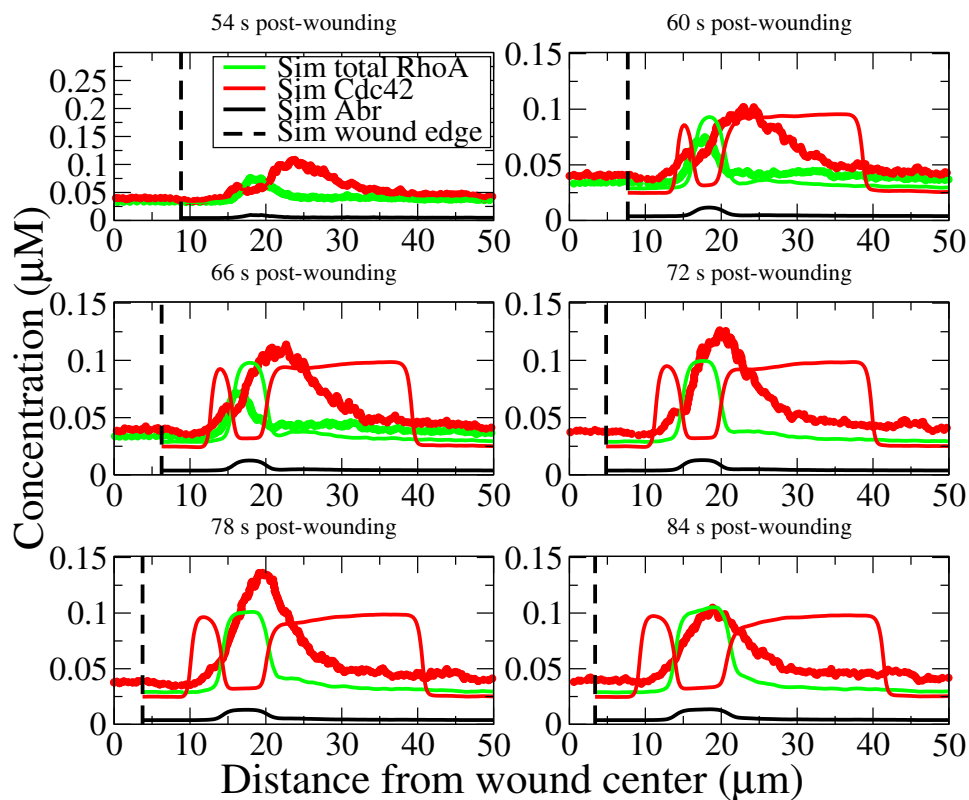


Figure 7.4: Results for Model 9 where PKC beta Rho GTPase initial conditions are used and PKCs are at control levels. Rho GTPase data from the corresponding PKC manipulation are shown for comparison (circles/thick curves). However, RhoA data are not shown after 72 s since RhoA activity begins to dive below the focal plane.

Figure 7.5 shows the simulation where PKC beta is overexpressed by two-fold. Again, the simulation begins with initial conditions given by data. After 60 s, the simulated RhoA zone begins to overtake the broad Cdc42 zone. By 72 s, RhoA has completely suppressed Cdc42 and filled the domain.

In this simulation, we observe the annihilation of the Cdc42 zone. The criterion for zone maintenance is not satisfied (**C1**) since PKC beta overexpression is too strong. As such, we perform another simulation where PKC beta activity is overexpressed by less than two-fold.

7.3. Simulations of PKC manipulations

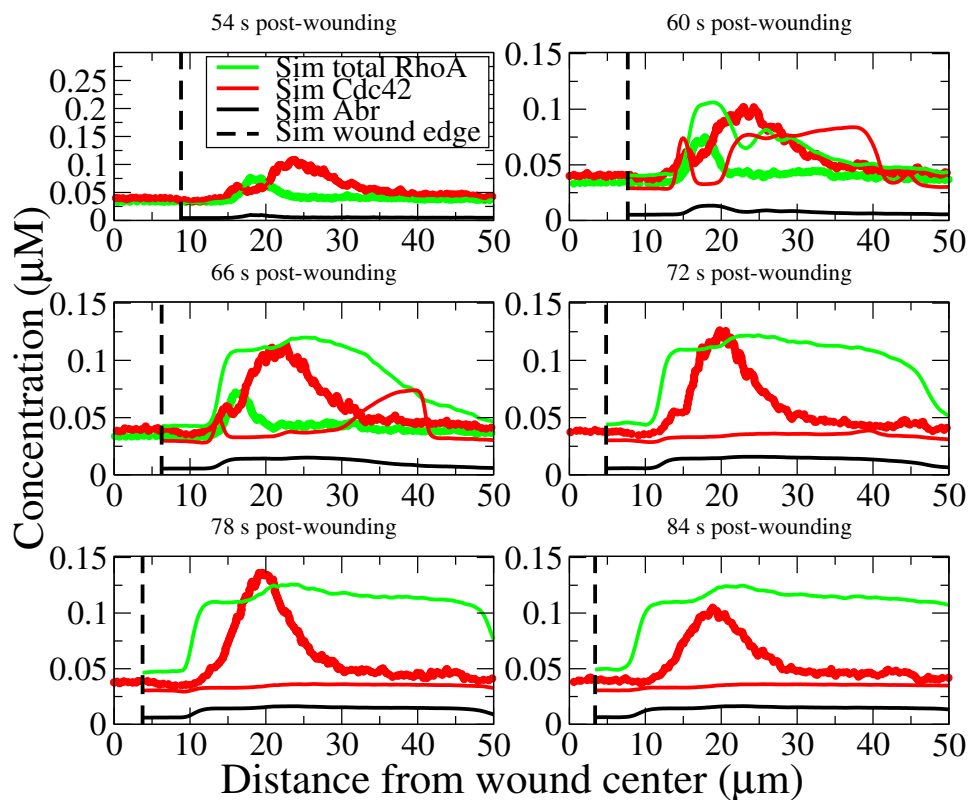


Figure 7.5: As in Figure 7.4, showing results for Model 9 where PKC beta is overexpressed by two-fold.

Figure 7.6 shows the simulation results where PKC beta is overexpressed by 1.5-fold. The first panel shows the initial conditions given by data.

At 60 s, simulated Cdc42 broadens and still sandwiches the RhoA zone. Comparing the RhoA zone to the RhoA zones in Figures 7.4 and 7.5, we see that overexpressed PKC beta impacts the zone intensity, as well as the width. Greater PKC beta activity leads to increased RhoA zone intensity, as well as breadth. The simulated RhoA zone widens at the expense of the Cdc42 zone. Comparing the Cdc42 zone to Figure 7.4, we see that PKC beta activity does not impact the Cdc42 zone intensity significantly. We have already discussed this issue as Cdc42 insensitivity to PKC beta when modulated through a GEF.

While zones are maintained (**C1**), Model 9 does not satisfy the remaining criteria **C2** and **C3**. By direct comparison to data, the Cdc42 zone height and width do not quantitatively match. As well, qualitatively, the data does

7.3. Simulations of PKC manipulations

not indicate that Cdc42 sandwiches the RhoA zone. Model 9 is unable to account for experimental observations.

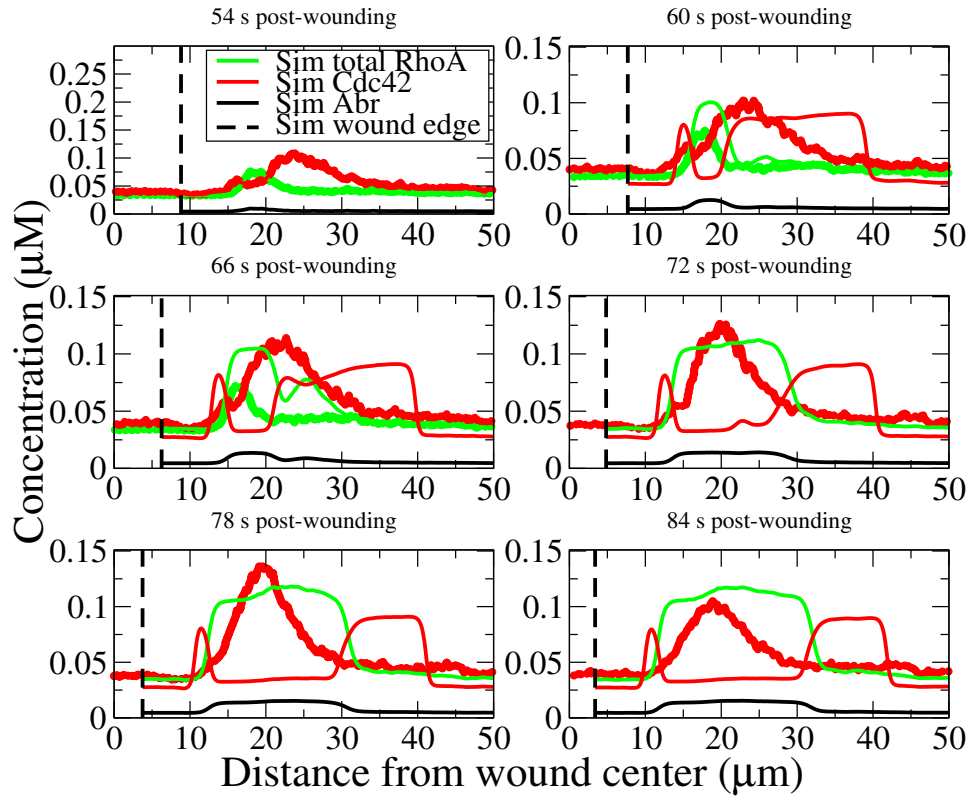


Figure 7.6: As in Figure 7.4, showing results for Model 9 where PKC beta is overexpressed by 1.5-fold.

7.3.2 Expression of dominant-negative PKC beta

Figure 7.7 shows the simulation results where PKC beta activity remains at control levels. In the first panel, we show the initial conditions which are given by data. Without modifying PKC beta activities, we observe the simulated Rho GTPases at background activities throughout. At 84 s, simulated RhoA and Cdc42 features above background are visible. We do not evaluate these results against model validation criteria since we have not modified PKC beta activities yet.

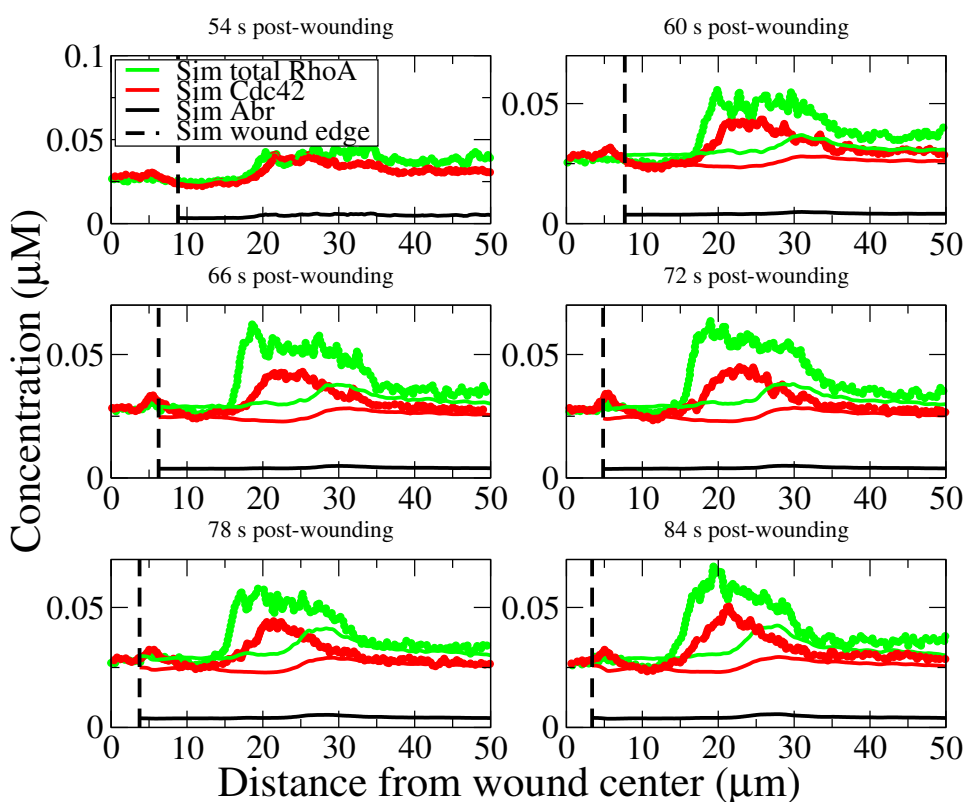


Figure 7.7: Results for Model 9 where dominant-negative PKC beta Rho GTPase initial conditions are used and PKCs are at control levels. Rho GTPase data from the corresponding PKC manipulation are shown for comparison (circles/thick curves).

Figure 7.8 shows the simulation results where we express dominant-negative PKC beta by modifying PKC beta activities to half the control

7.3. Simulations of PKC manipulations

levels. The first panel shows initial conditions given by data. Throughout the panels, we observe background activities of simulated RhoA and Cdc42 because the manipulation serves to increase the Rho GTPase thresholds. Even when Rho GTPase thresholds were at control level, zones could not be maintained. Additionally, in comparison to Figure 7.7, the above background features of RhoA and Cdc42 are smoothed out. Since zones are not maintained (C1), Model 9 cannot account for experimental observations.

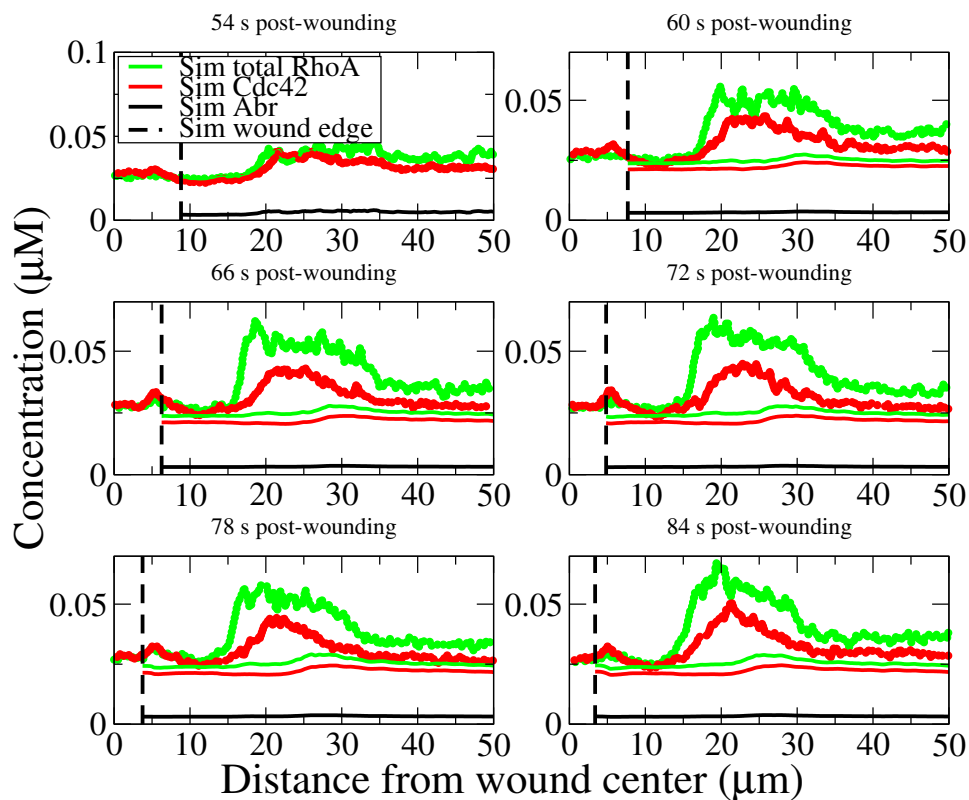


Figure 7.8: Results for Model 9 where dominant-negative PKC beta is expressed at half the control activity. Rho GTPase data from the corresponding PKC manipulation are shown for comparison (circles/thick curves).

7.3.3 Overexpression of PKC eta with inverted Rho GTPase zones

Here, we simulate PKC eta overexpression where Rho GTPase zone inversion has occurred. From 54 – 84 s post-wounding, the data already show inverted

7.3. Simulations of PKC manipulations

Rho GTPase zones (Figure 7.9).

Figure 7.9 shows simulation results where PKC ϵ activities remain at control levels. In the first panel, we show initial conditions where the Cdc42 zone is closer to the wound edge than the RhoA zone. Throughout the simulation, Rho GTPase activities are at background levels. We compare these results to the next simulation where PKC ϵ activity is modified.

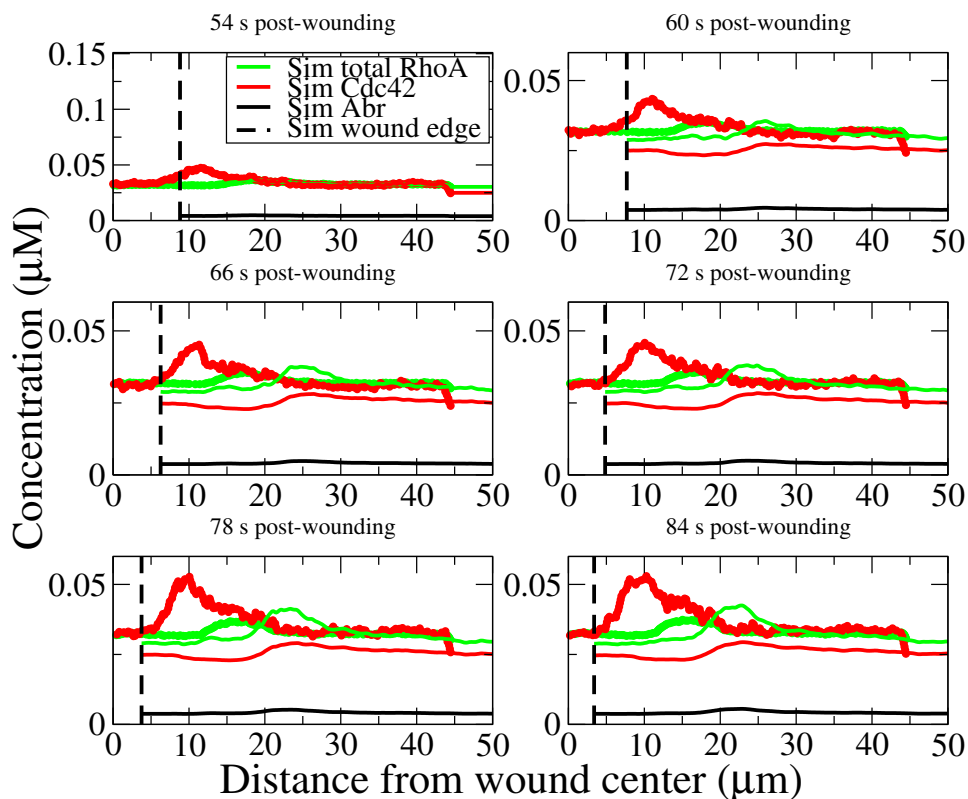


Figure 7.9: Results for Model 9 where overexpressed PKC ϵ Rho GTPase initial conditions are used and PKCs are at control levels. Rho GTPase data from the corresponding PKC manipulation are shown for comparison (circles/thick curves).

Figure 7.10 shows simulation results where PKC ϵ activity is overexpressed by two-fold. Again, Rho GTPase activities remain at background levels throughout. In comparison to Figure 7.9, the simulated Rho GTPase activities appear further suppressed. This manipulation lowers the Rho GTPase thresholds and background activities.

7.4. Revisiting fits of background activation rates to Rho GTPase activity

In this simulation, zones are not maintained (C1). Therefore, Model 9 cannot account for experimental observations.

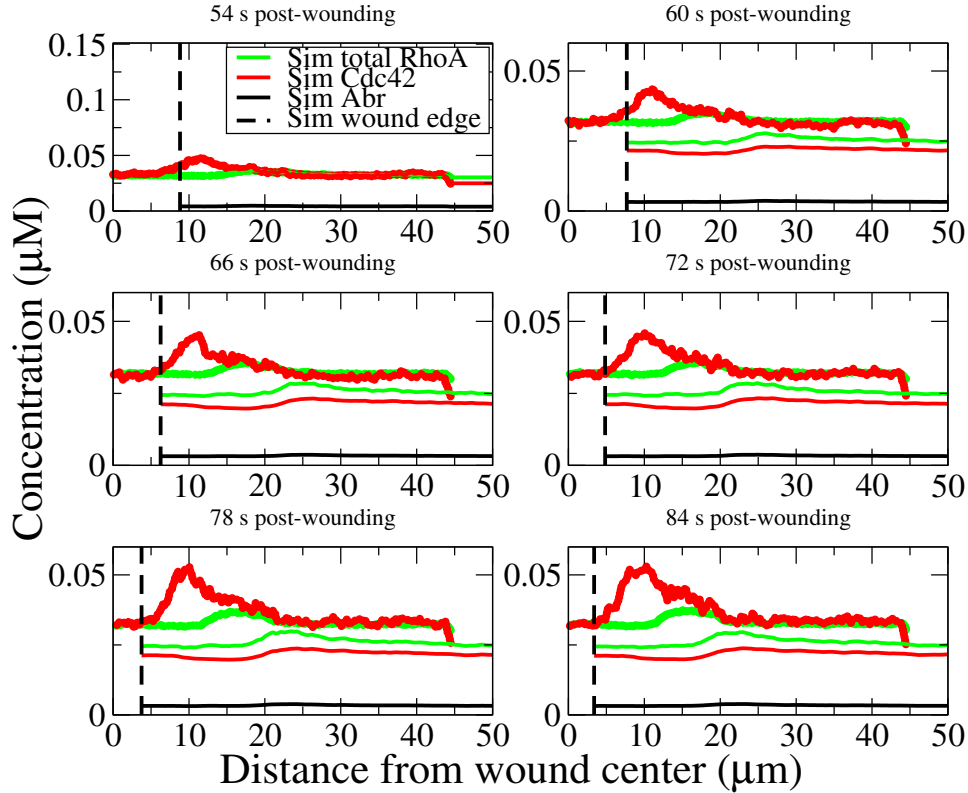


Figure 7.10: Results for Model 9 where PKC eta is expressed at twice the control activity. Rho GTPase data from the corresponding PKC manipulation are shown for comparison (circles/thick curves).

7.4 Revisiting fits of background activation rates to Rho GTPase activity

Simulations with Model 9 fail to capture the expression of dominant-negative PKC beta and the overexpression of PKC eta. Both simulated manipulations could not sustain zones. In the overexpression of PKC beta, however, zone maintenance was possible in the simulation. Qualitative and quantitative improvements to the overexpressed PKC beta simulation results are needed.

We can think of two immediate improvements to the simulation of PKC

7.4. Revisiting fits of background activation rates to Rho GTPase activity

beta overexpression. First, in Figure 7.5, a very broad RhoA zone is observed. The broad RhoA zone extends over regions of background PKC activities. This indicates that RhoA is bistable even when PKC activities are low. However, we argued that zone maintenance should not be possible at basal PKC activities, meaning that Rho GTPases should be monostable (Section 5.3.2). To enforce this assumption of monostability, we specify nonlinear constraints on the basal RhoGTPase activation rates $k_0^r(x, t)$, $k_0^c(x, t)$. We test whether PKC activities are partly responsible for regulating the discreteness of Rho GTPase zones. If this assumption is valid, we expect our simulation results to show narrower Rho GTPase zones, where zone expansion has been curbed.

The second improvement addresses the Cdc42 zone insensitivity to PKC beta. As in Section 5.5, we allow PKCs to modulate the background inactivation rate of Cdc42 ($k_7(x, t)$, Equation 5.13), instead of the background activation rate of Cdc42 ($k_0^c(x, t)$). Recall that the bifurcation diagram (Figure 4.5) indicates Cdc42 sensitivity to changes in k_7 .

7.4.1 Constrained fitting of $k_0^r(x, t)$ to control RhoA activity

In this section, we implement the first improvement to simulate the overexpression of PKC beta. We fit the basal activation rates to control Rho GTPase activities. Fits are performed with MATLAB's `fmincon` where we have supplied a nonlinear constraint on $k_0^r(x, t)$. We contrast these constrained fits with the previous unconstrained fits (Model 9).

We decouple the RhoA fit from the Cdc42 fit. Two RhoA fits are performed, with each considering a different nonlinear constraint. One RhoA fit is subject to the constraint:

$$\text{Region 2} \quad 0.75k_{\text{ctrl}}^r \geq k_{\text{basal}}^r + k_{\text{PKC}}^r \frac{\beta_H}{1 + \alpha_1 \eta_L} \quad (7.1)$$

where β_H and η_L are from Section 6.3.1. This constraint imposes RhoA in a single, low background level wherever PKC eta activity is low (i.e., outside of the RhoA zone; Region 2). Recall that a fold change of 0.75 in the basal RhoA activation rate results in monostable RhoA activity. Model 10 is defined in the following way:

Model 10. The RhoA fitted model with a nonlinear constraint (Equation 7.1) on $k_0^r(x, t)$.

Equations 6.4, where $\beta(x, t)$ and $\eta(x, t)$ are detailed PKC activity profiles from control data.

7.4. Revisiting fits of background activation rates to Rho GTPase activity

Parameters Listed in Figure 7.11, satisfying the nonlinear constraint in Equation 7.1.

Advection velocity $v_c(t)$ such that wound edge locations agree with control data throughout (Figure 7.1).

Figure 7.11 shows the RhoA fit using Model 10. The simulation results capture the control RhoA zone's height, width and speed of amplification adequately. If we contrast this to the unconstrained fit (Figure 7.2), we observe a minor difference in the simulated background activities. The difference produces a slightly higher sum of squared residuals (SSR) in the Model 10 fit ($0.059 \mu\text{M}^2$) than the Model 8 fit ($0.053 \mu\text{M}^2$).

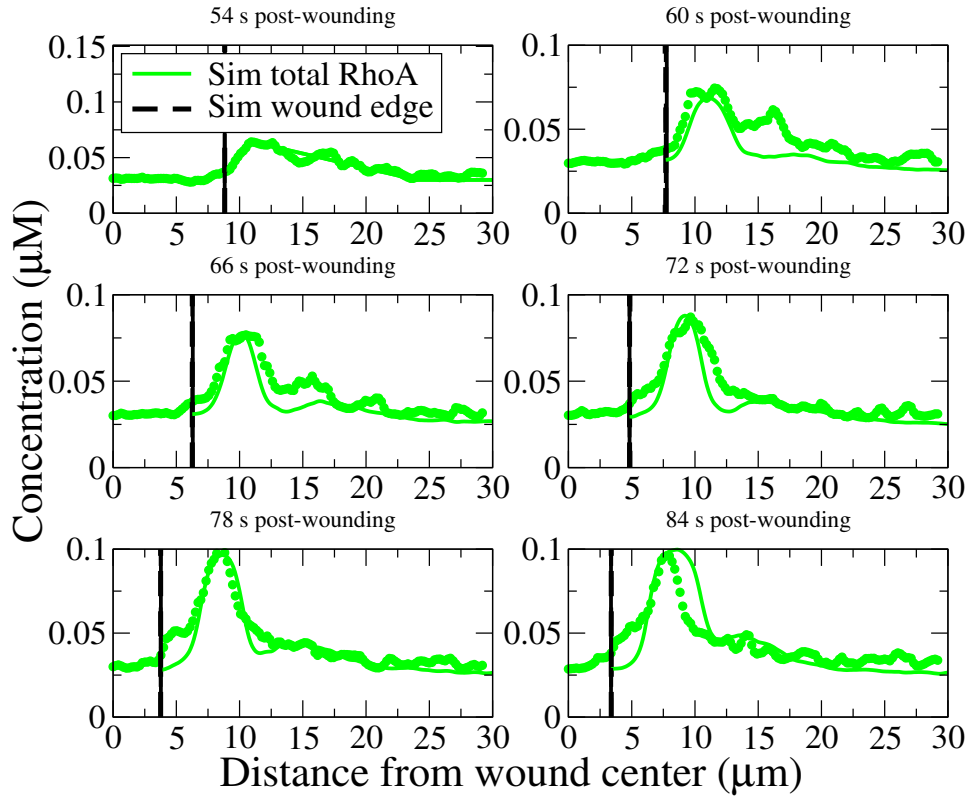


Figure 7.11: Model 10 fits to control RhoA activity. Fitted parameters that resulted in a sum of squared residuals of $0.059 \mu\text{M}^2$ were: $k_{\text{basal}}^r = 0.0027 / \text{s}$, $k_{\text{PKC}}^r = 0.29 / \mu\text{M}/\text{s}$, $\alpha_1 = 24.83 / \mu\text{M}$, $\beta_0^r = 0.46 \mu\text{M}$. Control data are shown for comparison (circles/thick curves).

7.4. Revisiting fits of background activation rates to Rho GTPase activity

The second RhoA fit is subject to multiple nonlinear constraints:

$$\text{Region 1} \quad k_{\text{ctrl}}^r \geq k_{\text{basal}}^r + k_{\text{PKC}}^r \frac{\beta_H}{1 + \alpha_1 \eta_H} \quad (7.2)$$

$$\text{Region 2} \quad 1.25k_{\text{ctrl}}^r \geq k_{\text{basal}}^r + k_{\text{PKC}}^r \frac{\beta_H}{1 + \alpha_1 \eta_L} \quad (7.3)$$

$$\text{Region 3} \quad 0.75k_{\text{ctrl}}^r \geq k_{\text{basal}}^r + k_{\text{PKC}}^r \frac{\beta_L}{1 + \alpha_1 \eta_L} \quad (7.4)$$

where $\beta_{H,L}$ and $\eta_{H,L}$ are from Section 6.3.1. These constraints impose RhoA in a single, low background level wherever both PKC beta and PKC eta are low (i.e., outside both GTPase zones; Region 3). The constraints were explained in detail in Section 5.3.2.

Model 11 is defined in the following way:

Model 11. The RhoA fitted model with nonlinear constraints (Equations 7.2-7.4) on $k_0^r(x, t)$.

Equations 6.4, where $\beta(x, t)$ and $\eta(x, t)$ are detailed PKC activity profiles from control data.

Parameters Listed in Figure 7.12, satisfying the nonlinear constraints in Equations 7.2-7.4.

Advection velocity $v_c(t)$ such that wound edge locations agree with control data throughout (Figure 7.1).

Figure 7.12 shows the RhoA fit using Model 11. The simulation results capture the RhoA zone just as well as Model 8 and Model 10. However, the background activities are visibly worse, increasing the sum of squared residuals to $0.071 \mu\text{M}^2$.

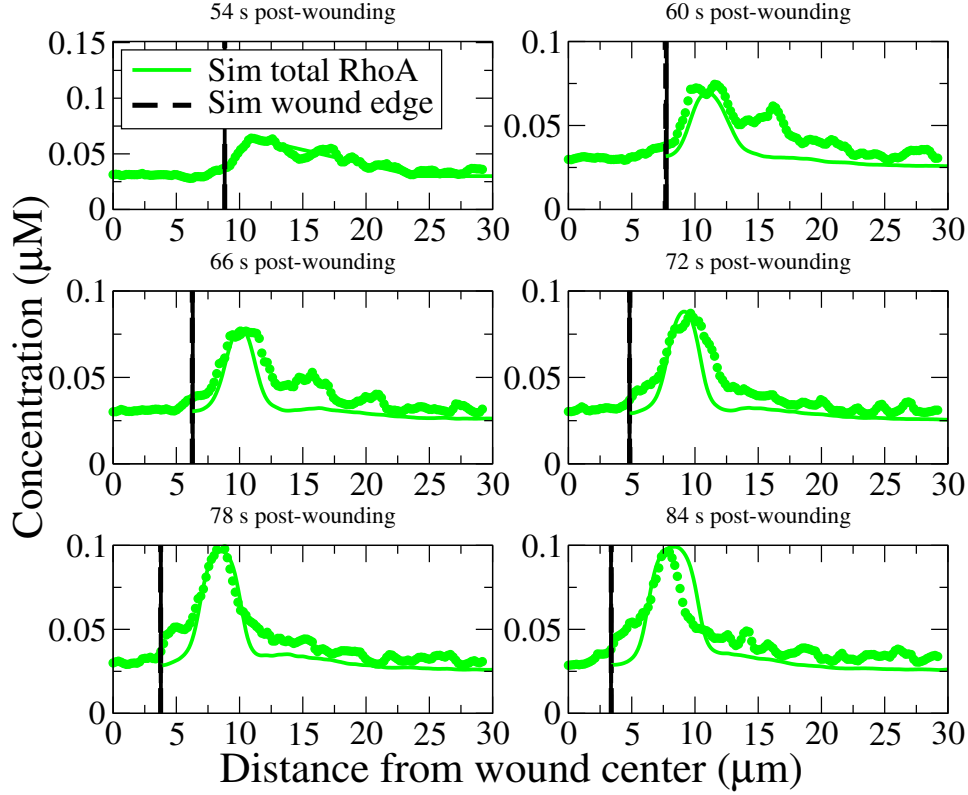


Figure 7.12: Model 11 fits to control RhoA activity. Fitted parameters that resulted in a sum of squared residuals of $0.071 \mu\text{M}^2$ were: $k_{\text{basal}}^r = 0.0057 / \text{s}$, $k_{\text{PKC}}^r = 0.096 / \mu\text{M}/\text{s}$, $\alpha_1 = 17.25 / \mu\text{M}$, and $\beta_0^r = 42.06 \mu\text{M}$.

Simulating overexpression of PKC beta

Using the calibrated Models 10 and 11, we simulate the overexpression of PKC beta, ignoring Cdc42 for now. Figure 7.13 shows the simulation results where PKC beta is overexpressed by two-fold. Results from Model 9 (green), Model 10 (olive), and Model 11 (blue) are compared. In the first panel, we see that each simulation begins with initial conditions given by data.

As the simulation progresses, we observe that Model 11 produces a narrower and more focused RhoA zone. If we consult Figure B.1, we see that the RhoA zone breadth is limited to regions where PKC activities are high. Therefore, under the assumption that GTPase zones should not form at basal PKC activities, we have shown that PKC activity profiles are partly responsible for discrete GTPase zones. To implement this assumption, we

7.4. Revisiting fits of background activation rates to Rho GTPase activity

applied two different nonlinear constraints to the RhoA fits, but found that only Model 11 was successful.

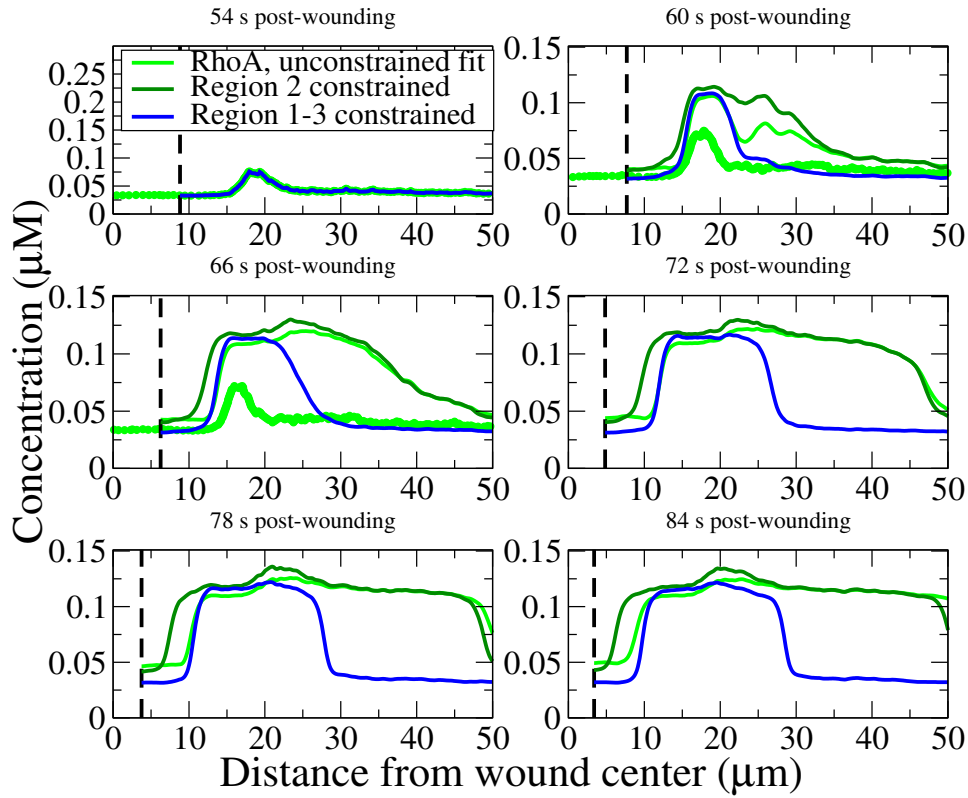


Figure 7.13: Results for Model 10 (olive) and Model 11 (blue) where PKC beta is overexpressed by two-fold. The unconstrained fit from Model 8 is shown for comparison (green). RhoA data from the corresponding PKC manipulation are also shown for comparison (circles/thick curves). However, RhoA data are removed after 72 s because RhoA dives below the focal plane.

7.4.2 Constrained fitting of $k_0^c(x, t)$ or $k_7(x, t)$ to control Cdc42 activity

Applying the nonlinear constraints (Equations 7.2-7.3) resulted in a restriction of the extreme RhoA broadening that was previously observed. We adopt these constraints to fit either $k_0^c(x, t)$ or $k_7(x, t)$. The latter is expected to address the Cdc42 zone insensitivity to PKC beta.

When we attempt a constrained fit of either basal Cdc42 (in)activation

rate, the fits result in a loss of the Cdc42 zone, and background Cdc42 activity throughout the simulation. Since we cannot calibrate the Cdc42 control simulation under these constraints, we do not proceed further and refrain from simulating PKC manipulations.

7.5 Conclusions

In this chapter, we performed a full nonlinear parameter fit of the model to control data. We first adjusted the advection velocity of the wound edge to match data at all time points. Then we fitted RhoA in isolation successfully. Next we attempted to fit the full system, including Cdc42. The model made assumptions about PKC localization and Rho GTPase initial conditions. We assumed that PKC localization in each manipulation was the same as the control. The Rho GTPase initial conditions were assumed to be given by data. The model was fitted and not subject to any nonlinear constraints. The calibrated model could account for the control (without reproducing the RhoA shoulder), but was unable to account for the observed PKC manipulations.

We took a second look at model assumptions and the fitting procedure. We assumed that Rho GTPase zones are unable to form when PKC activities are at background, thereby assuming that Rho GTPases are monostable over regions of low PKC activity. As such, we imposed a nonlinear constraint on the parameter fits, enforcing GTPase monostability in regions of low PKC activity. With these constraints, we fitted the model to RhoA control data. We simulated PKC beta overexpression, and compared the simulations from constrained fits to simulations from unconstrained fits. We observed that the assumption on zone formation at PKC resting levels, which imposed the nonlinear constraint, was effective at curbing broad RhoA zones. Lastly, we found that fits to Cdc42 were thoroughly unsuccessful, and therefore the model could not account for the control data. We were unable to proceed in reproducing PKC manipulations.

Based on these results, we ask whether Rho GTPases should be monostable in regions of low PKC activities. Experimentally, this would mean that a resting cell is unable to sustain GTPase zones. Moreover, if a resting cell could be locally perturbed by Rho GTPases, without a zone forming, the assumption would be valid. If the assumption is warranted, we would be confident in applying the nonlinear constraints in Equations 7.2-7.4. However, we require additional experimental evidence regarding this assumption.

Chapter 8

Conclusions

In this thesis, we tested whether PKCs could account for Rho GTPase patterning in single cell wound healing. We started with a Rho GTPase model from Simon et al. (2013), and allowed PKCs to affect the Rho GTPase basal (in)activation rates with increasing spatial detail. We tested models with spatially constant PKCs, as well as spatially distributed PKCs. The spatially distributed PKCs were either represented as simple step functions, or were given by explicit PKC activity profiles from data. While our model variants could account for the control, they were unable to recapitulate PKC manipulations so far.

We addressed five questions about how PKCs exert their influence on Rho GTPases (Section 2.5). We will review each question in turn. The first question asked whether PKC beta upregulated Rho GTPase activity by enhancing activation (through a GEF) or by depressing inactivation (through a GAP). A similar question applied to PKC ϵ . To answer this question, we performed a bifurcation analysis on the Rho GTPase basal (in)activation rates in Chapter 4. The bifurcation diagrams identified parameter regimes of GTPase bistability, and hence regimes where zone maintenance was possible. The diagrams were used primarily for parameter estimation, but they also showed that nearly equivalent effects on GTPase activity occurred through either increasing the basal activation rate, or decreasing the basal inactivation rate, and vice versa. Correspondingly, the bifurcation diagrams of basal activation rates were reflections of the bifurcation diagrams of basal inactivation rates. The bifurcation diagrams did not immediately suggest that PKC modulation of either basal GTPase rate (i.e., through GEFs or GAPs) was more likely.

It is possible, however, that PKC modulation of basal Rho GTPase inactivation rates is more likely to occur. In Chapters 5-7, we noticed that Cdc42 was insensitive to changes in PKC beta activity when the basal Cdc42 activation rate was modulated. Allowing PKC beta to affect the basal Cdc42 inactivation rate increased Cdc42's sensitivity. From this, we can conclude that PKC regulation of Rho GTPase GAPs is more likely to quantitatively account for observed GTPase zone intensities. Our future model (Model **FM**)

will allow PKCs to affect the basal inactivation rates.

The next question we asked was whether the spatial distribution of PKCs was important in accounting for the observed GTPase zones. By increasing spatial detail in the PKC activity profiles, we showed that the spatial distribution was indeed important in accounting for GTPase patterning. The first model with spatially constant PKCs failed to explain PKC manipulations, allowing us to conclude that PKC spatial detail was necessary. Furthermore, when spatially distributed PKCs were implemented as step functions, we reproduced the RhoA shoulder, a subtle feature in Rho GTPase patterning. The RhoA shoulder within the Cdc42 zone appeared as a result of total PKC η absence from the Cdc42 zone.

For the next model, we requested and received detailed PKC activity profiles. But the PKC data was from another experiment, and was not synchronized with the RhoA and Cdc42 data. We compensated for the differences in datasets by aligning PKC activity peaks to RhoA activity peaks. Unfortunately, this was not enough to resolve issues between datasets. As a result, the detailed PKC activity profiles did not recapitulate the RhoA shoulder in GTPase patterning. The loss of the RhoA shoulder was due to mismatched datasets which allowed the presence of PKC η within the Cdc42 zone. This motivates Model **FM** to eschew the detailed PKC activity profiles, and adopt step function representations of the PKCs.

The third question we asked was why PKC η only appeared in the RhoA zone, and was absent from the Cdc42 zone. To mimic this, we implemented PKC localization that was Rho GTPase-dependent. In the end, this dependency was rejected because it was unjustified. Instead, we know that PKCs are activated by the lipid DAG, so DAG-dependence is likely the cause of PKC localization. We did not explicitly consider DAG in this thesis, so we took the spatially detailed PKC activity profiles at face value.

Still, we wonder why PKC η localizes to a narrower region than PKC β , even though DAG presence is broad. We speculate that it is possible that PKC η weakly competes for DAG, and is therefore more likely to be present in regions abundant in DAG. Since DAG is mostly concentrated in the RhoA zone, this would explain why PKC η is present only in that narrow region.

The fourth question we asked also concerned PKC η localization. We asked how PKC η could be absent from the Cdc42 zone and still exert influence over it. Our first simple spatial model defined PKC η as essentially zero within the Cdc42 zone, hence the Cdc42 zone was completely unaffected by PKC η . We tried to cure the Cdc42 zone insensitivity to PKC η by using explicit PKC activity profiles. The PKC profiles had a

gradient of PKC η running through the Cdc42 zone. We were unable to test whether this was the correct improvement because we only had data to simulate PKC η overexpression with inverted GTPase zones. Due to inverted GTPase zones, PKCs did not encompass the Cdc42 zone in the usual way (Figure B.3). A better test would be to run a simulation with control Rho GTPase initial conditions and PKC η overexpression. Sufficient changes to the Cdc42 zone intensity would validate the use of detailed PKC profiles. Unfortunately, we did not try this due to time constraints.

Another way to address PKC η 's influence on the Cdc42 zone is through the implementation of PKC competition for DAG. In this scenario, PKC η competes with PKC β for DAG, only in the RhoA zone. Indirectly, PKC η can affect the Cdc42 zone, without being present there, by modifying PKC β which does extend over the Cdc42 zone. We envision implementing PKC competition for DAG in Model **FM**.

Our last question asked whether PKCs affected activation rates linearly, or not. This can be related to a question about how DAG modulates PKC effects on Rho GTPases. We found that the basal activation rates must saturate with PKC β , in order to successfully reproduce a control experiment. The saturation possibly reflects the finite amount of DAG, and the finite expression of PKC attainable. Model **FM** will also employ PKC saturation.

In the end, our main challenges have been uncertainties in data and the assumptions we have made. In particular, we suggest that PKCs and Rho GTPases be measured simultaneously in a control experiment. This would resolve our issues with merging datasets.

We would also like clarification on an assumption we have used. We assumed that at background PKC activities, as in a resting cell, Rho GTPase zones are impossible to sustain (i.e., are monostable). This led us to impose a monostable constraint on Rho GTPases wherever PKC activity was low. We saw that PKC activity profiles were partly responsible for the discrete Rho GTPase zones. In order to validate this assumption, we would like an experiment which locally perturbed Rho GTPase activities in a resting (unwounded) cell. The perturbation could be an injection of constitutively active RhoA or Cdc42. If zones are unable to form, our assumption would be justified.

We are optimistic that PKCs can account for Rho GTPase patterning, and will ultimately allow us to investigate Rho GTPase zone inversion. We are optimistic that it would be fruitful to take what we have learned here to motivate the next model. In the absence of detailed PKC activity profiles without dataset issues, Model **FM** should make the following assumptions:

- PKC activity profiles can be represented as simple step functions, as in Models 3, 4.
- PKC localization should be inferred from one dataset – the Rho GTPase control. That is, the zone localization definition applied to Rho GTPase control activities should dictate control PKC zones and recruitment. In simulated manipulations, we would use the same control PKC zones but adjust the PKC activity levels. This is a new assumption that has not been attempted.
- PKCs should affect the basal inactivation rates, as in Model 4.
- The basal rates should saturate with PKC activity, as in Models 6, 7.
- Regions of background PKC activity should not be able to sustain zones, and GTPase activities should be monostable there, as in Models 3-7, 10, 11.
- PKC competition for DAG should be implemented. This is a new assumption.

Again, we would use the model to simulate PKC manipulations, and test whether the experimental observations can be accounted for.

Bibliography

- Mutsuki Amano, Masaaki Ito, Kazushi Kimura, Yuko Fukata, Kazuyasu Chihara, Takeshi Nakano, Yoshiharu Matsuura, and Kozo Kaibuchi. Phosphorylation and activation of myosin by Rho-associated kinase (Rho-kinase). *Journal of Biological Chemistry*, 271(34):20246–20249, 1996.
- William M Bement, Craig A Mandato, and Mary N Kirsch. Wound-induced assembly and closure of an actomyosin purse string in *Xenopus* oocytes. *Current Biology*, 9(11):579–587, 1999.
- William M Bement, Ann L Miller, and George von Dassow. Rho GTPase activity zones and transient contractile arrays. *Bioessays*, 28(10):983–993, 2006.
- William M Bement, Emily M Vaughan, Hoi-Ying E Yu, Amber Lasek, Nick Vitale, and Troy A Hornberger. Lipid domain-dependent regulation of single cell wound repair. Unpublished manuscript, 2012.
- Hélène A Benink and William M Bement. Concentric zones of active RhoA and Cdc42 around single cell wounds. *The Journal of Cell Biology*, 168(3):429–439, 2005.
- TH Chuang, X Xu, V Kaartinen, N Heisterkamp, J Groffen, and GM Bokoch. Abr and Bcr are multifunctional regulators of the Rho GTP-binding protein family. *Proceedings of the National Academy of Sciences*, 92(22):10282–10286, 1995.
- Céline DerMardirossian and Gary M Bokoch. GDIs: central regulatory molecules in Rho GTPase activation. *Trends in Cell Biology*, 15(7):356–363, 2005.
- Aron B Jaffe and Alan Hall. Rho GTPases: biochemistry and biology. *Annual Review of Cell and Developmental Biology*, 21:247–269, 2005.
- Craig A Mandato and William M Bement. Contraction and polymerization cooperate to assemble and close actomyosin rings around *Xenopus* oocyte wounds. *The Journal of Cell Biology*, 154(4):785–798, 2001.

Hiroaki Miki and Tadaomi Takenawa. Regulation of actin dynamics by WASP family proteins. *Journal of Biochemistry*, 134(3):309–313, 2003.

Cory M Simon, Emily M Vaughan, William M Bement, and Leah Edelstein-Keshet. Pattern formation of Rho GTPases in single cell wound healing. *Molecular Biology of the Cell*, 24(3):421–432, 2013.

Emily M Vaughan, Ann L Miller, Hoi-Ying E Yu, and William M Bement. Control of local Rho GTPase crosstalk by Abr. *Current Biology*, 21(4):270–277, 2011.

Appendix A

Zone amplification factors from box-and-whisker plots

In Chapter 2, we present Rho GTPase data in PKC manipulations. Changes in Rho GTPase zone intensity are quantified in box-and-whisker plots, and compared to the control Rho GTPase zones. We express the changes in Rho GTPase zone intensity as a fold change relative to the control. These fold changes are used as zone amplification factors in simulated PKC manipulations to scale the initial conditions.

		Intensity (A.U.)		fold change relative to control
		Control	OEPKCbeta	
30 s	RhoA	6.0	12.0	2
	Cdc42	8.0	21.0	2.6
60 s	RhoA	13.2	14.3	—
	Cdc42	20.4	35.6	1.7

Table A.1: Fold change in RhoA and Cdc42 zone activities, relative to control, when PKC beta is overexpressed. Based on mean intensity data (in arbitrary units) taken from Figure 2.2 D. Fold changes that are not statistically significant are indicated by —.

		Intensity (A.U.)		fold change relative to control
		Control	DNPKCbeta	
RhoA	Zone	39.4	19.2	0.49
	Background	24.1	25.0	—
Cdc	Zone	49.1	19.7	0.40
	Background	29.0	27.1	—

Table A.2: Fold change in RhoA and Cdc42 zone activities, relative to control, when dominant-negative PKC beta is expressed. Based on mean intensity data (in arbitrary units) taken from Figure 2.2 E. Fold changes in background activity that are not statistically significant are indicated by —.

Appendix A. Zone amplification factors from box-and-whisker plots

		Intensity (A.U.)		fold change relative to control
		Control	OEPKCeta	
30 s	RhoA	8.0	1.6	0.2
	Cdc42	6.8	3.0	0.44
60 s	RhoA	20.4	2.4	0.12
	Cdc42	15.4	7.2	0.46

Table A.3: Fold change in RhoA and Cdc42 zone activities, relative to control, when PKC eta is overexpressed. Based on mean intensity data (in arbitrary units) taken from Figure 2.2 F.

		Intensity (A.U.)		fold change relative to control
		Control	DNPKCeta	
RhoA	Zone	37.7	35.1	—
	Background	24.0	57.2	2.4
Cdc	Zone	49.3	40.3	—
	Background	31.2	45.5	1.46

Table A.4: Fold change in RhoA and Cdc42 background activities, relative to control, when dominant-negative PKC eta is expressed. Based on mean intensity data (in arbitrary units) taken from Figure 2.2 G. Fold changes in zones that are not statistically significant are indicated by —.

Appendix B

Amalgamating PKC and Rho GTPase datasets

In Chapter 6, we used explicit PKC activity profiles given by control data. Due to differences in datasets, the PKC profiles had to be shifted to correct for localization to the control Rho GTPase zones. In Chapter 7, we have Rho GTPase data for each PKC manipulation. In each PKC manipulation, we must correct the PKC activity profile and shift it to overlap the RhoA zone. The following figures illustrate these corrections.

B.1 Overexpression of PKC beta

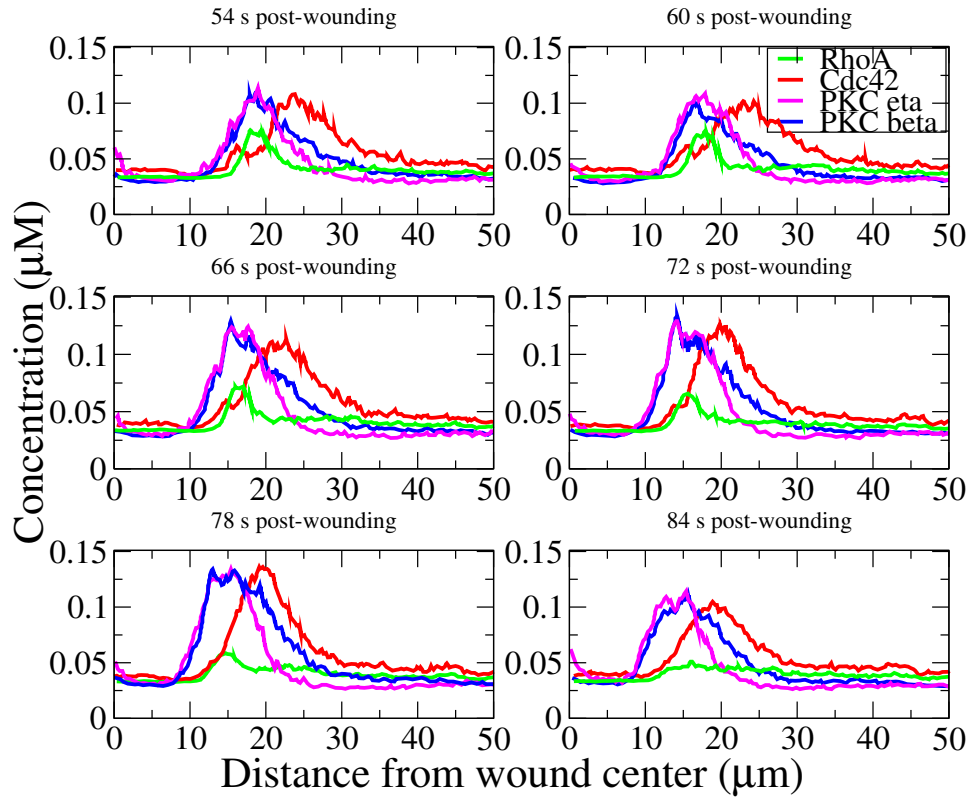


Figure B.1: Alignment of control PKC profiles with Rho GTPase profiles in PKC beta overexpression. PKC profiles are aligned with Rho GTPase data as is (unshifted). The wound edge is not shown but is towards the left. At 72 s, the RhoA zone dives away from the focal plane.

B.2 Expression of dominant-negative PKC beta

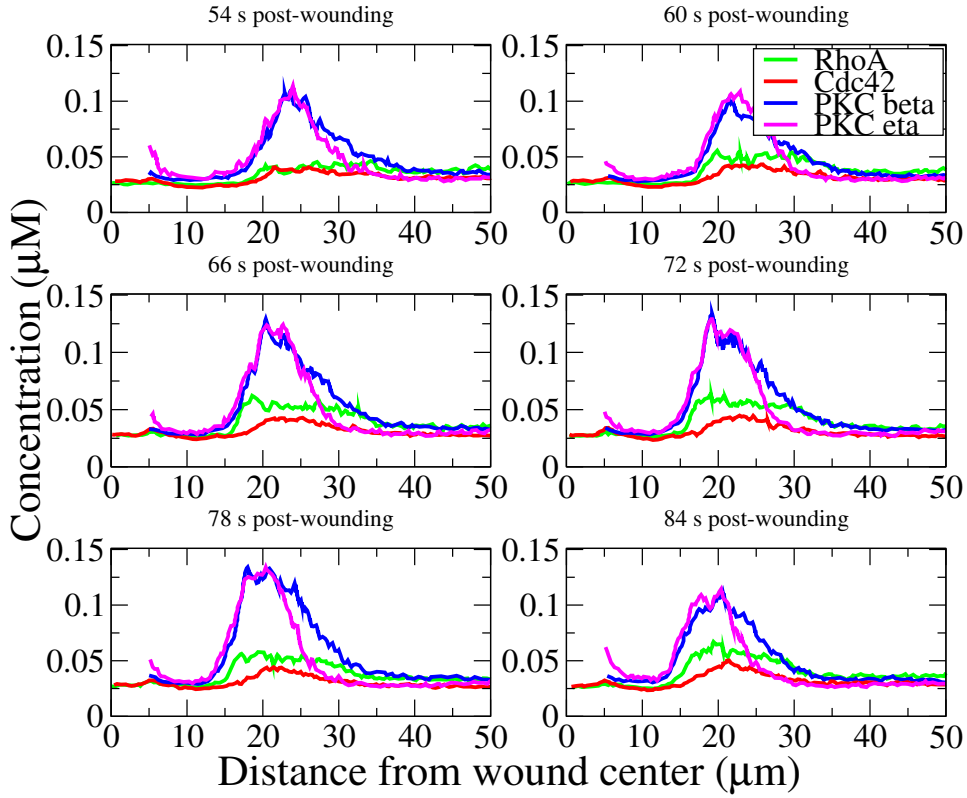


Figure B.2: Alignment of control PKC profiles with Rho GTPase profiles in dominant-negative PKC beta expression. PKC profiles are aligned with Rho GTPase data when shifted 5 μm away from the wound center. The wound edge is not shown but is towards the left.

B.3 Overexpression of PKC eta with inverted Rho GTPase zones

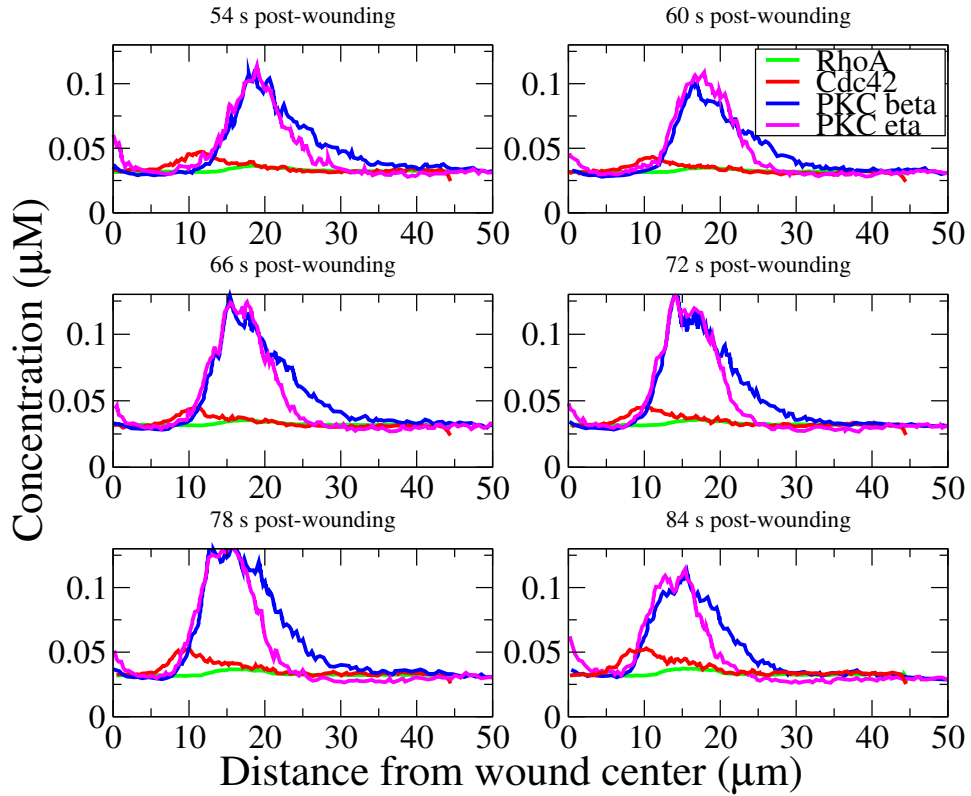


Figure B.3: Alignment of control PKC profiles with Rho GTPase profiles in PKC eta overexpression. PKC profiles are aligned with Rho GTPase data as is (unshifted). The wound edge is not shown but is towards the left.